PREDICTION OF NATURAL SNOWDRIFT ACCUMULATION IN ALPINE AREAS

N. Berg
N. Caine

PREDICTION OF NATURAL SNOWDRIFT ACCUMULATION IN ALPINE AREAS

A final report to USFS Cooperative Agreement 16-388-CA, Rocky Mountain Forest and Range Experimental Station, USDA Fort Collins, Colorado.

1975

N. Berg
N. Caine
Department of Geography
University of Colorado
Boulder, Colorado

PREFACE

This is the final report of USFS Cooperative Agreement 16-388-CA entitled Prediction of Natural Snowdrift Accumulation in Alpine Areas. It has as an objective the definition of a set of hypotheses concerning snowdrift accumulation in the form of a simulation model and the testing of the resulting model through field verification.

The authors wish to acknowledge the support of the Institute of Arctic and Alpine Research (INSTAAR) at the University of Colorado. Special thanks are due to Mr. J. Clark, Research Climatologist, who provided encouragement and support in the field. Likewise, the knowledge of machinery of Dr. M. Grant, R. Ring, and particularly H. Moulton, maximized the probability of success for the bi-weekly winter sorties into the alpine. We are also deeply indebted to Dr. J.D. Ives, Director of INSTAAR, who made available equipment, space, and transportation during the winter field seasons 1973-74 and 1974-75.

Sincere thanks are due also to Dr. M. Martinelli and especially Dr. R.A. Schmidt, of the US Forest Service, without whose patient encouragement this study would not have been successful.

The assistance of several individuals greatly eased the collection of field data. During the 1973-74 winter Marcia Clements made numerous trips to the alpine under often severe conditions. Frederick Bauer spent portions of the summers of 1973 and 1974 as rod-man for the topographic surveying. Finally, Elizabeth Berg spent many hours in the alpine as the companion to the senior author.

Provision of computer time by the National Center of Atmospheric Research and the University of Colorado Computing Center is gratefully acknowledged.

TABLE OF CONTENTS

LIST OF TABLES

LIST OF FIGURES

INTRODUCTION

In regions of seasonal snow accumulation where woody vegetation is scarce, relocation of fallen snow by wind is a common occurrence. The ground surface topography plays an important role in eolian snow redistribution in that lee slope depressions act as catchments for blowing snow. The result of this process is striking in late spring and early summer when snow may exist only adjacent to natural or artificial drainage channels in high plains regions or to the lee of alpine solifluction terraces. Understanding of the relationships between topography and snow redistribution is incomplete and often of a qualitative nature. Knowledge of natural snowdrift formation is applicable to the assessment of snow loading in snow avalanche zones and to the site selection of snow fences for augmentation of natural drift accumulation. The efficient management of artificial and natural drift accumulation, which knowledge of the redistribution processes should allow, would therefore provide opportunities for optimizing hydrologic management in alpine and midwestern plains regions.

Objective

This study seeks to define the role of wind-drifted snow in the mass budget of alpine snowbanks through derivation of a quantitative simulation model for the prediction of snowdrift accumulation. It is aimed specifically at utilizing existing theoretical knowledge of the processes of eolian snow sedimentation. The deposition and subsequent accumulation of snow into drifts is analogous in many ways to eolian sand dune development and subaqueous deltaic and current ripple formation. In this latter regard Allen (1968, p. 318) specified the general problem:

> The fate of the settling grains, in relation to the form, structure, texture, and fabric of the resultant leeside deposits, constitutes one of the most difficult of all the many problems of sediment transport-deposition.

Literature Synopsis

Initial research on the mechanics of sediment entrainment and deposition in low density fluids was conducted by Bagnold (1941) through laboratory and field experimentation. Since this beginning, numerous aspects of eolian sand movement have been investigated, some of which will be incorporated into the present analysis for lack of comparable understanding of eolian snow processes. A comprehensive review of the eolian sand movement literature is presented in Cooke and Warren (1973).

Specific concern with the deposition of eolian snow particles has involved both empirical and theoretical analyses. Several conceptual hypotheses have been presented on the general mechanics of snow deposition. Radok (1968) noted that although surface erosion and deposition depend upon 1) snow content in the suspension zone and 2) horizontal mass flux divergence; accumulation or ablation occurs by a net vertical mass transport through a self-maintaining saltation layer. Concomitant shear stress changes and formation of negative pressure gradients (Mellor, 1965) initiate the variations in the horizontal drift flux which result in sediment deposition. Odar (1965) suggested that while an object introduced into the boundary layer changes the boundary layer gradient, if the gradient remains above a certain limit, no deposition results.

Aside from these conceptual arguments, which to date have not been rigorously tested against empirical evidence, recent work on the deposition of wind-blown snow has involved statistical and scale model investigations.

Early investigations of snow deposition by the wind were concerned with the encroachment of wind-drifted snow onto road and railways. Research by Finney (1939) is typically quoted in this vein. Theakson (1973) has followed a similar direction to that of Finney's early research. Other scale model studies concerned with the practical problems of snow-drifting include the analysis of geometric scaling criteria applicable to hardware modelling (Calkin, 1975) and the work of Nayak,

Garrison, and Cermak (1974) on drifting around a proposed industrial complex. Recent work on natural snowdrift formation has been completed by Tabler (1975) from primarily an empirical standpoint utilizing regression analysis. His analysis provides valuable insights to the processes of snowdrift development but may be limited to the locale at which the regression coefficients were determined.

Scope and Limitations

The approach used in the present study develops from the outline of previous work. This shows that statistical and scale model studies may provide adequate empirical information but do not place sufficient emphasis upon the interacting physical processes which result in snow deposition. It is only through understanding of these processes that knowledge of the system could be applied in situations removed from that which provided the initial model. For this reason the research described here approaches the problem from a theoretical standpoint. As Allen's comment suggests, however, the problem is complex and it is necessary to resort to relevant flume and wind-tunnel observations to resolve some parts of it. It is also necessary to integrate information from several disciplines, notably fluid dynamics and sedimentology, as a basis for analysis.

The model is relatively simplistic and, at present, is deterministic but an attempt has been made to incorporate all the significant process variables. Future modification should expand the model's utility rather than compromise its current status. The simulation investigates the process interactions at a single drift site. In nature, several catchments commonly exist in-line such that blow-past from one site becomes input for a catchment further downwind. Extending it to the multiple catchment situation should not involve major alterations to the model presented here.

The primary concern of the model is determination of the location of deposition of wind-blown snow particles. On the following pages a set of hypotheses on snowdrift development are proposed which specify the relationships between particle deposition, ground topography, and airflow. Four sections can be identified and described separately. These are 1) initial ground topographic configuration; 2) airflow across this topography; 3) grain movement; and 4) depositional mechanisms. Field documentation of drift development allows verification of the functional relationships that comprise the model. Experimentation with the model in the form of a "sensitivity" analysis provides a means to ascertain which relationships most effect the outcome.

A MODEL FOR ALPINE SNOWDRIFT ACCUMULATION

Central to the problem of particle deposition is the presumption that sedimentation occurs when the tractive force of the fluid flow is no longer sufficient to transport the grains. Such a reduction in force, as produced by a decrease in wind speed, can be a purely meteorological response to the regional climatic substructure, in which case deposition will be random with respect to ground topography. Alternatively, airflow responds to changes in topography, following the principle of continuity. If the flow boundary narrows, as with movement over or around a topographic high point, wind shear increases. Conversely, expanding flow, downslope or into topographic depressions, decreases the fluid speed and shear. Observations show the preferrential relocation of snow to the lee of microtopographic high points (figure 1). Specification of the interrelationships between particle deposition and topography is the ultimate aim of the modelling effort.

Figure 2 is a general flowchart of the structure of the model. The ground surface over which the snow particles move is the primary static input to the model. Rules for the specification of the airflow speed and direction over varied topography define the tractive force for grain movement. From knowledge of the ground topography and airflow across it, zones may be specified in which the flow speed is insufficient for grain movement and which become potential drift accumulation sites. It is further necessary to specify the actual grain transport quantities and trajectories with respect to the ground and airflow parameters. A final task involves the depositional mechanisms controlling the settlement location of the grains. These of necessity must include provision for accounting for the allocation of 1) deposited snow to various locations on the topographic grid; and 2) "blow-past", the proportion of incoming snow which passes beyond the catchment.

Figure 1. Snowdrift survey, Niwot Ridge, mid-July, 1974.
Dotted line is snow surface. Horizontal and vertical axes values are in meters.

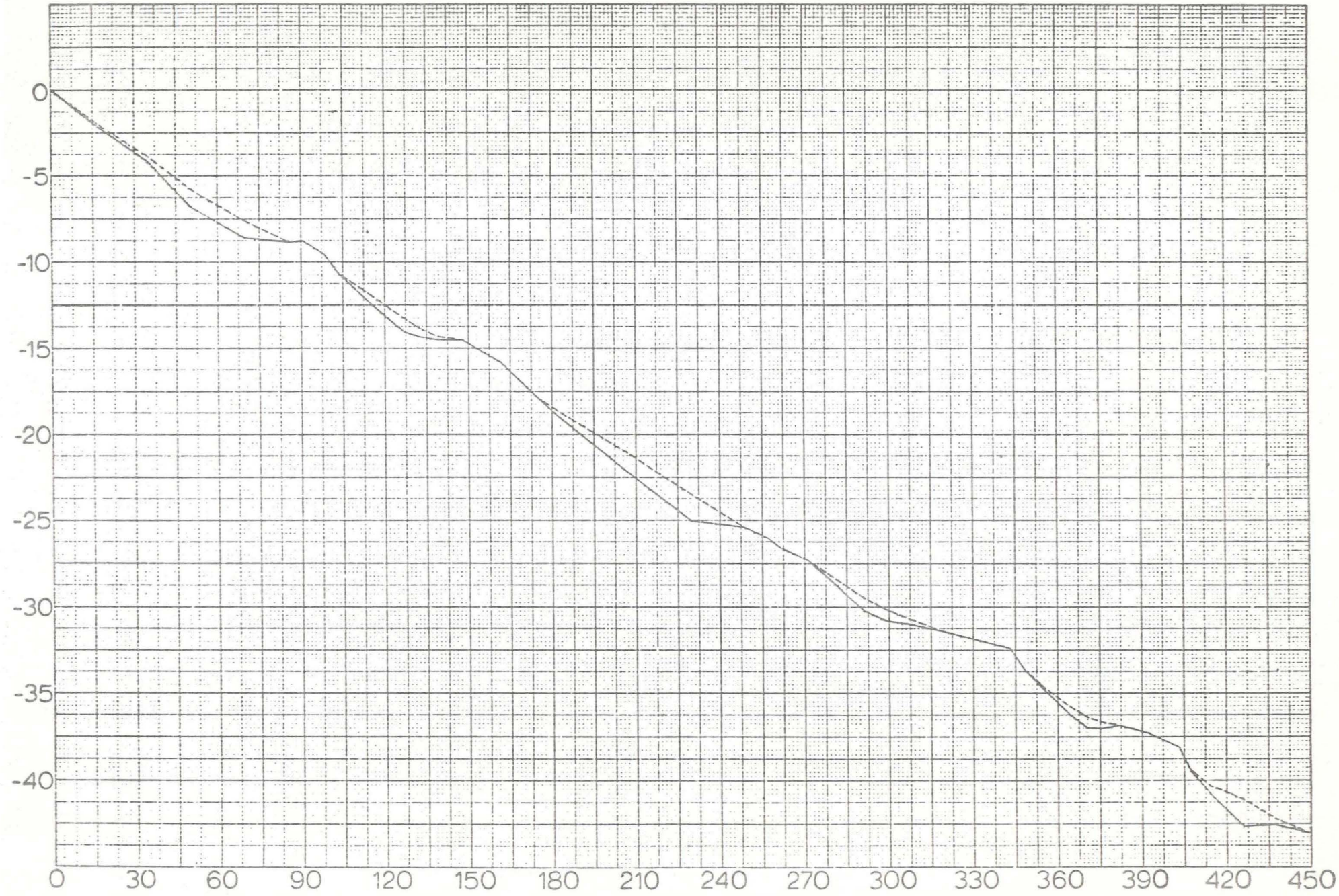
0
-5
-10
-15
-20
-25
-30
-35
-40
0
30
60
90
120
150
180
210
240
270
300
330
360
390
420
450

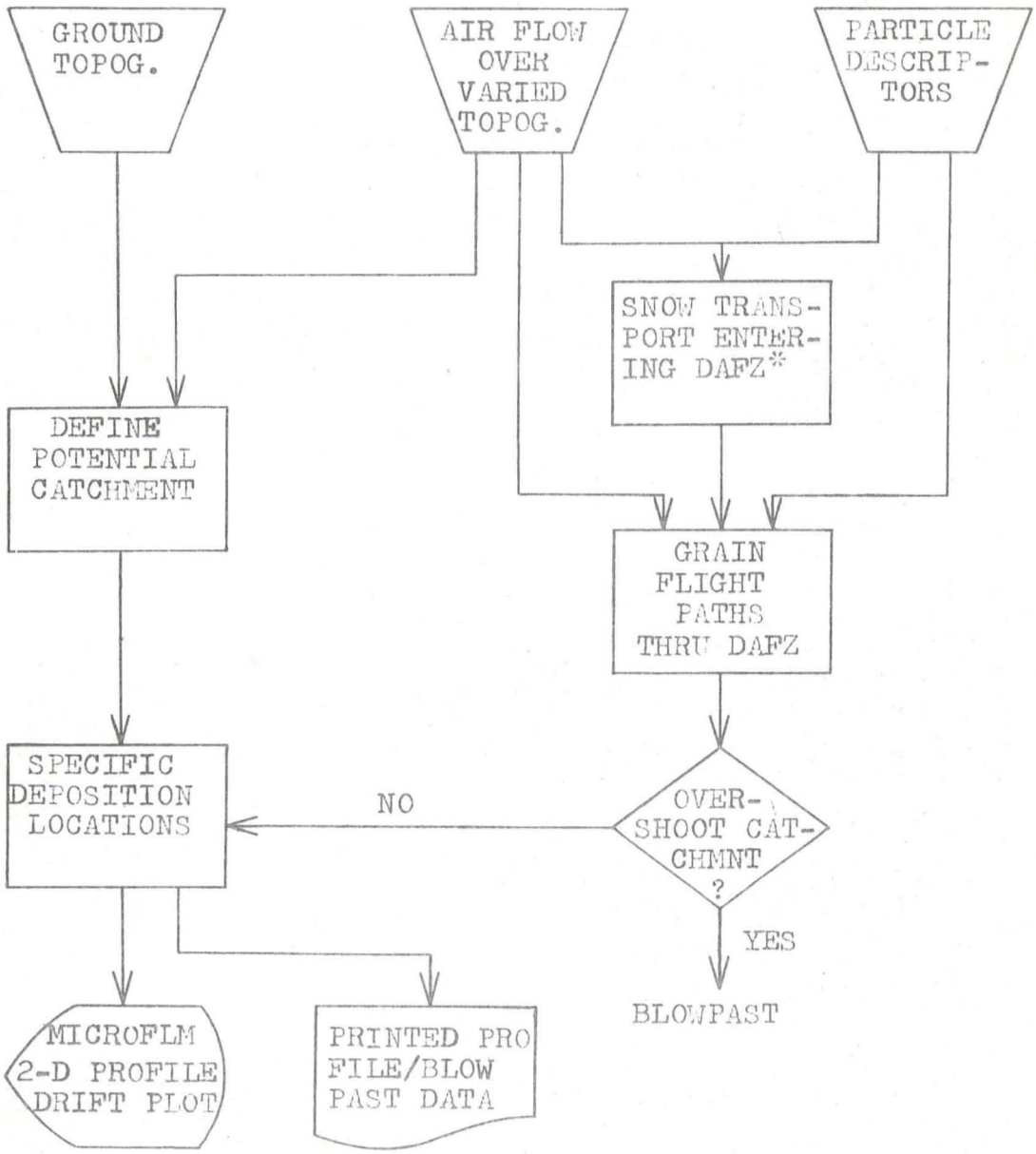

Figure 2. Flowchart of general structure of the snow-drift accumulation model

*DAFZ refers to Drift Accumulation Flow Zone: the area of potential deposition plus the lower atmospheric region immediately above the potential drift

In the following paragraphs the major components of the model are discussed in sequence.

Ground Topography

A two-dimensional Cartesian coordinate system is followed through all sections of the model. Input topographic data consists of up to 50 x-z coordinate pairs which specify the ground points. Point (0,0) is defined by the user as the anticipated location downwind of which deposition begins. Subroutine TOPIN resets the x-z coordinates so that point (0,0) is in the proper location and function TOPO interpolates between input x-values to calculate the z-value for any specified x-value. Figure 3 illustrates a simple topographic configuration in which three slope segments are specified.

Airflow

Prior to quantitative consideration of the airflow regime a general discussion of the mechanisms involved provides a basis for further analysis. The types of flow encountered in typical blowing snow settings are characterized by relatively high Reynolds Numbers wherein flow is everywhere turbulent. Only in situations where air speed is low--typically below the threshold speed of snow entrainment by wind--is the laminar situation even approached.

Four realms of air movement are important with respect to redistribution of blowing snow particles in a topographic situation like that of figure 3. Upwind of the origin the flow velocity is sufficient to transport particles. Typically, flow will be over a quasi-planar surface in which a steady state condition--in the mean--develops and for which flow parameters can be calculated successfully. Flow in this region is assumed to approximate that considered in traditional boundary layer analysis for which there is a long upwind approach slope.

When the wind flows over the crest of a slope into a topographic depression such that streamlines diverge, velocity decreases and--by the Bernoulli theorem--

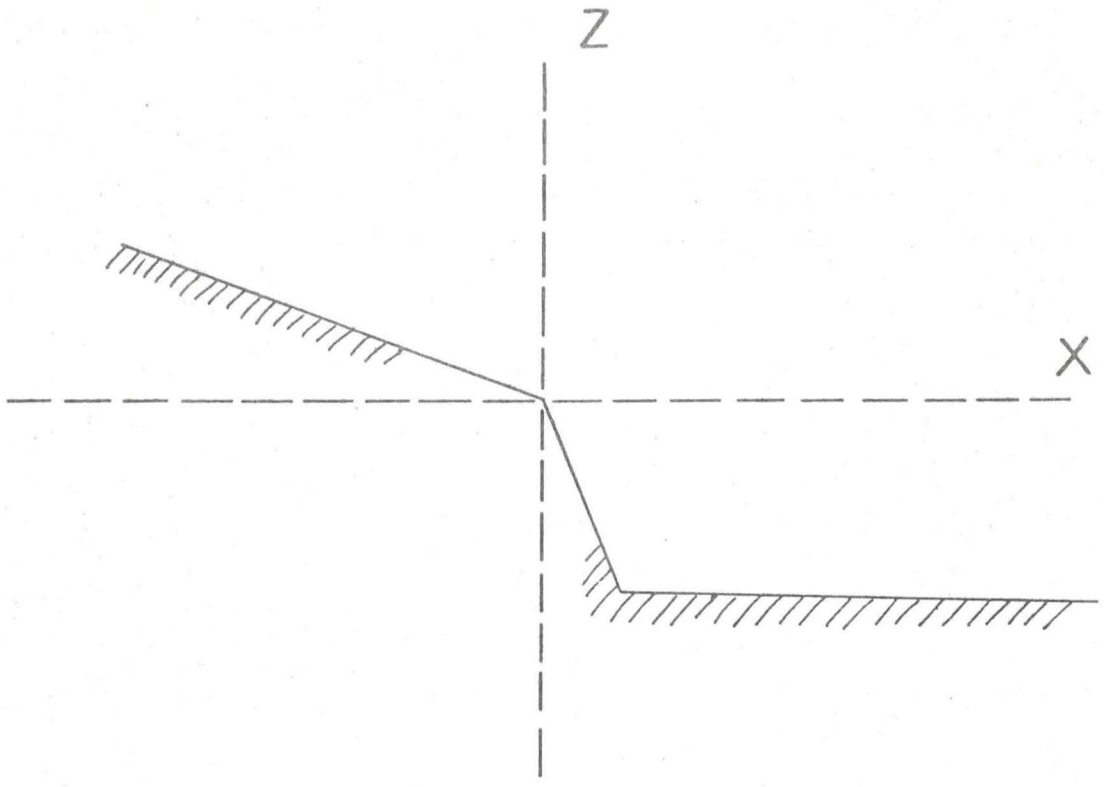

Figure 3. Definition sketch of three-segment slope topography with Cartesian coordinate system.

pressure increases with distance. The positive pressure gradient augments the existing effect of internal friction to severely decelerate the air parcels. In the region closest to the bounding surface these effects are most marked so that if flow expansion is great enough some fluid particles are stopped while others have their direction of motion reversed (Mellor, 1965). An eddy region of reversed flow results which is bounded by the solid boundary below and by a line--in the two-dimensional case--of zero velocity above which intersects the solid boundary downstream at the point of flow reattachment. Boundary layer separation has occurred with the criteria for separation being that $dU/dz = 0$ at the wall (figure 4). Sharp discontinuities in the solid boundary--at the origin in figure 3--trigger separation.

A major consequence of the separation of viscous fluids is the generation of vortex layers (Allen, 1968). In the case of separation caused by flow expansion a free vortex layer develops which is not bounded by a rigid boundary. If an abrupt surface discontinuity exists the vortex layer should steadily increase in thickness with distance from the separation point (figure 5) and be bounded below by the separation streamline. The vortex wedge is a zone of mixing where turbulence is intensified from that immediately upwind of the separation point (Arie and Rouse, 1956; Raudkivi, 1967).

Beyond the point of flow reattachment the fourth flow regime is characterized by the redevelopment of a boundary layer flow similar to that upwind of the separation point (Plate and Lin, 1965). In this region, the flow characteristics of the mixing/vortex region gradually revert to those which follow the logarithmic profile law.

Figure 6 illustrates the idealized case in which flow expansion is abrupt and separation is triggered at the origin.

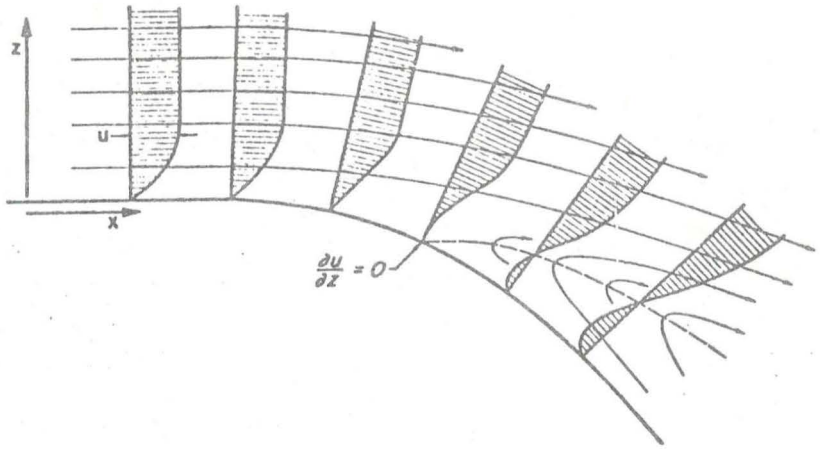

Figure 4. Boundary layer separation resulting from flow expansion (Mellor, 1965, p. 32).

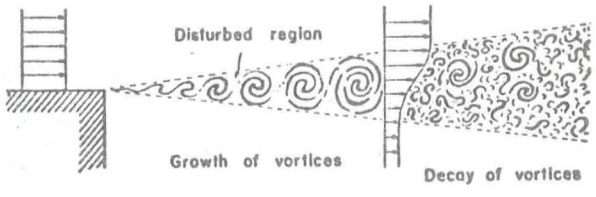

Figure 5. Growth of vortices in a free turbulence shear layer (Allen, 1968, p. 14).

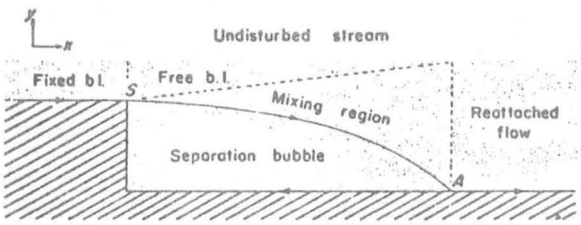

Figure 6. Flow regimes of a reattaching half-jet (Allen, 1968, p. 318).

The foregoing discussion implicitly considers two-dimensional flow. That flow separation may be three-dimensional is unquestioned (e.g., Cooke and Brebner, 1961; Chang, 1970) but the approach described here considers only two-dimensional flow for the sake of computational simplicity.

(i) Flow calculations for the undisturbed boundary layer

Numerous field and laboratory experiments show the adequacy of the logarithmic wind profile in conditions where near-surface thermal gradients are insignificant. Schmidt (1972) adopted the logarithmic profile in his analysis of the sublimation of wind-blown snow and experimentation in Antarctica by Budd, Dingle and Radok (1966) utilizing data from 129 wind profiles under blowing snow conditions showed no systematic deviation from the logarithmic profile.

Subroutine SHRVEL calculates frictional velocity, U_*, by either equation (1) utilizing values of wind speed U_z at height z and a surface roughness characteristic z_o, or through equation (2) from wind speeds $U_{z(1)}$ and $U_{z(2)}$ at heights z(1) and z(2),

$$U_* = U_z k \; / \; \ln(z/z_o) \tag{1}$$

$$U_* = k((\ln z(1) + \ln z(2))/2) \; (U_{z(1)} - U_{z(2)})/(z(1)-z(2)) \tag{2}$$

where k is von Karman's constant and z_o is commonly referred to as the roughness length of the surface. If equation (2) is used

$$z_o = \exp(\ln z - (U_z k \; / \; U_*)). \tag{3}$$

An alternate defintion for z_o derived by Budd, Dingle and Radok (1966) from field measurements during blowing snow is

$$z_o = \frac{10^{-(1.404 - (0.039\, U_{10}))}}{1000} \tag{4}$$

where U_{10} is wind speed at 10 m height. Subroutine VELIN defines the ratio

U_z/U_{max} where U_{max} is the velocity at the top of the boundary layer.

Use of the unmodified logarithmic law for non-horizontal surfaces is not entirely valid by reason of the continuity argument expressed in a previous section. Nevertheless it is the most generally applicable relationship that is currently available and will be assumed adequate for the present purposes.

(ii) Flow downwind of origin

Few field data are available which specify airflow conditions across topographic irregularities on the micro-scale. Furthermore, theoretical analysis of this condition is inadeqaute (Plate and Lin, 1965; Raudkivi, 1966). However, some information on natural and artificial flow regimes similar to that occurring at an eolian snow depositional site is available from natural sedimentary environments and from wind tunnel and flume experiments. Few of these data refer specifically to a blowing snow situation.

iia) Flow expansion in natural sedimentary environments

Notable similarities in particle and fluid movement patterns exist between eolian sand dunes, subaqueous ripples and deltas, and snowdrifts. Particularly illustrative is the resemblance in infill processes. As suggested in figure 7a, sand dunes and subaqueous ripples advance by sand infilling immediately to the lee of a sharp slope discontinuity. Similarly, initial snowdrift and delta accumulation occurs through deposition of material to the lee of a stationary slope discontinuity. Observations by the authors and others (e.g., R.A. Schmidt, oral comm., 1974) show that the snowdrift fills in during intermediate stages with a sharp slope discontinuity--figure 7b--similar to the dune slipface. Knowledge of flow over dunes is limited but it is one of the few natural flow regimes which exhibits similarities to flow over snowdrift catchments.

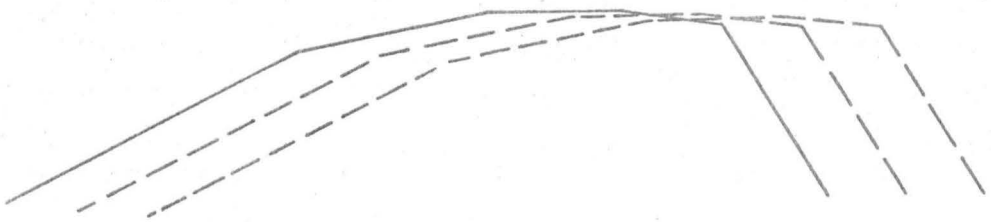

Figure 7a. Schematic representation of sand dune movement.

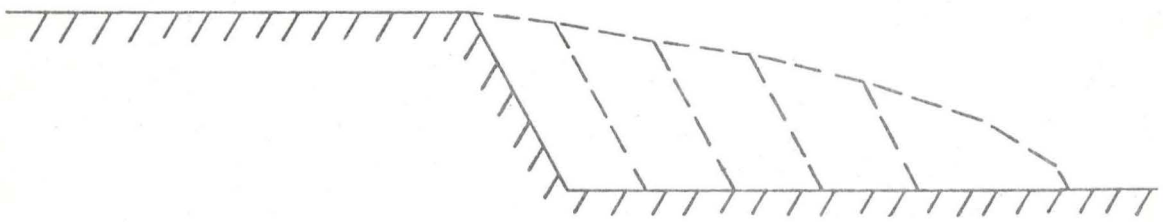

Figure 7b. Schematic representation of snowdrift infill.

If a Reynolds Number is defined using the vertical dimension, l, of a sand dune as the length parameter, a measure of similarity between sand dune, snowdrift and other similar types of flow can be determined. Measurements by Inman et al (1966) showed the wind speed above the summit of a 7-meter high dune to be approximately 7.5 mps. Measurements by Berg (1975) give similar results. Assuming an air temperature of 20°C, the corresponding "step" Reynolds Number, R_s, (Allen, 1968), given by

$$R_s = \frac{lU}{v}, \qquad (5)$$

where v is kinematic viscosity and U is wind speed, is 3.5×10^6. While lower temperatures exist in the blowing snow environment many drift catchments are on the order of 7 meters in height and there is no reason to believe that wind speeds should vary systematically between the dune and snowdrift environments (the senior author has experienced both high and low winds in both environments). For the following discussions R_s is considered to equal 10^6 for both the eolian sand and snow regimes.

In an extensive analysis of the development of subaqueous current ripples, Allen (1968) stated that R_s for ripple marks is also on the order of 10^6. Such findings suggest similarities in the flow regimes for the three environments.

Comprehensive micrometeorological wind measurements are not available for sand movement areas but several subjective observations of flow in such areas are relevant to the snowdrift case. Whereas workers argue about the efficacy of eddy flow to the lee of the dune crest for entrainment of dune sand, the existence of a flow reversal is less controversial. Inman et al (1966) reported backflow of mean speed equal to two mps with a maximum reverse flow of five mps. In similar observations, Hoyt (1966) also recorded reverse flow as well as noting this flow to be powerful enough to move sand. The senior author has seen vegetative matter

moving up dune slipfaces and felt a rain of sand, originating from above eye level, while standing in the lee of a large dune. That reverse flow should occur is bolstered by theoretical arguments. By dynamical similarity separation bubbles should develop if $R_s \doteq 10^6$. Allen (1968, p. 133) strongly affirms this contention:

> Although it may be difficult to establish in the field the existence of unsteady separation bubbles captive to dunes, there are the soundest of theoretical reasons for the belief that such eddies do occur. To deny the implications of the large Reynolds numbers afforded by wind dunes would be to deny the deepest foundations of modern fluid dynamics.

A second observation on sand movement on dunes concerns the transport of grains at the slope discontinuity. Under high wind speed conditions, the senior author and others (e.g., Cooper, 1958) have observed a wedge-shaped region, synonomous with the mixing region of figure 6, which is so sand-filled as to reduce visibility. This plume of high sand concentration fades with increasing distance leeward from the slipface crest. The similarity to snow pluming off ridge crests is striking and the conclusion to be drawn is that high turbulence intensity, particularly with respect to the magnitude of the "up" turbulent component, must exist in the near mixing region to suspend sand grains.

ib) Artificially-induced flow expansion

Successful quantification of the airflow regime must rely upon wind-tunnel and flume data from conditions which most closely simulate flow over irregular topography. Half and full jet flow have been investigated by numerous workers (e.g., Tollmien, 1926; Liepmann and Laufer, 1947; Albertson et al, 1950; Tani, 1958; Laursen and Toch, 1959; Abbott and Kline, 1962; and Naib, 1966) and appear to approximate reasonably flow over abrupt slope discontinuities. These flow regimes are similar in that abrupt flow expansion results at locations where the boundary walls diverge. Raudkivi (1967) and Allen (1968, p. 166) note that "a

fundamental similarity" exists between two-dimensional flow over negative steps and flow past a subaqueous ripple. By dynamic similarity arguments, such similarities should pertain to flow at snowdrift catchments.

Several properties of step flow are important in the current analysis. Much of the following discussion is taken from the excellent summary of Allen (1968).

Fluid movement through an axisymmetric jet into a bounded fluid region is termed reattaching full jet flow. In such a regime, the reattachment of separated flow to an adjacent solid boundary has relevance to flow over irregular terrain. When two adjacent portions of a fluid move at different speeds, the slower-moving portion is entrained and accelerated such that pressure is reduced whereby the entire fluid flow turns toward the region of reduced pressure. Such a phenomenon, the Coanda effect, accounts for the reattachment of a two-dimensional jet to an adjacent wall--thereby forming a separation bubble--if the boundary wall is not inclined too steeply from the plane of the jet (Squire, 1956) (figure 8). In full-jet flow the distance from the orifice to the reattachment point, or the length of the separation bubble, L_b, varies with both the step height, H, and the orifice width, d, such that L_b/H appears to be a function of d/H (figure 8) (Bourque and Newman, 1960; Sawyer, 1960). Further consideration of full-jet flow will be delayed until discussion of airflow to the lee of the step.

Analysis of reattaching half-jets show a similar association between the ratio step height to separation bubble length and the ratio of boundary layer thickness to step height. Although theoretical analysis by Abramovich (1963) resulted in a constant value of 6.1 for L_b/H, his own experimental work showed L_b/H to be strongly dependent upon d/H. The experimental data of Abramovich (1963), Bourque and Newman (1960), and Sawyer (1960) as well as that from diffuser flow by Abbott and Kline (1962) plus other relevant data on this relationship are presented in figure 9. Variations in Reynolds Number and boundary layer thickness probably

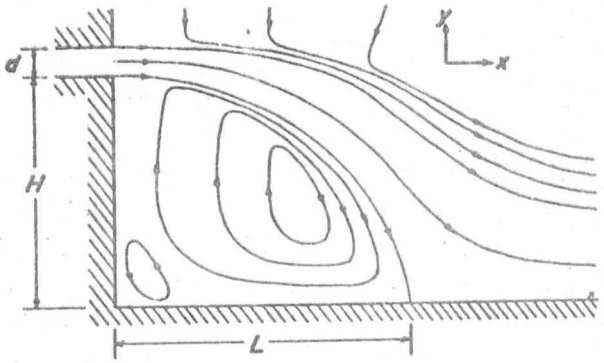

Figure 8. Pattern of motion in a reattaching jet (after Sawyer, 1960, p. 551).

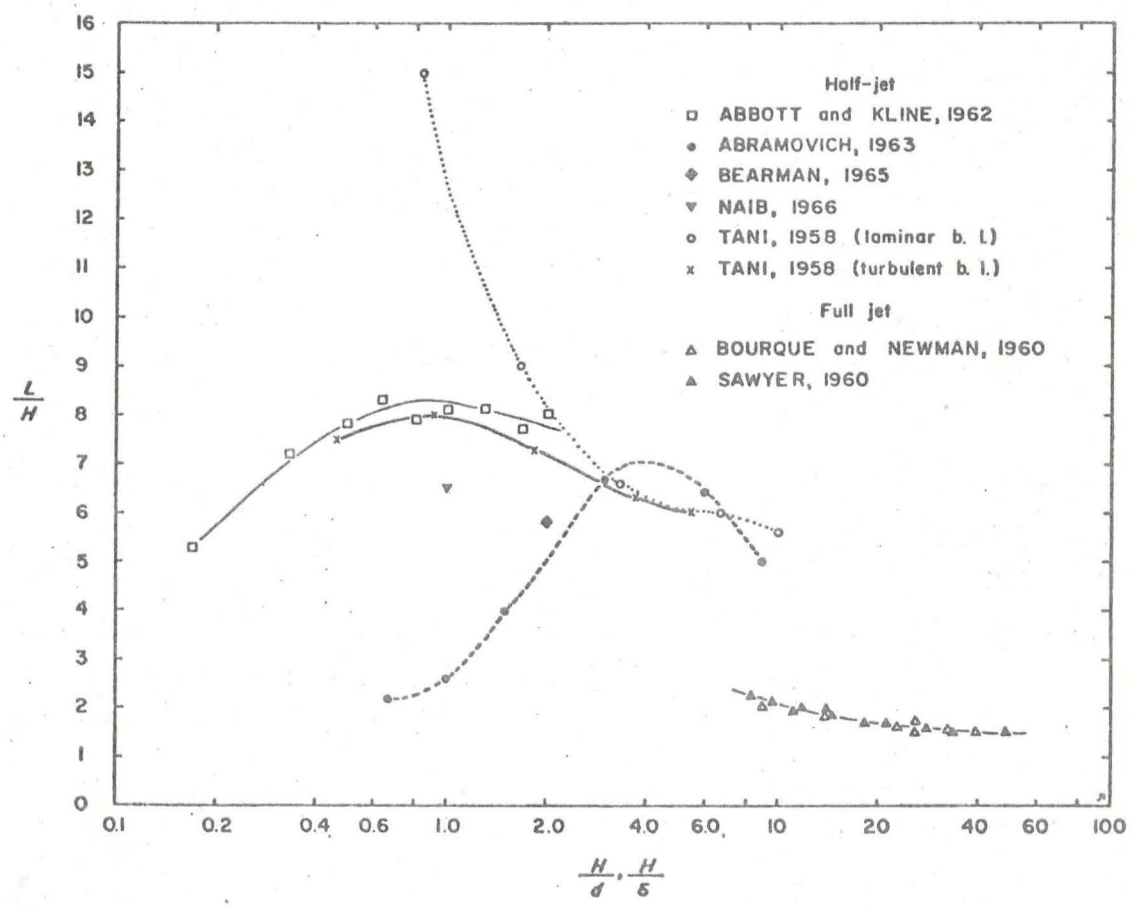

Figure 9. L_b/H as a function of H/d or H/δ for reattaching jets and half-jets, where d is flow depth and δ is boundary layer thickness (Allen, 1968, p. 157).

explain many of the discrepancies in the data (Allen, 1968).

The two-dimensional turbulent reattaching half-jet closely resembles flow occurring over irregular topography as well as subaerial dune and subaqueous ripple situations. Besides the question of separation bubble length the airflow properties to the lee of the separation point are of importance. In this regard it is necessary to specify as accurately as possible the entire flow field.

Empirical and theoretical evidence shows that reverse flow occurs in the eddy region below the separation streamline. Abramovich's theoretical results (Abramovich, 1963) are plotted on figure 10 along with a comparison to the experimental results of Naib (1966). In this connection U_2 is reverse flow velocity and U_1 is maximum forward flow speed at a non-dimensional distance x/H from the separation point. It is apparent that reverse flow speeds can be appreciable, up to 0.4 of the maximum forward speed, and backflow varies with position in the separation bubble. Raudkivi's work on step flow confirmed the existence of reverse flow of varying intensity although the flow regime was incompletely known (Raudkivi, 1967). From their measurement of flow over a wall positioned normal to a splitter plate, Arie and Rouse (1956) also described reverse flow in the eddy zone. These observations confirm similar observations of reverse flow to the immediate lee of subaerial dune crests. In the subaqueous environment, Allen (1968) considered reverse flow in the eddy region of current ripples to equal a constant value of one-quarter of the maximum forward flow speed at all locations within the separation bubble. The mean of 22 measurements of the ratio reverse flow velocity to forward flow velocity in the separation bubble to the lee of a model delta was found by Jopling (1960) to equal 0.25.

At this point discussion has considered the properties of the eddy zone, especially its spatial dimensions and airflow regime. It is now necessary to consider flow through the mixing region and in the zone of boundary layer redevelopment.

The spatial configuration of the mixing region must be defined as well as the horizontal and vertical mean and fluctuating velocity components. Along the separation streamline velocity equals zero. This streamline forms the lower border of the mixing region and its angular orientation may be determined from figure 9 as will be described in a later section. Flume and wind-tunnel analyses by several workers (e.g., Tollmien, 1926; Jopling, 1960; Naib, 1966) and theoretical analysis by Abramovich (1963) yield values for the upper mixing region angle, α, ranging from 5 to approximately 6.1 degrees with a mean of 5.39 degrees from the horizontal.

Data on the airflow distributions within the mixing zone is scarce. Working with submerged unbounded full jets Albertson et al (1950) found the longitudinal velocity distribution within the mixing region to closely approximate the normal probability function. Flow across a given section within this zone is represented by one of the two symmetrical halves of the normal probability curve. The free stream flow speed, which is considered equal to the boundary layer flow velocity or is defined by the logarithmic profile law, is scaled downward from the upper boundary of the mixing region according to the normal probability distribution. (figure 11) This approach does not consider flow reattachment so air speed in the eddy zone is taken to equal zero.

An alternative approach is that used by Naib (1966) utilizing a formula developed by Schlichting (1930, discussed in Naib, 1966) for wake flow. In this procedure air speed within the mixing zone, $U_{z,x}$, at distance x from the separation point and height z is related to the maximum reverse flow speed at x, $U_{b,x}$, and the maximum forward flow speed at the upper boundary of the mixing region at x, $U_{m,x}$, in the following manner

$$U_{z,x} = U_{m,x} - (1 - N^{1.5})^2 (U_{m,x} - U_{b,x}) \qquad (6)$$

where

$$N = (z - z_{b,x}) / (z_{m,x} - z_{b,x}) \qquad (7)$$

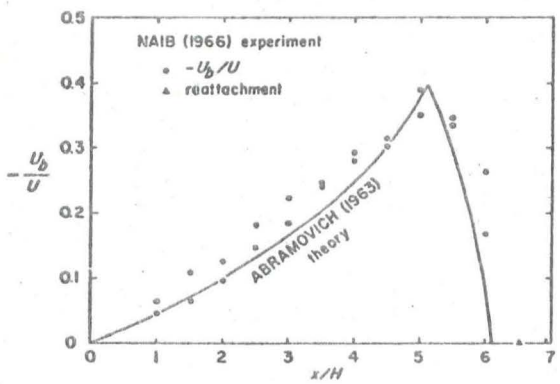

Figure 10. U_2/U_1 (U_b/U) as a function of x/H for the reattaching half-jet. Abramovich (1963) theory compared with experimental results of Naib (1966) (Naib, 1966, p. 205).

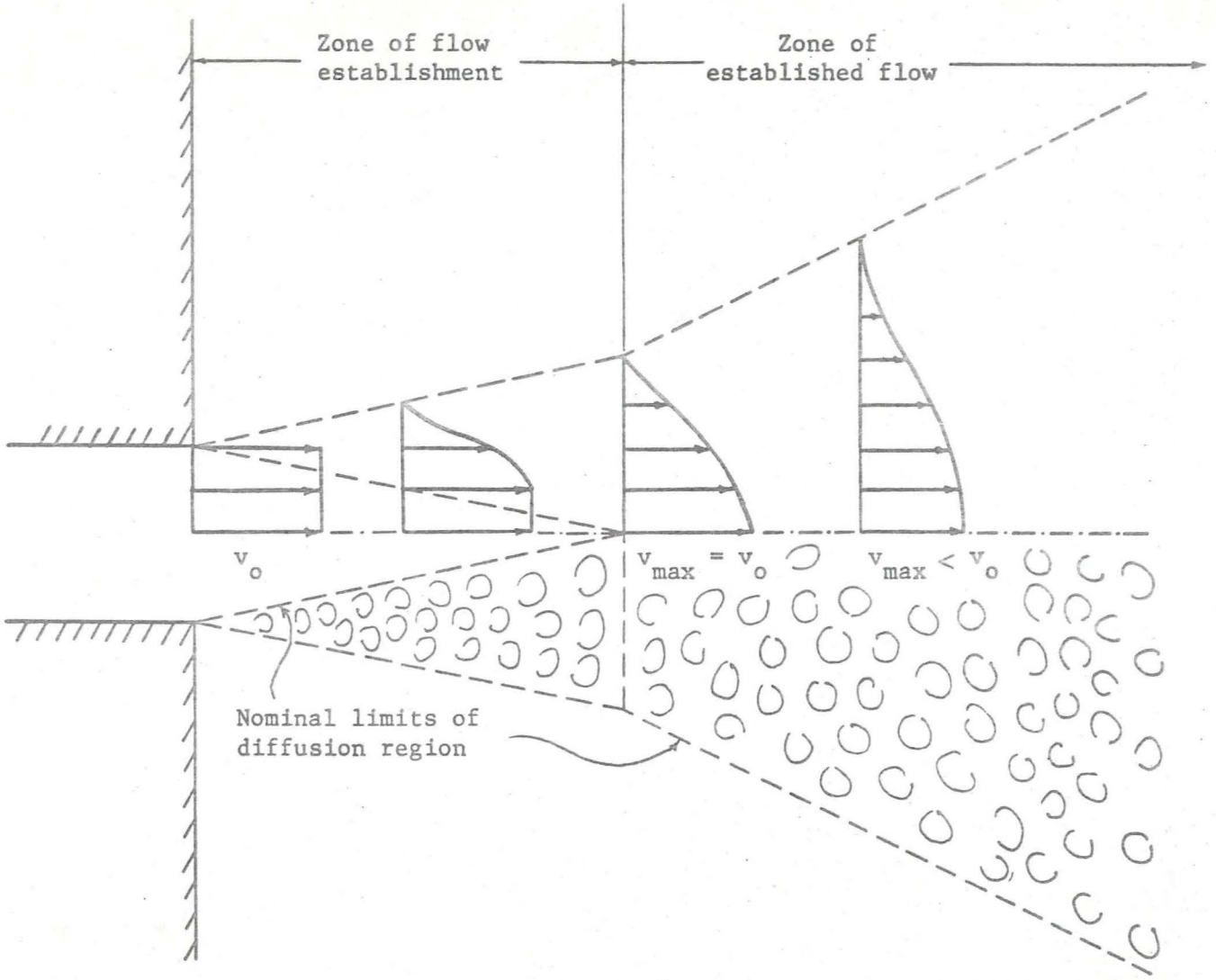

Figure 11. Schematic representation of diffusion of a full free jet (after Albertson et al, 1950, p. 640).

and $z_{b,x}$ and $z_{m,x}$ are the heights at which $U_{b,x}$ and $U_{m,x}$ occur, respectively. In his empirical evaluation of equation (6) under flow condtions where the Froude Number equalled 0.5, Naib (1966) found a good correspondence between the experimental data and the values predicted by equation (6) (figure 10).

Besides determination of the mean horizontal velocity component at a specified height within the mixing region, the horizontal and vertical turbulence intensities and mean vertical velocity must be specified. A literature search produced no references to the mean vertical velocity component within the mixing zone. Consideration of the high level of vorticity in this region suggests, however, that in the mean there is insignificant vertical motion in that the downward vortex action cancels the upward motions.

The effects of turbulence are perhaps more important. Work by Tani (1958), Raudkivi (1967), and Arie and Rouse (1956) showed that the intensity of the horizontal turbulence component within the mixing region reaches one-quarter of the maximum flow speed outside the mixing zone. Similarly, the vertical turbulence component reaches a maximum of 1/8 of the maximum flow velocity. Furthermore, the intensity of these turbulence components appears to follow a normal probability distribution across a given section of the mixing region whereby the maximum 0.25 or 0.125 U_1 values are attained in the center of the mixing zone.

In wind-tunnel experimentation on flow reattachment downwind of two-dimensional model hills Plate and Lin (1965) noted that the height of the redeveloping boundary layer, H_{bl}, follows a power law of the form

$$H_{bl} = A_2 (x - L_b)^{C_2} \tag{8}$$

as suggested by Elliot (1958, discussed in Plate and Lin, 1965) (figure 12). Empirical analysis of the flow profile plots show $C_2 = 0.5$. It remains to determine the coefficient A_2.

① UNDISTURBED BOUNDARY LAYER (OUTER LAYER)
② REGION OF HILL INFLUENCE (MIDDLE LAYER)
③ REGION OF REESTABLISHING BOUNDARY LAYER (INNER LAYER)
④ BLENDING REGION BETWEEN MIDDLE AND OUTER LAYER
⑤ BLENDING REGION BETWEEN INNER AND MIDDLE LAYER
⑥ STANDING EDDY ZONE
⑦ POTENTIAL OUTER FLOW

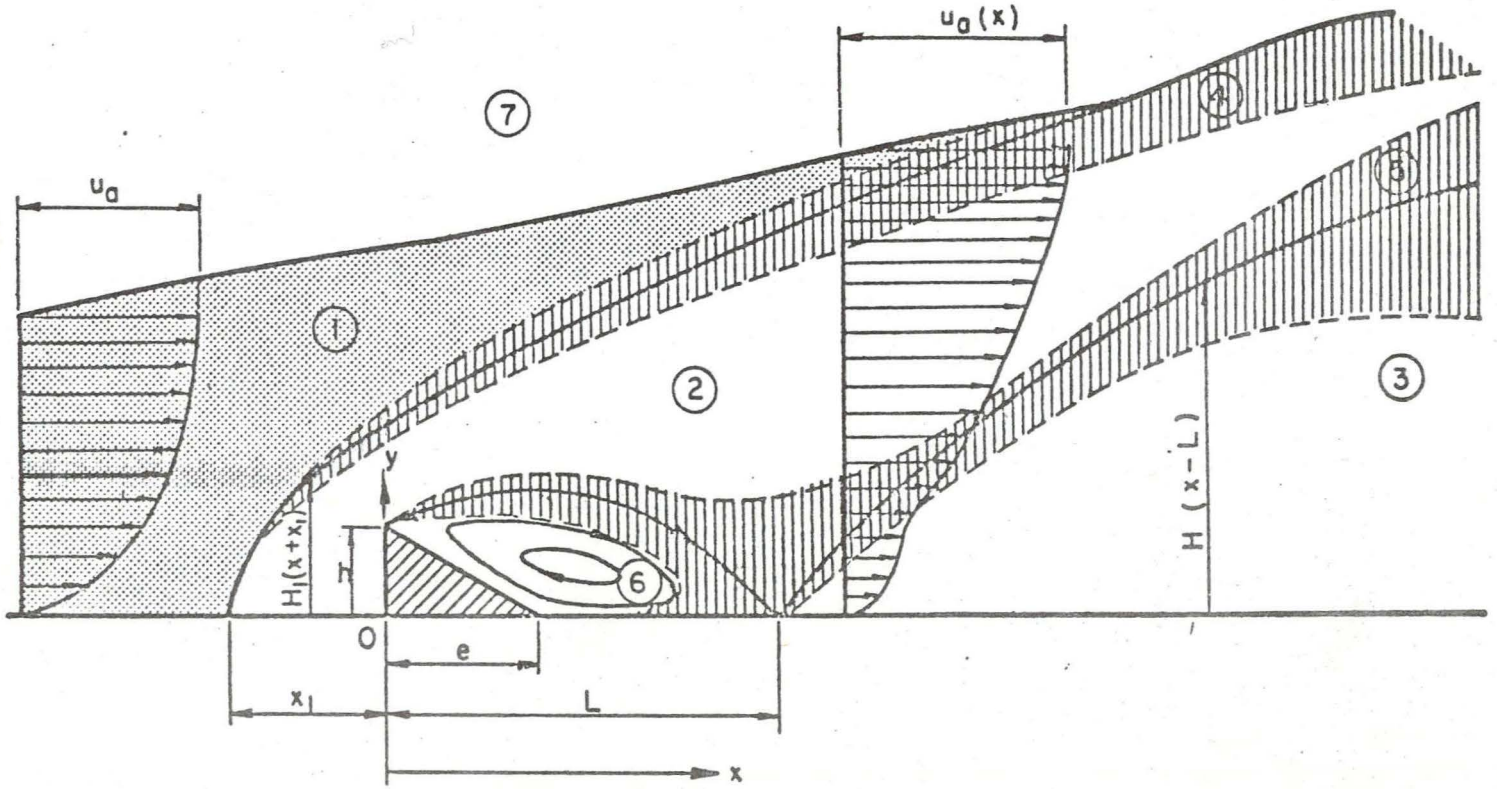

Figure 12. Definition of flow zones (Plate and Lin, 1965).

A measure of the influence of the model hill on the flow regime is the wall shear stress coefficient, C_f. If the value of C_f is known at a location upwind of the separation point, $C_{f(0)}$, then the ratio $C_f/C_{f(0)}$ measures the influence of the model hill on the downwind flow profile. Evidence shows $C_f/C_{f(0)} = 1.0$ at the location where the non-dimensional ratio $x/H = 65$ (Plate and Lin, 1965, p. 67, fig. 40). At $x/H = 65$, H_{bl} is assumed equal to the original boundary layer height, d, and all components of equation (8) are known except for A_2. Solution for A_2 allows equation (8) to be used to define the height of the redeveloping boundary layer at any x-location.

ii) Flow calculations in the mixing and eddy zones

In order to specify the flow velocities in the eddy and mixing regions the boundaries of these zones must be defined in the drift accumulation model. The upper boundary of the mixing region is defined as angle α and is taken to equal 5.39 degrees unless α is input by the user. Determination of the lower mixing region angle, β, is more complicated. Information on figure 9 shows the separation bubble length, L_b, to be a function of boundary layer thickness, d, and step height, H. Subroutine DTEND utilizes the data in figure 9 by linearizing the curves into five segments and disregarding the lower H/d values of Tani (1958), laminar boundary layer, and Abramovich (1963). The parameter H is easily specified when the upwind approach angle of the step is horizontal and when the riser is vertical. In nature, however, such a configuration seldom exists. Definition of H therefore becomes somewhat arbitrary; the procedure for its determination is given as follows.

Step height is defined in the direction perpendicular to the line extending leeward from point (0,0) along the upwind approach slope--whose angle is designated WNDRD--(figure 13). The lower end of the normal is located at the ground surface z-value at which a specified ground slope value--CRTSP input by the user--

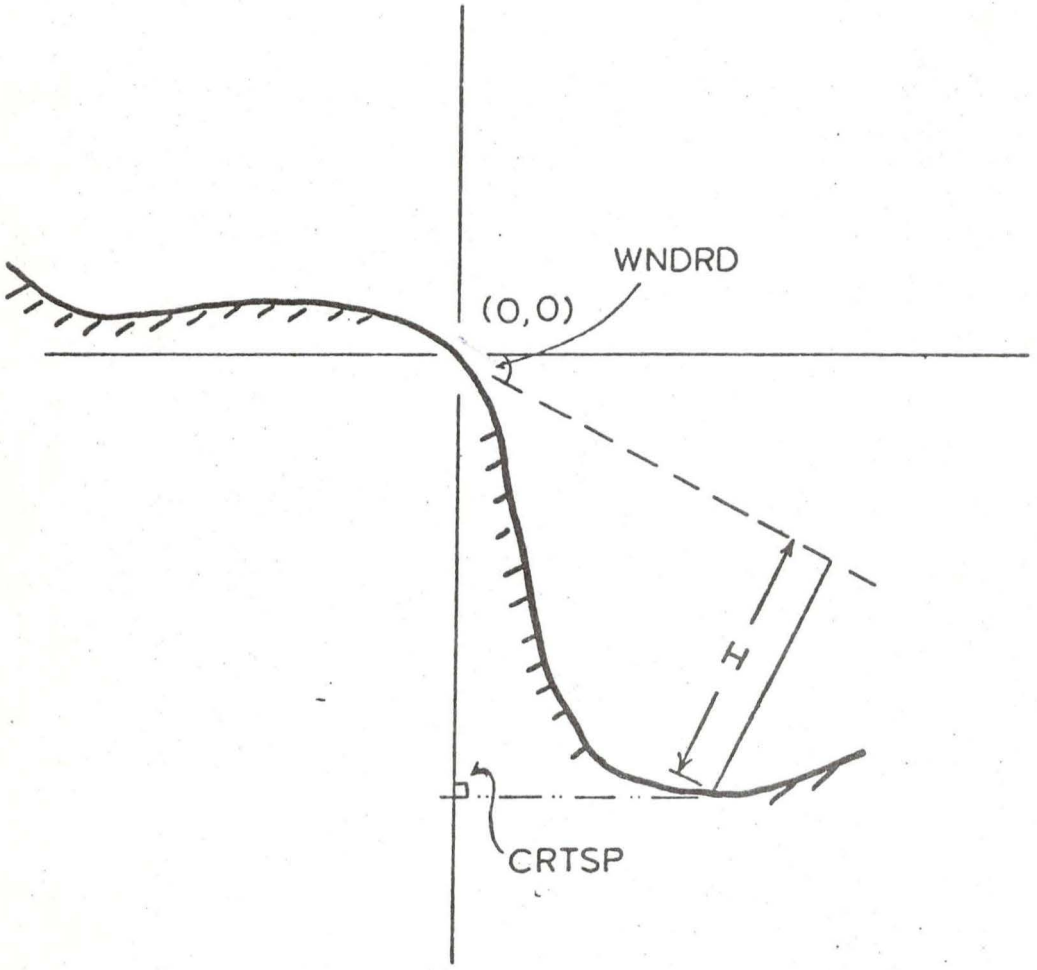

Figure 13. Schematic representation of determination of step height, H, from knowledge of critical slope, CRTSP, and approach angle, WNDRD.

is first reached (figure 13). The value for H follows from simple trigonometric operations.

Given H, L_b is determined from the linearization of figure 9 data. For example, for the condition in which the ratio H/d is less than 0.5,

$$L_b = H\ ((7.6\ H/d) + 4) \tag{9}$$

and β is the arctan (H/L_b).

It remains to specify the horizontal and vertical velocity components within the mixing and eddy flow zones.

Subroutines NAIB and ALBRT provide for derivation of the horizontal speed distribution within the mixing zone. If zero backflow is input the Albertson procedure is used whereas if a constant negative reverse flow value or a positive reverse flow value is input to the model, velocity values based upon the Naib approach (equation 6) result. As suggested in a previous paragraph, the effects of turbulence are significant and should be included in the model. At the present time, however, the model calculates only the mean horizontal velocity and assumes the value of zero for the mean vertical velocity in both the mixing and eddy regions.

Flow within the separation bubble is determined by subroutine EDDY which provides alternatives for the flow calculation. Options of either 1) zero reverse flow, 2) constant reverse flow, or 3) variable backflow (equation 6) are available. Both the backflow/forward maximum flow ratio, U_2/U_1, and the location of maximum backflow within the separation bubble can be specified as input parameters. Alternatively, the model utilizes the value 0.4 and 0.82 for these parameters as defined by Naib (1966).

(iv) Flow calculations in the zone of boundary layer redevelopment

To completely specify flow beyond the reattachment point the height of the redeveloping boundary layer must be known as well as the velocity distribution above and below this height. The model assumes that the location at which $C_f/C_{f(0)} = 1.0$ denotes the point at which the boundary layer is fully redeveloped and $H_{bl} = d$ at this point. Given this assumption, equation (8) can be solved for A_2 after which H_{bl} may be determined for any distance beyond flow reattachment. The speed of the airflow at H_{bl} is further assumed to be directly proportional to the height of the boundary layer; thus at $x = 32H$, $H_{bl} \doteq 9.9$--assuming $L_b = 10$, $H = 2$, and $d = 15$. Furthermore, at $x = 32H$ the velocity at the top of the boundary layer is approximately 0.66 of that upwind of the origin.

Flow velocity within the boundary layer follows the logarithmic profile law while flow above the boundary layer is assumed to follow the mixing region profile as defined by subroutines NAIB or ALBRT.

Particle Movement

Under low temperature conditions blowing snow particles may be considered to be hard ice spheres of approximately 0.1 mm diameter (Mellor, 1965). In many respects these particles move in a manner similar to sand. An obvious differentiating feature between sand and snow is the inherent thermodynamic instability of snow particles and the consequent importance of the sublimation of wind-blown snow and the cohesion of deposited snow grains. These differences notwithstanding, consideration of the mechanisms of wind-blown sand is relevant since more is known about some facets of sand movement than analogous facets of eolian snow movement.

It is necessary to establish initial conditions for particle movement in the region of undisturbed flow and to calculate flight trajectories for grains through the mixing and eddy regions. Specifically, rules must be developed to 1) apportion total mass transport between the various modes of grain movement; 2) define hori-

zontal and vertical particle speeds for particles in creep, saltation, and suspension; 3) calculate drift densities at varying heights for suspended grains; and 4) define particle trajectories at the entrance into the mixing zone and within the mixing and eddy regions.

(i) Grain motion prior to entrance to the mixing region

Three modes of transport have been distinguished for wind-blown sand. (1) In creep transport particles move by rolling and sliding without leaving the surface. Grains in creep transport typically receive their impetus for motion from the impact of saltating grains falling from the air stream. (2) Saltation occurs when particles bound along the surface, impacting to eject other grains into saltation or to impel particles in creep transport or to rebound themselves into the airflow. Saltating grains travel in curved trajectories under the influence of gravity and wind forces (Bagnold, 1941). (3) Particles held in suspension travel in the air stream and seldom contact the surface; vertical mixing processes hold up the suspension load (figure 14).

Measurements by many workers (e.g., Mellor and Radok, 1960; Dingle and Radok, 1961; Budd, Dingle, and Radok, 1966) of drifting snow densities in the lower boundary layer document the existence of the suspension transport mode for blowing snow. Photographic analysis of low-velocity blowing snow events by Japanese researchers (e.g., Kobayashi, 1972) demonstrate the importance of saltation in such meteorological regimes. Although creep exists as a wind transport mode of snow, this process has received little investigation (Mellor, 1965).

The model is constructed so that particle movement analysis is completed for one grain size fraction at each iteration. A transport quantity, q_d, in g cm^{-1} sec^{-1}, is required as input for each size fraction. The value of q_d is apportioned between the three transport modes by the following procedure.

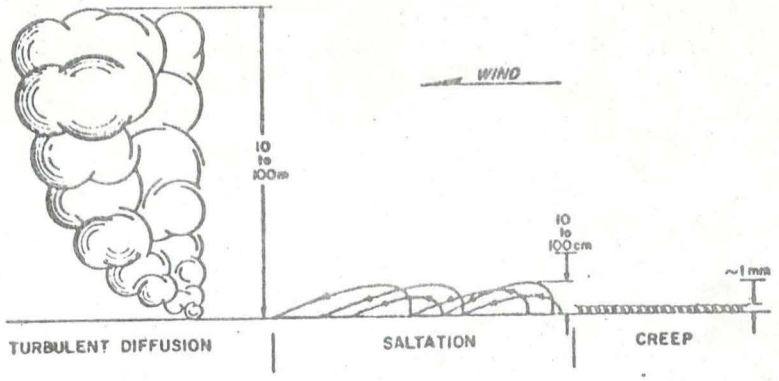

Figure 14. The three modes of transport for blown snow (Mellor, 1965, p. 5).

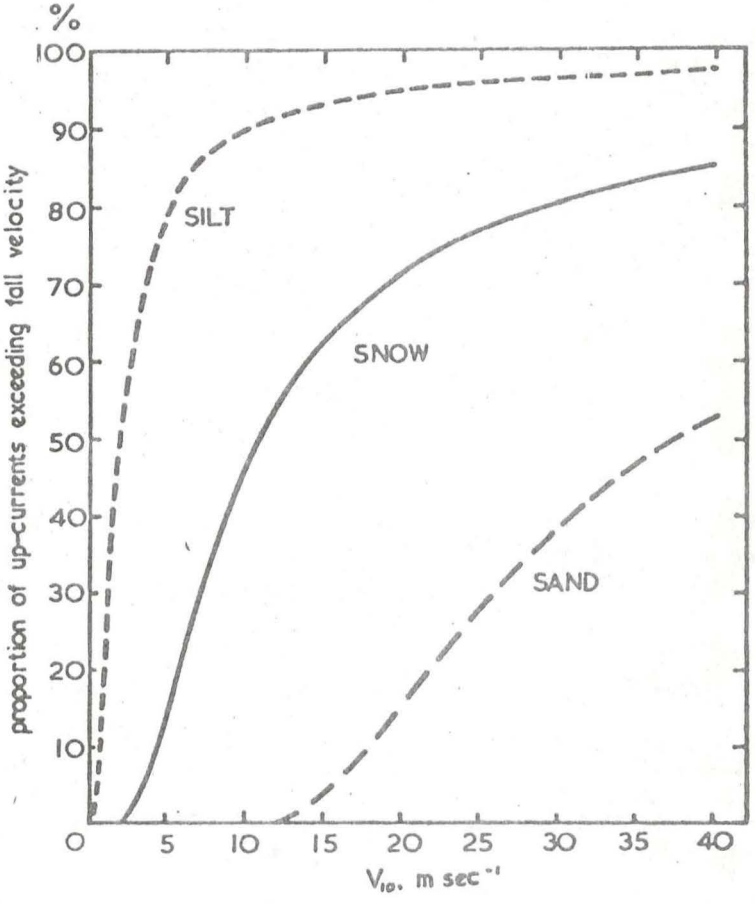

Figure 15. Cumulative frequency curves of suspension up-currents for silt, snow, and sand (Radok, 1968, p. 14).

The terminal velocity of fall, w, for grains of diameter D is calculated from equation (10)

$$w = cD \quad (D \text{ in mm, } w \text{ in mps}) \tag{10}$$

where c takes the value 2.2 for angular grains, 2.7 for subangular to subrounded grains, and 3.2 for round blowing snow particles. Values of the coefficient c are adapted from those quoted by Budd (1966, p. 60) and Mellor (1965, p. 12). Equation (10) is adequate for grain diameters between ca. 60 microns and 1.5 mm. It assumes that particle fall velocity is constant with height thereby implying uniform snow particles that do not change size with height. The non-dimensional fall velocity coefficient w_* is defined by

$$w_* = w / kU_* \tag{11}$$

where k and U_* are as previously defined.

Radok (1968) has developed an equation for the probability distribution, P(W), of boundary layer atmospheric up-currents which exceed the particle fall velocity (figure 15). For a given wind velocity regime and particle size, the fraction of q_d alloted to suspension transport is calculated through solution of equation (12); the remainder of q_d being allocated to creep and saltation:

$$P(W) = (2/\pi)^{1/2} \int_{0.36w_*}^{\infty} e^{-x^2/2}\, dx \; . \tag{12}$$

The suspension load, q_{sus}, therefore becomes equal to q_d P(W).

ia) Suspension transport

Considering the simplified case of constant fall velocity, the "drift density", n_z, at height z in g m^{-3} can be calculated from the following relationship (Shiotani and Arai, 1953; Mellor and Radok, 1960):

$$n_z = n_{z(1)} \, (z/z(1))^{-w_*} \qquad (13)$$

where $n_{z(1)}$ is specified as the drift density at height z(1). Equation (13) assumes that horizontal particle velocity is equal to wind speed (Mellor, 1965).

To facilitate computation of the suspension load the lower atmospheric boundary layer is considered to be comprised of a set of layered units which increase in thickness with increasing height. Given the configuration of the mixing region and especially angles A and B synonymous with α and β (figure 16), particles entering the mixing zone at a distance x equal to the anticipated leeward end of the drift--point 1 in figure 16--will be carried past the drift accumulation. In fact, grains entering the mixing zone between heights 1 and 2 (figure 16) will also be transported beyond the catchment. Subroutine SUSP divides the region below the level designated by point 2 (figure 16)--defined as a constant fraction, 0.666, of the height at point 1--into a discrete number of layers the lowest of which borders the saltation layer; the thickness of each succeeding layer is a specified multiple of the thickness of the adjacent lower unit. Additional layers are defined above the point 2 level, each of these being of constant thickness. The 0.666 value can be adjusted as an input parameter as can the ratio of layer thicknesses.

Rearranging equation (13) so that the ratio $n_z/n_{z(1)}$ becomes the argument of the equation and considering z(1) as the height of the lowest suspension load layer, drift density proportions are calculated for each layer. These values are summed and the fraction allocated to each layer is determined as a proportion of the sum $n_{z(i)}/n_{z(1)}$ where i represents a specified layer and ranges from one to the total number of layers, T. Specifically,

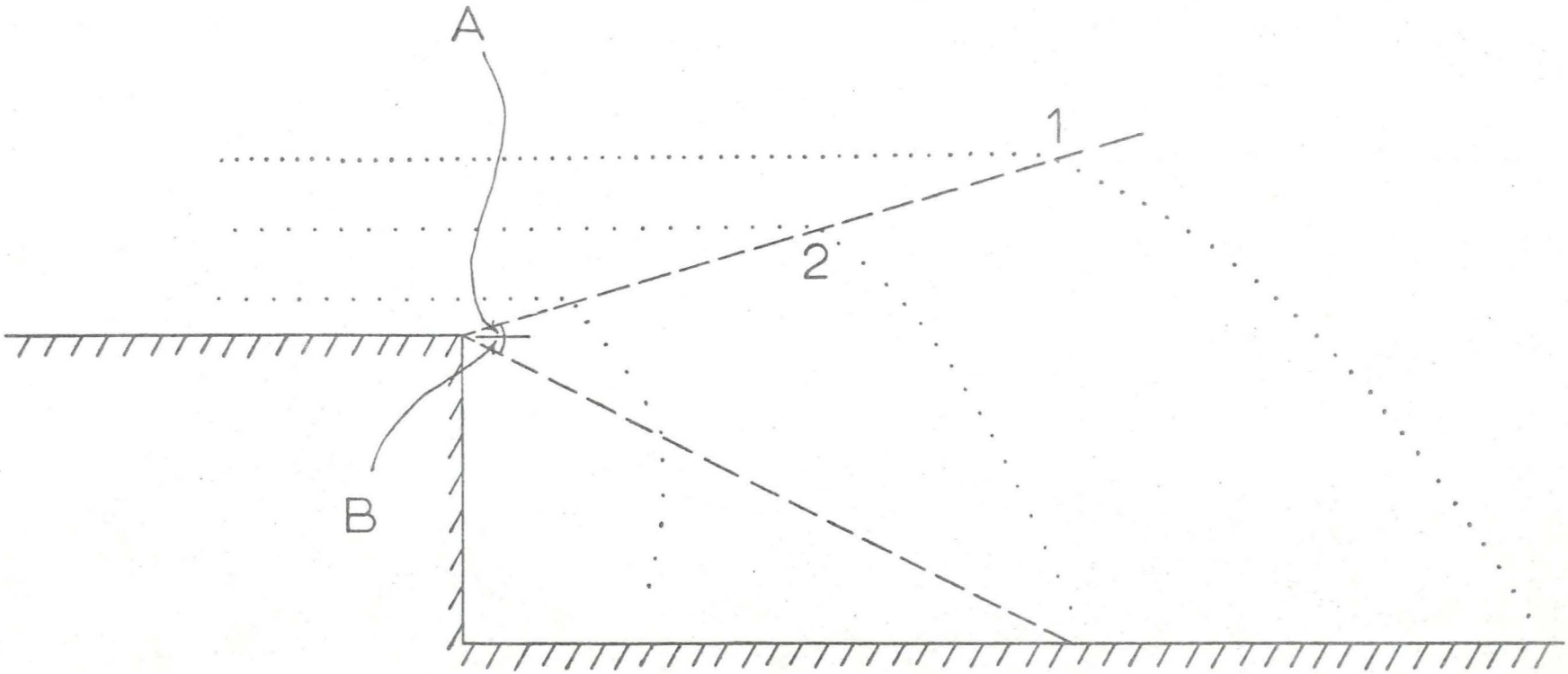

Figure 16. Schematic representation of grain movement at a backward-facing step.

$$q_{sus(i)} = q_{sus} \frac{n_{z(i)}}{\sum_{i=1}^{T} \frac{n_{z(i)}}{n_{z(1)}}} \quad . \qquad (14)$$

Following the work of Bagnold (1941) and Mellor (1965), the speed of suspended particles is assumed to equal that of the wind at the specified height.

ib) Creep transport

The remaining transport load--$q_d - q_{sus}$--moves as saltation and creep. Little is known about creep transport in either the eolian sand or snow environments. The available quantitative data relate to the proportion of the total eolian sand load that is carried in the creep mode. For grains with a mean diameter equal to .25 mm Bagnold (1941) found that creep was typically about one-quarter of the total load. With suspension negligible in the sand situation this amounts to creep being one-third of the saltation transport. With sand between 0.15 and 0.25 mm diameter Chepil (1945) recorded the creep fraction as 0.157 while for grains between 0.25 and 0.83 mm diameter the ratio was 0.249. Creep to saltation load ratios reported from field measurements by Ishihara and Iwagaki (reported by Horiakwa and Shen, 1960) varied between 0.065 and 0.166. Horikawa and Shen (1960) found the ratio to be independent of wind speed and to be approximately 0.20. A final observation, made by Sharp (1964), is that creep probably becomes more significant as the coarser grain fraction increases. In the eolian snow environment creep transport exists (Mellor, 1965) although in an extensive photographic study of saltation at low wind speeds Kobayashi (1972) made no mention of creep.

Two factors become apparent with respect to creep transport. Both the empirical and subjective data suggest that the creep to saltation load ratio increases with increasing grain size. Second, it appears that creep is less evident in the snow movement case than in eolian sand movement. The model initially considers creep load to be a constant fraction, 0.1, of the saltation load; this

value is adjustable through an input parameter. The creep load coefficient is weighted by a grain-size factor so that small grain size reduces the creep transport value. Currently this weighting factor is the square root of the ratio of grain diameter, in mm, to 0.1.

No data is available on the speed of grains in creep transport although intuitively the rate of movement must be a function of wind speed. Since creeping grains move primarily as a result of impact by saltating particles, once this impetus is removed, as is the case beyond the brink of the drift deposit, then grains in creep will have zero velocity. The speed of all grains in creep transport is therefore assumed equal to zero at the entrance to the mixing region. All creep transport is further assumed to occur at the surface so that the z-coordinate at the intersection of the creep load with the mixing zone is (0,0).

(ic) Saltation transport

The final component of the total transport, the saltation load, involves two important factors. It is necessary to determine the average height of the saltation curtain so that the lowest layer of suspension transport can be defined. Further, the mean path length of saltating grains is a significant parameter for determination of the rate of drift infill near the lip of the catchment. Besides the relevant work on saltation of sand particles, the photographic analyses of Kobayashi (1972) and Mellor and Radok's derivation of snow saltation trajectories (Mellor and Radok, 1960) provide the basic information used in the current modelling effort. Radok's application of Owen's theoretical analysis of the mechanics of sand saltation is a third major source (Radok, 1968).

Extensive photography of grains in saltation led Kobayashi (1972) to suggest saltation as the main mode of eolian snow transport in low wind speed regimes (up to 10 mps at 1 m height). His analyses showed that saltating snow grains follow a parabolic path--as opposed to sand saltation which better fits

a rose curve (Bagnold, 1941; Chepil and Milne, 1939). Measurements by the senior author of Kobayashi's photographic data show the angle of grain impact to vary from 8.7 to 12.8 degrees (Kobayashi, 1972). These values compare with values of 10 to 16 degrees found by Bagnold (1941) for saltating sand. Use of horizontal blowing snow traps provided Kobayashi with empirical data on the relationship between wind speed and saltation path length. For horizontal surfaces in which the air is "saturated" with snow particles the mean saltation path length, L_s, is related to wind speed at one meter height, VI, by equation (15),

$$L_s = 0.011\ VI \quad (L_s \text{ in meters, VI in mps up to 10 mps}). \tag{15}$$

For less saturated conditions path lengths increase so that

$$L_u = 0.0285\ VI \tag{16}$$

where L_u refers to the unsaturated saltation path length. In further discussion, Kobayashi relates the saturated condition to a depositional regime. In a mountainous area on upslopes ranging from 16° to 28° saltation path lengths measured 20-30% shorter.

Alternative methods for derivation of saltation path length can be developed from Mellor and Radok's extension of Bagnold's work (Mellor and Radok, 1960). Bagnold (1936, 1941) developed a relationship between the mean saltation path length, L, the final horizontal velocity component of the grain just prior to impact, U_f, the acceleration due to gravity, g, and the initial vertical velocity of the saltating grain, w'. For saltating sand

$$U_f / L = g / w' \quad . \tag{17}$$

Furthermore, w' is a linear function of U_* so that

$$w' = BU_* \tag{18}$$

where B takes the value 0.8 for sand. From the graphic analysis of two saltating snow particle trajectories using Bagnold's method (Bagnold, 1936), Mellor and Radok (1960) altered equation (17) to

$$U_f / L = 0.65\ g / w' \quad . \tag{19}$$

On somewhat arbitrary ground Mellor and Radok equate w' with U_* although in a footnote (Mellor and Radok, 1960, p. 344) suggest that

$$w' = CU_* \tag{20}$$

where C may be as large as 3 or 4. Rearrangement of equation (19) yields

$$L = U_f\ w' / (0.65\ g) \quad . \tag{21}$$

It remains to provide values for U_f and w'.

Bagnold (1941) stated that with a relatively thick layer of saltating sand the horizontal particle speed at impact approaches the wind speed at the high point of the saltation path trajectory and the falling velocity of the particle approaches the fall velocity for particles of the specified grain size. Svasek and Terwindt (1974) concur with this opinion, although they simply may be reiterating Bagnold's statements. When the initial velocity of rise is small the final fall and horizontal velocities are proportionately less than the maximum possible. Owen's theoretical analyses of the saltation phenomenon are relevant here.

From theoretical considerations Owen (1964) found w' to approximate U_* and the mean height of the saltation layer, h, to also be a function of U_* as follows:

$$h = U_*^2 / 2g \quad . \tag{22}$$

A second formula for h has been presented by Iversen (1975) based upon wind-tunnel and theoretical considerations of saltation on the surface of Mars. In this formulation

$$h = \frac{\rho_f U_*^2}{\rho_s g} \quad . \tag{23}$$

Although saltation layer thickness values computed from (22) and (23) may appear low, the few available data suggest that most saltation does occur close to the surface. Rusin (1959) commented that 70 to 80% of all transport occurs at lower than 4 cm height. Similar experiments by Kungurtsev (1956) showed 73 to 91% of drifting snow to occur between zero and 10 cm above the surface.

Owen was further able to specify the wind speed at height h, U_h, as

$$U_h = D' U_* \tag{24}$$

where

$$D' = U_z / U_* - 2.5 \ln(2gz / U_*^2) \quad . \tag{25}$$

Radok (1968) applied Owen's concepts to blowing snow and found reasonable agreement between Owen's predicted values and Budd, Dingle and Radok's empirical data (Budd, Dingle, and Radok, 1966). Thus equating U_h in equation (24) with U_f in equation (19) and considering w' equal to approximately 1.5 U_* solution of (21) is possible.

The angle of saltation grain impact, ϕ, is suggested by Bagnold (1941) to be given approximately by,

$$\phi = \arctan (w / U_f) \quad . \tag{26}$$

A grain size parameter is not included in the Kobayashi treatment and is only of secondary importance in Owen's analysis. Nevertheless, Sharp (1964) commented from field observations that grain impact angle increases with increasing grain size. Since an increase in impact angle probably relates to a decrease in path length a grain size factor should be included. For want of adequate data, L is weighted by a square root factor of the ratio of grain diameter to a suggested mean diameter of 0.1 mm.

Subroutine SALT allows derivation of saltation path length by either the Kobayashi method or the alternative described above. Simple modifications allow change in the values of the various parameters included for determination of impact angle, mean saltation layer thickness, and mean saltation path length.

A final consideration with respect to the saltation load involves the calculation of the intersection of saltating grain flight trajectories with the mixing region boundary. Grains impacting at an angle ϕ to the horizontal meet the mixing region wedge whose upper boundary is determined by angle A (figure 16). It is assumed that all saltating grains of given grain diameter under a specified wind regime impact at the same angle ϕ and that the saltation transport, q_{salt}, is apportioned equally from x = 0 to x = xsalt (figure 17). Between z = 0 and z = zsalt a specified number of layers, ILAY, are constructed, each with 1/ILAY fraction of q_{salt}. These layers are treated similarly to the suspension load layers, as described in the following section.

i) Grain movement through the mixing and eddy zones

Results from the transport mode subroutines, SUSP, SALT, and SLTINT, include information on the location of intersection of grains in suspension, creep, or saltation with the upper boundary of the mixing region, as defined by angle A (figure 16). It is necessary to determine the grain flight paths through the mix-

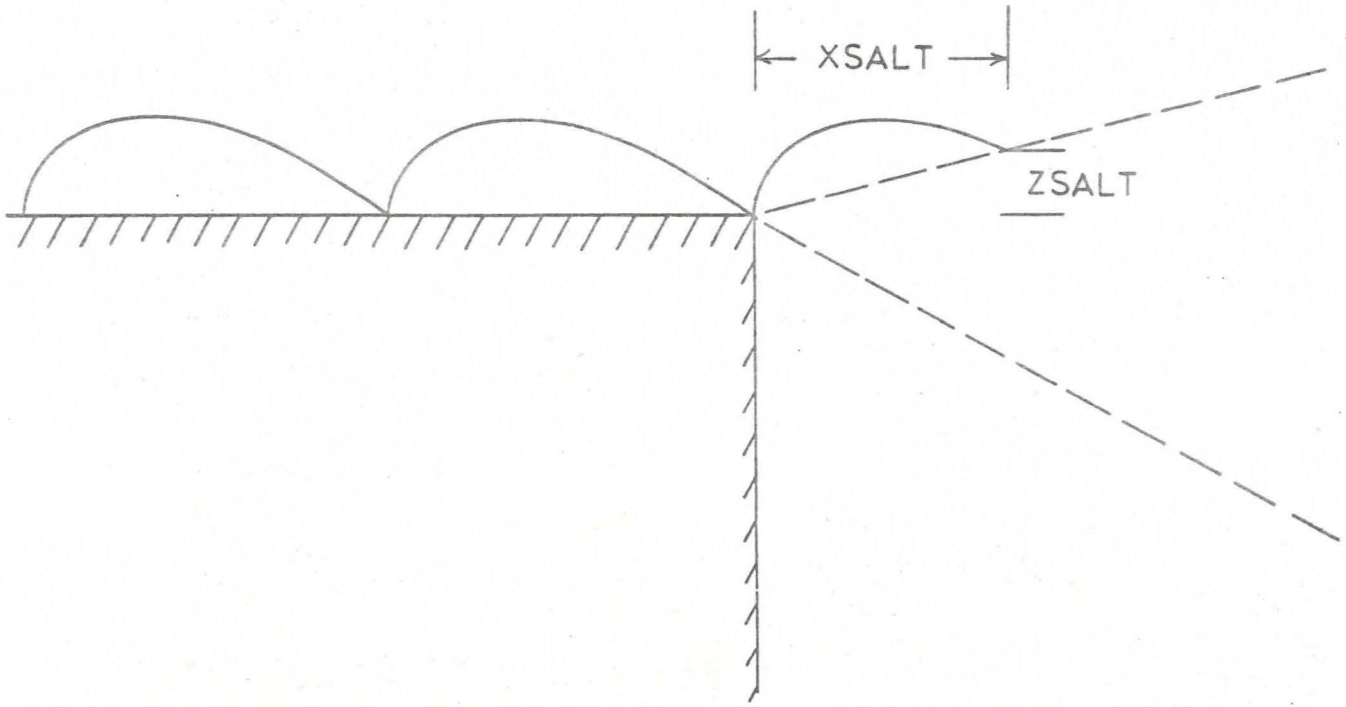

Figure 17. Schematic representation of saltation grain movement at the mixing region boundary.

ing zone until eventual settlement into the drift or transport beyond the eddy zone. In the following discussion the "no slip" condition is assumed (Mellor, 1965) so that grains move at the same velocity as the adjacent air flows.

Given the initial z-coordinate of the intersection of a transport grain layer with the upper mixing region boundary, flight trajectories of particles through the mixing zone are derived from knowledge of the geometric configuration of the mixing region. Essentially two angular measurements are required; these are derived in subroutines CELL and DTEND. The x-value at intersection is easily calculated from knowledge of z_{int}, the z-value of the relevant creep, saltation or suspension layer, and the tangent of angle A. The lower edge of the mixing region is similarly determined given x and the tangent of angle B, which designates the line of zero velocity. The difference between the upper and lower z-values is scaled by a constant, the resulting value, $z_{tot(I)}$, being the width of one layer within the mixing region and considered unit I in the flight trajectory computation. From z_{int}, = z_1, is subtracted the reciprocal of $z_{tot(I)}$, yielding the next z-value, z_2 for consideration. Utilizing either the Albertson or Naib mixing region velocity distributions, a horizontal component U_2, equated to the wind speed of the particle, is calculated for location z_2. Considering further the vertical component to equal w and to be constant through the mixing region, manipulation of simple trigonometric relationships yields a value for x_2 via the following equation:

$$x_{i+1} = x_i + \frac{(z_i - z_{i+1})\ (U_{i+1})}{w} \qquad (27)$$

where i specifies the layer under consideration. At each newly-defined x, the mixing region boundaries are again determined; the difference between top and bottom border values is divided by the constant $z_{tot(i)}$ with the resulting value subtracted from z_i to yield z_{i+1}. The iteration continues until either x_{i+1} is

greater than the anticipated leeward extent of the drift--as calculated in subroutine CTOP--or the blowing snow parcel enters the eddy zone and contributes to the drift accumulation.

The foregoing analysis implicitly assumes the approach angle of the wind to be horizontal. In nature, this condition is seldom fulfilled since, even if the ground surface upwind of the trap lip is horizontal, infilling by snow takes a generally downslope form (approximately along angle B in figure 16). This then feeds back to change the approach angle of the wind to the lip of the trap which migrates downwind as infilling occurs. The resulting downslope component becomes more pronounced, particularly if the ground slopes downward to windward. The model accounts for this change in the axial orientation of the approaching flow by defining the mean ground/snow slope over a specific input distance upwind. Grain path computations are calculated with respect to this axis.

Depositional Mechanisms

Prior to complete specification of the snowdrift, the final major task involves consideration of the depositional processes by which parcels of blowing snow, moving through the mixing and eddy zones, settle into final resting locations. Subroutines CELL and CTOP define a set of cells which, when considered in totality, comprise the spatial configuration of the snowdrift. It is necessary to determine the spatial configuration of the cells, including their lateral and upper and lower extents, as well as to develop a set of rules providing for allocation of the blowing snow parcels into specific cells.

The accounting cells are rectangular in shape and are bounded at the base by the ground topography as defined in subroutines TOPO and TOPIN. The width or lateral extent of all cells is equal and can be specified by an input parameter. If not user-defined, cell width is taken as 0.5 meters. Currently the relevant arrays are allocated 200 storage locations by the model. If the program deter-

mines from the specified cell width value that more than 200 cells will be required, the cell width is redefined to provide for a maximum of 200 cells.

Determination of the actual configuration of the upper surface of the drift is an important aspect of the entire modelling effort. This surface is defined with respect to the tractive force required for grain movement.

Theoretical and empirical consideration show grain movement to be a function of the shear stress imparted by the fluid onto the grains in such a way that a boundary stress value exists below which movement will not occur (e.g., Bagnold, 1941; Owen, 1964; Radok, 1968). Although stress values can be indexed readily by flow velocity values, complete specification of the relationship between velocity and initiation of grain deposition is not possible since it depends upon secondary factors like grain shape and angularity (Williams, 1964). Furthermore most of the empirical information available involves observation of the flow speed at which movement is initiated rather than at which deposition starts. This is unfortunate in that factors such as surface hardness (Kotlyakov, 1961) complicate the determination of such "threshold" velocity values. The available data for threshold entrainment values, U_{+}, center on values approximating 3 mps and do not vary over an inordinate range (Table 1). For this reason the model assumes U_{+} to be the criterion differentiating between areas of deposition and erosion.

For a given x-value the cell top is specified as the z-location within the mixing zone at which U, as determined from the mixing zone velocity distribution, equals U_{+}. The drift surface is thus specified by the locus of points within the mixing region--or at the border of the mixing and eddy zones if $U_{+} = 0$--which represent the spatial location at which $U = U_{+}$. If U_{+} is assigned a value greater than zero then the potential drift surface will extend past the flow reattachment point and into the zone of boundary layer redevelopment. The location of the final cell is arbitrarily defined at the point where the cell height is less than

Table I. Eolian snow grain entrainment velocities.*

Reference	Height (m)	Comments	U_t (mps)
Croce, 1943, discussed in Schneider, 1962	10	Depends upon surface hardness	7
Kungurtsev, 1956	2	Velocity below which wind cannot transfer snow	2.4
Rusin, 1959	5	Hourly mean velocity from Antarctic measurements	6
Kotlyakov, 1961	10	Depends upon surface hardness	5
Dyunin and Komarov, 1963	1		2.71
Mellor, 1965	10	Depends upon snow hardness	3
Dyunin, 1967	1	From $q = 5(V1/3 - 1)^3$	3
Radok, 1968	10	Derived from Owen's theoretical analysis	1.8

*If a range of values is given the lowest is quoted here under the assumption that the onset of deposition occurs under the lowest energy conditions.

0.1 units high.

The effect of the changing axial orientation of the wind with increasing infill is included in the model. The effect of including this factor is to shorten the drift if the ground approach is downslope and to lengthen the drift if the ground approach is upslope.

As the snow particles move through the mixing region each parcel of grains eventually (1) crosses the separation streamline, where dU/dz = 0, (2) alights in the redeveloping boundary layer zone, or (3) passes beyond the catchment. In the latter case the amount of such "blowpast" is recorded and these particles may be deposited downwind in another snowdrift catchment. If the parcel lands in the redeveloping boundary layer zone it will be deposited in the accounting cell with the appropriate x-location. Alternatively, when the parcel crosses the $U = U_t$ boundary it will move into an accounting cell. If the Albertson method is utilized, the parcell will be deposited in that cell. If, however, reverse flow is determined via the Naib procedure, the parcel continues to move backward in the eddy region. In the latter case it eventually comes to rest in another accounting cell, depending upon the respective magnitudes of the particle fall velocity and the reverse flow speed. The model is constructed so that a parcel entering a filled cell is allocated to the next leeward cell which is not filled.

The areal extent occupied by a blowing snow parcel within an accounting cell is a function of grain packing. Subroutine PACK accepts as input either the final snowdrift deposit density, void ratio, or porosity. From any one of these, the other two are calculated from the following relationships (Bader, 1962; Mellor, 1964):

$$P = (\rho_i - \rho_d) / \rho_i \ , \tag{28}$$

$$e = (\rho_i - \rho_d) / \rho_d \ , \tag{29}$$

and $$\rho_d = \rho_i (1 - P) , \quad (30)$$

or $$\rho_d = \rho_i / (1 + e) \quad (31)$$

where P is deposit porosity, e deposit void ratio, ρ_i ice density, and ρ_d deposit density. Ice density is assumed equal to 0.917 g cm^{-3} unless otherwise specified through an input parameter. Prior to modification by metamorphic processes, the maximum attainable density of deposited snow particles is probably less than 0.5 g cm^{-3}. The maximum recorded density after extensive laboratory piston tapping and jarring of particles is 0.58 g cm^{-3} (Anderson and Benson, 1963).

General procedural characteristics of the model

Output from the computer simulation model consists of graphical and printed information. Microfilm plots of drift accumulation at the completion of each infill event show the sequence of intermediate stages of infill. Microfilm rather than line printer plots are included because of the high precision possible with the microfilm grid network and the relative ease with which microfilm plotting routines can be devised. If required, line printer plot routines can be developed. The printed output specifies 1) the original input data; 2) any modifications of the input data; 3) output of various parameters, such as frictional velocity, that drive the computations; and 4) the actual description of the drift infill sequence. With specific regard to 4), several features are important. These are a) the accounting cell dimensions and ground topography; b) snow heights per cell; c) total proportion of each cell filled; d) proportion of each cell occupied by each grain size fraction; e) blowpast per event; and f) cross-sectional area occupied by snow. Output 4d) allows investigation of the modal downwind carry distance of each grain size fraction.

Utilization of the model will be enhanced if several procedural characteris-

tics are mentioned.

Each grain size fraction is treated independently and all computations are performed on one size fraction at a time. This may bias the facies output in that under certain circumstances, where mass transport is great or the duration of an event is long, the windward-most cells may be filled by one grain size fraction to an unrepresentative extent simply because that size fraction was the first to be considered. Second, the location of the separation point moves downwind as the catchment fills. This alters the proportion of incoming snow retained by the catchment by effectively reducing the space available for infill. As such, snow originating at steadily lower levels bypasses the trap.

FIELD PROCEDURES

Field studies were conducted to verify the drift accumulation model and to provide auxiliary information on other aspects of snowdrift development. Input parameters to the model are primarily meteorological and topographic in nature. Measurements of relevant environmental variables, specifically wind speed and direction, and blowing snow particle size and frequency were made for use as input to the model. Topographic surveys were made at three sites during the summers of 1973 and 1974 and drift accumulation at these sites was recorded during the winters of 1973-74 and 1974-75.

Field Area

There are several requirements for field sites in this study. They should be representative of alpine snowdrift situations and so need an adequate vertical relief (approximately two to three meters) to ensure drift accumulation. A variety of catchment situations including single and multiple in-line accumulation areas would also be useful.

Field sites must be accessible for frequent observation under extreme winter conditions and, in practice this becomes a limiting criteria. In this regard, the Institute of Arctic and Alpine Research's Mountain Research Station at the 2900 m level in the Indian Peaks region of the Colorado Front Range provides an excellent base of operations. From this facility alpine sites on Niwot Ridge, the most prominent alpine interfluve in the Indian Peaks region, are accessible on a year-round basis. An emergency shelter--hereafter designated "T-van"--maintained by INSTAAR and located at 3490 m elevation at timberline was selected as the field base (figure 18).

T-van is located approximately midway between two stations for which long-term meteorological information is available. Precipitation, temperature, and wind

Figure 18. Topographic map of general research area

The map is a section of the western portion of the Ward quadrangle of the USGS 7.5 Minute Series.

Approximate boundaries of the map are:

Northern edge	40° 4' North
Eastern edge	105° 33' West
Southern edge	40° 2' 30" North
Western edge	105° 37' 30" West

Legend:
T = T-van
M = Meteorological mast
1 = Slope site
2 = Tank trap site
3 = Krum site

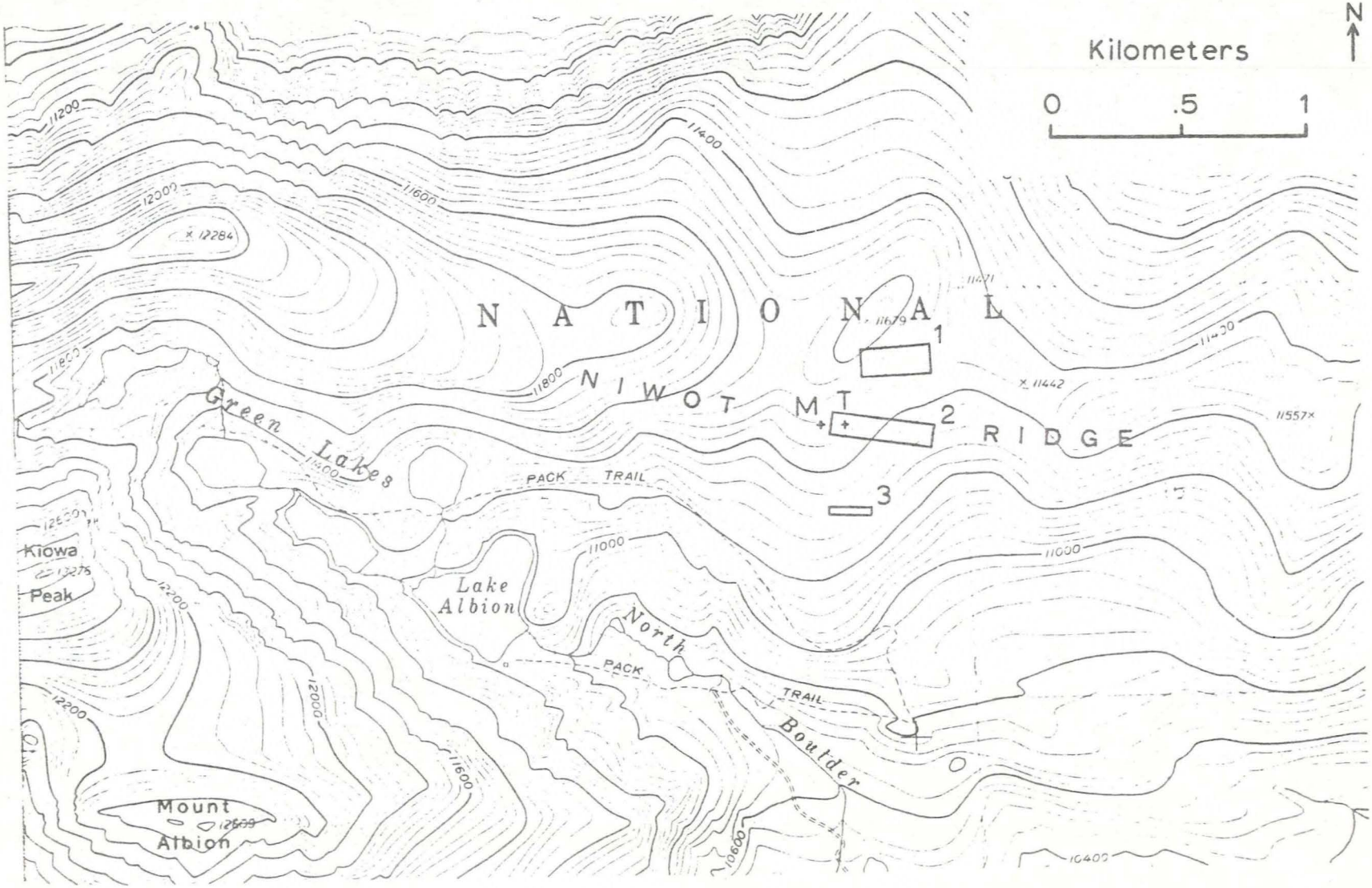
Kilometers
0 .5 1
N
NATIONAL
NIWOT MT
RIDGE
1
2
3
Green Lakes
PACK TRAIL
Lake Albion
North
PACK
TRAIL
Boulder
Kiowa
Peak
Mount
Albion
11200
11400
11600
11800
12000
12200
12284
11442
11557
11000
10600
10400

speed data have been kept since 1952 at the "Niwot Ridge" station, an alpine site located at the 3750 m level ca. four kilometers west of T-van on Niwot Ridge and "Como" station (3050 m) ca. five km east of T-van in the upper montane forest. Temperature and precipitation records from these two locations, and from a third station with a shorter period of record located less than one km west of T-van, were used in the current investigation.

The climatology of the area has been discussed by Barry (1972, 1973). Of particular interest to this project are the mean wind speed, precipitation and temperature characteristics of the winter season at the alpine Niwot Ridge station.

From 1952 to 1970 mean monthly wind speeds were greater than 10 mps--at ca. two m height--for all months between November and February inclusive. Data collected over the 1965-1970 period showed October and March also to have mean speeds greater than 10 mps with the January mean for this period equal to 13.9 mps. Although little quantitative wind direction information is available, the central part of Niwot Ridge is subjected "to the direct influence of westerly winds modified only slightly by the Continental Divide" (LeDrew, 1974). This refers to the vicinity of the field sites where drifting snow was studied.

The snow accumulation period at the Niwot Ridge station extends from mid- or late-October to mid-May. Mean monthly minimum temperatures are below 0°C from October through May with mean monthly maximums below the freezing point from November to April. Relatively low wind speeds in May and the presence of moist spring snow limit significant blowing snow events to the 6.5 month period from mid-October to the end of April.

Although precipitation gages in wind-swept locations are notorious for their inaccuracy (e.g., Larson, 1971; Rechard, 1975) the installation of a circular snow fence shield around the Niwot Ridge precipitation gage in 1964 has allowed reasonable precipitation totals to be estimated for the period since then (Barry, 1973).

The mean annual precipitation at the Niwot Ridge station is 102 cm water equivalent of which ca. 65% falls between mid-October and April 30. Since Niwot Ridge has an area of ca. 7.85 km^2 (USGS 7.5 Minute Series (Topographic) Ward quadrangle, 1954), the equivalent of ca. 4.1×10^7 cubic meters of water are susceptible to annual relocation by the wind.

Site Characteristics

On Niwot Ridge, local relief is the result of the development of periglacial terraces and lobes on south and east-facing slopes. Benedict (1970, p. 171) has described "turf-banked terraces" as "bench-like accumulations of moving soil that lack conspicuous sorting." These forms range up to four m in height at the riser, over 500 m long, and over 90 m wide (Benedict, 1970) and often form a stair-step configuration moving downslope. Depending upon aspect and windward tread orientation, snowdrifts form immediately leeward of the terrace lobes.

Three study sites were selected within ten minutes walking time of T-van (figure 18). (1) Site 1, "Slope" site, is located on the leeward slope of one of the major topographic high points on Niwot Ridge and includes five in-line snow accumulation troughs. (2) The "Tank Trap", site 2, is a single topographic catchment which usually retains snow until mid-August. (3) The third locality, "Krum" site, differs from the first two in that krumholtz vegetation located at the top of the terrace riser provides additional topographic relief. Other krumholtz islands cover ca. 40% of the ground for 250 m windward of Krum site. All three sites are similar in having a downslope approach from windward into the drift accumulation area.

Drift Documentation

The basic procedure for evaluating the drift accumulation model involves the comparison of two compatible data sets, one derived from field observations and the second from the model. For this purpose a ground topographic base profile must be

constructed upon which snow accumulation may be simulated.

An extensive theodolite survey of the three sites was made in July/August, 1973, and expanded during July, 1974, to provide ground control. Due to the high uni-directionality of snow-bearing winds on Niwot Ridge, it was decided that profile lines constructed parallel to the dominant wind direction would provide sufficient topographic control. Six lines--three at Slope site, two at the Tank Trap, and one at Krum--were delineated by conspicuous orange wooden stakes. Orientation of the lines was determined with reference to that of adjacent krumholtz tree islands. It was assumed that the direction of the long-term prevailing wind would be represented in the molding of the krumholtz as suggested by Koerner (1969). To compensate for errors in defining the prevailing wind direction, additional lines were surveyed at 10° offsets to the main lines, providing topographic control over a 20° directional range (figure 10). Figure 19 shows the cross-sectional profiles for the six main lines. At all three sites, an area 20 m in width on each side of each line was also surveyed to provide additional information on possible local topographic control of airflow direction.

During the 1973-74 and 1974-75 winter seasons, extensive monitoring of snowdrift accumulation was undertaken with the objective of delineating the location, depth, and spatial extent of accumulating drifts. Accumulation stakes, 1.8 m in length and marked at 10-cm intervals, were positioned 3 m apart on the central part of four of the six lines to allow observation of snow depths directly during the initial accumulation period. Eventual burial of the accumulation stakes forced a shift to abney level survey or probe measurements for snow depth documentation.

During the first winter abney level surveys were the primary tools for data acquisition. This method involved measurement of snow surface slope with respect to known control points, the orange location stakes. Typically a field assistant was employed so that two angular measures, in the up- and down-slope directions,

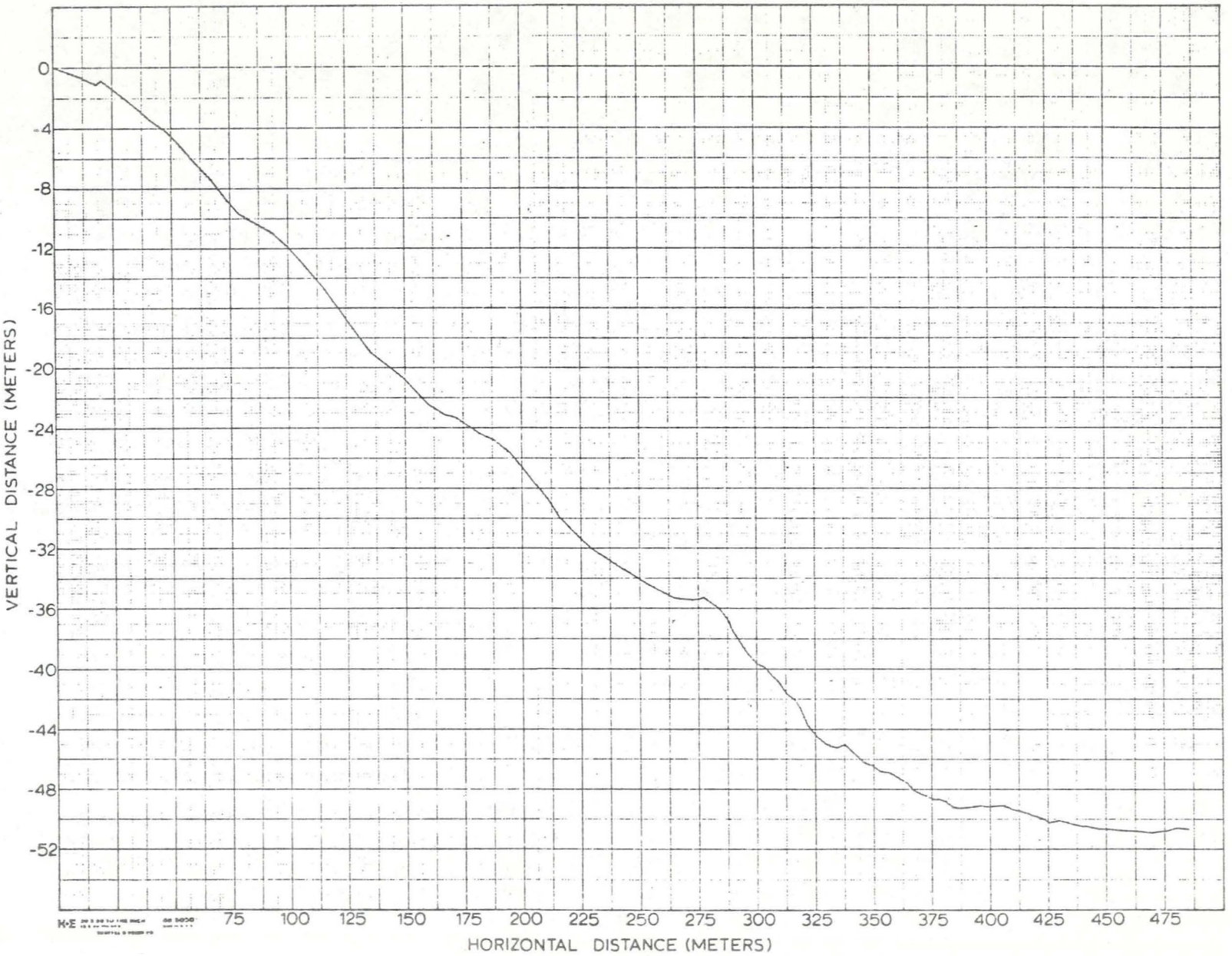

Figure 19a. Cross-sectional profile along ground surface at Tank Trap site, North line.

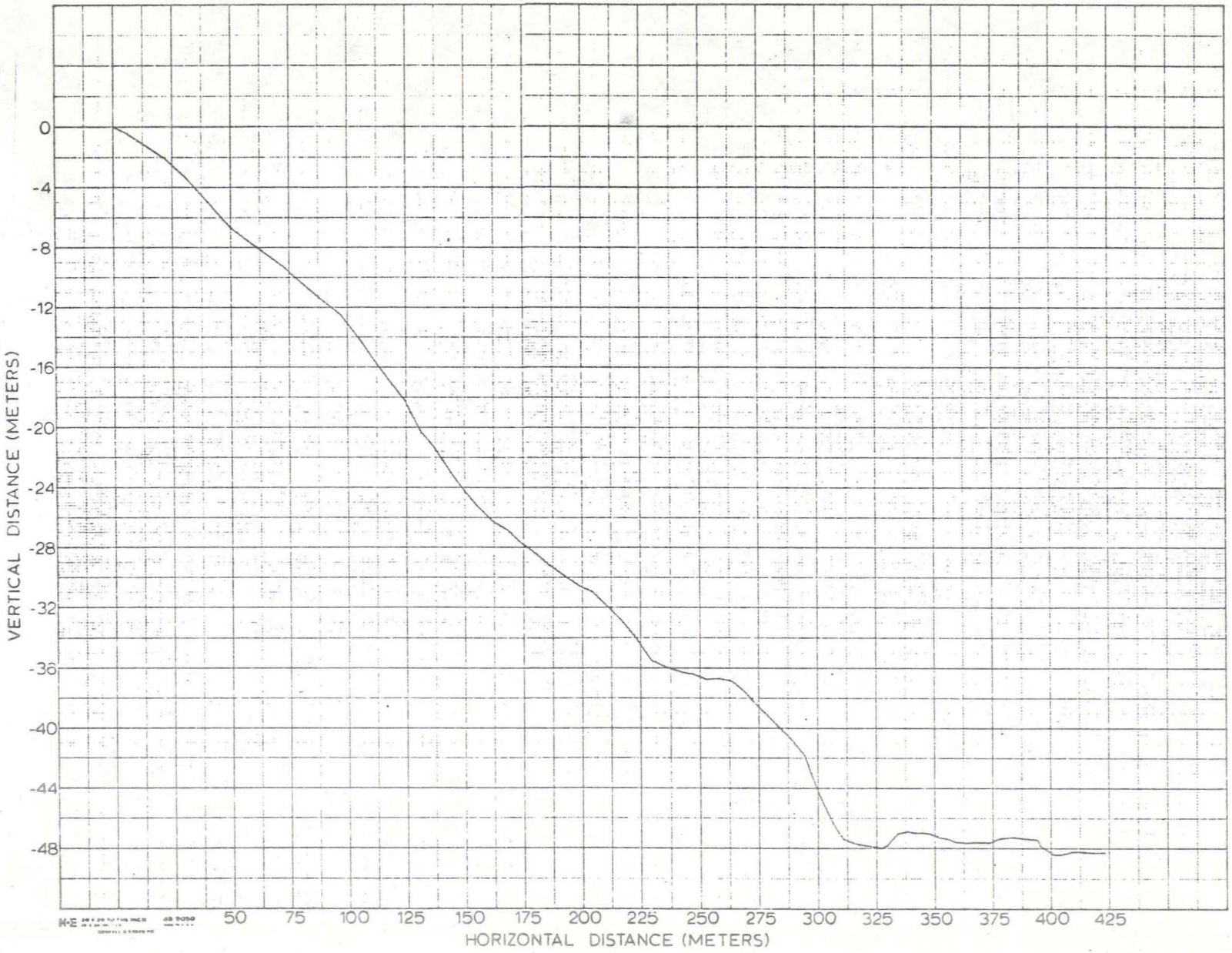

Figure 19b. Cross-sectional profile along ground surface at Tank Trap site, South line.

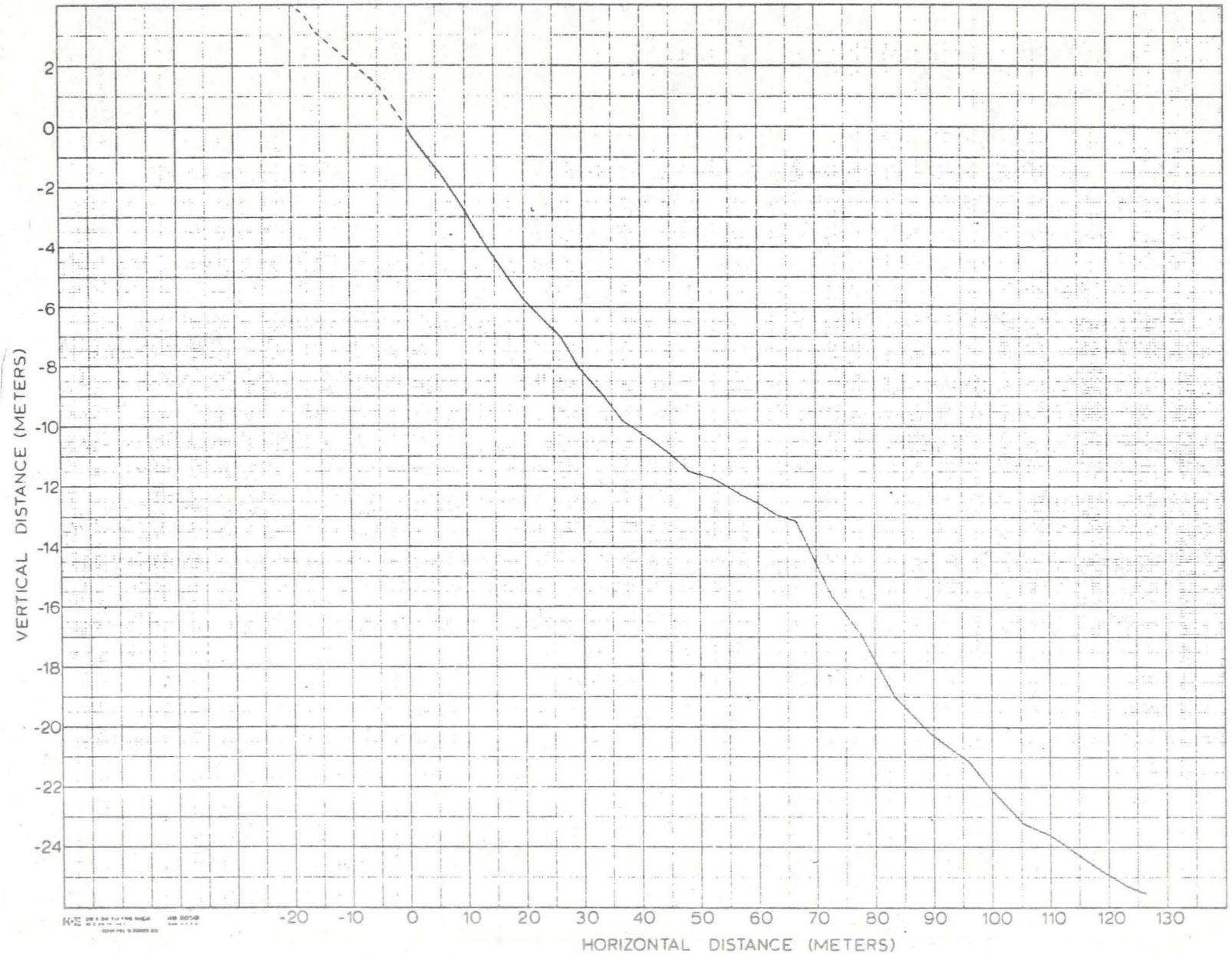

Figure 19c. Cross-sectional profile along ground surface at Krum site.

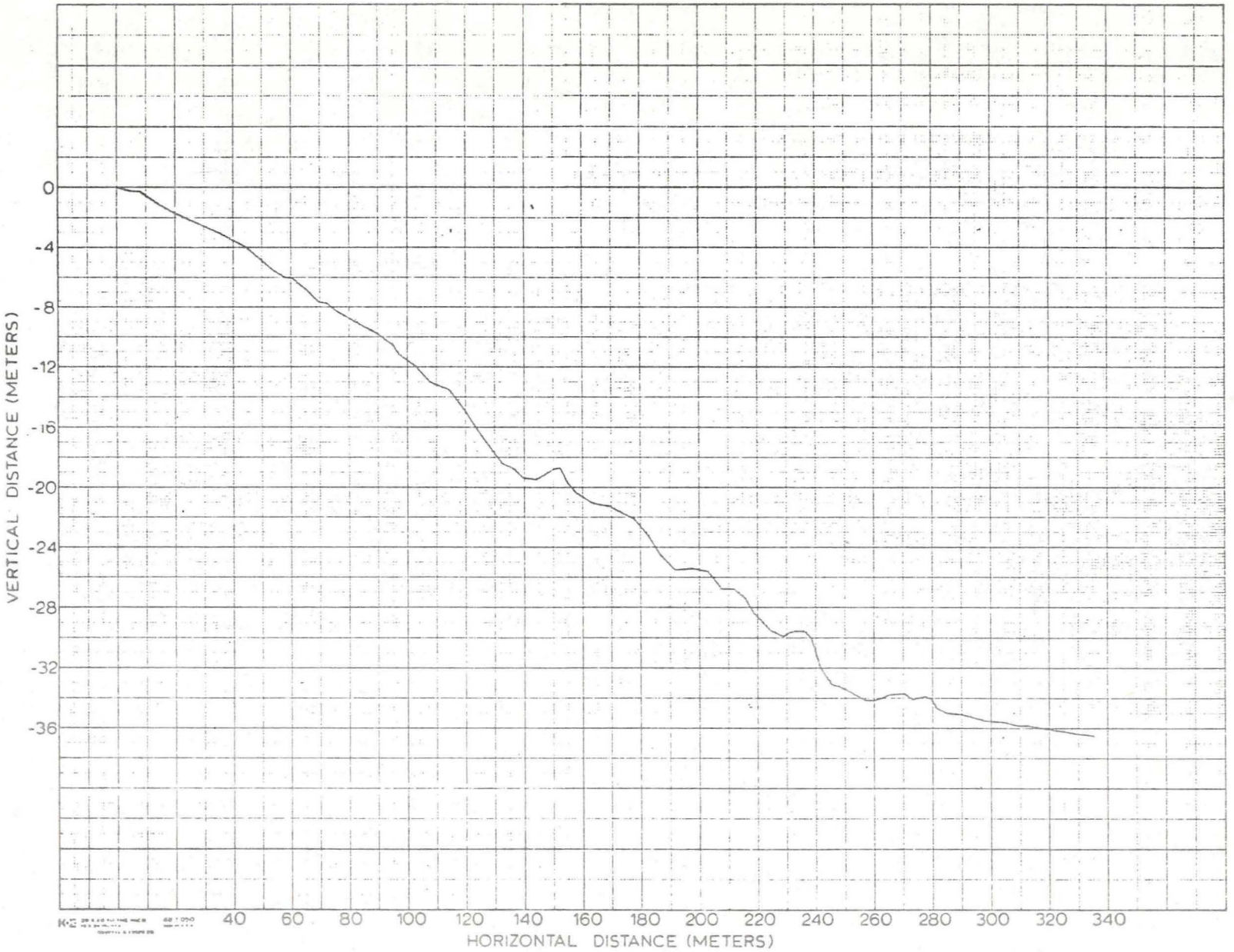

Figure 19d. Cross-sectional profile along ground surface at Slope site, South line.

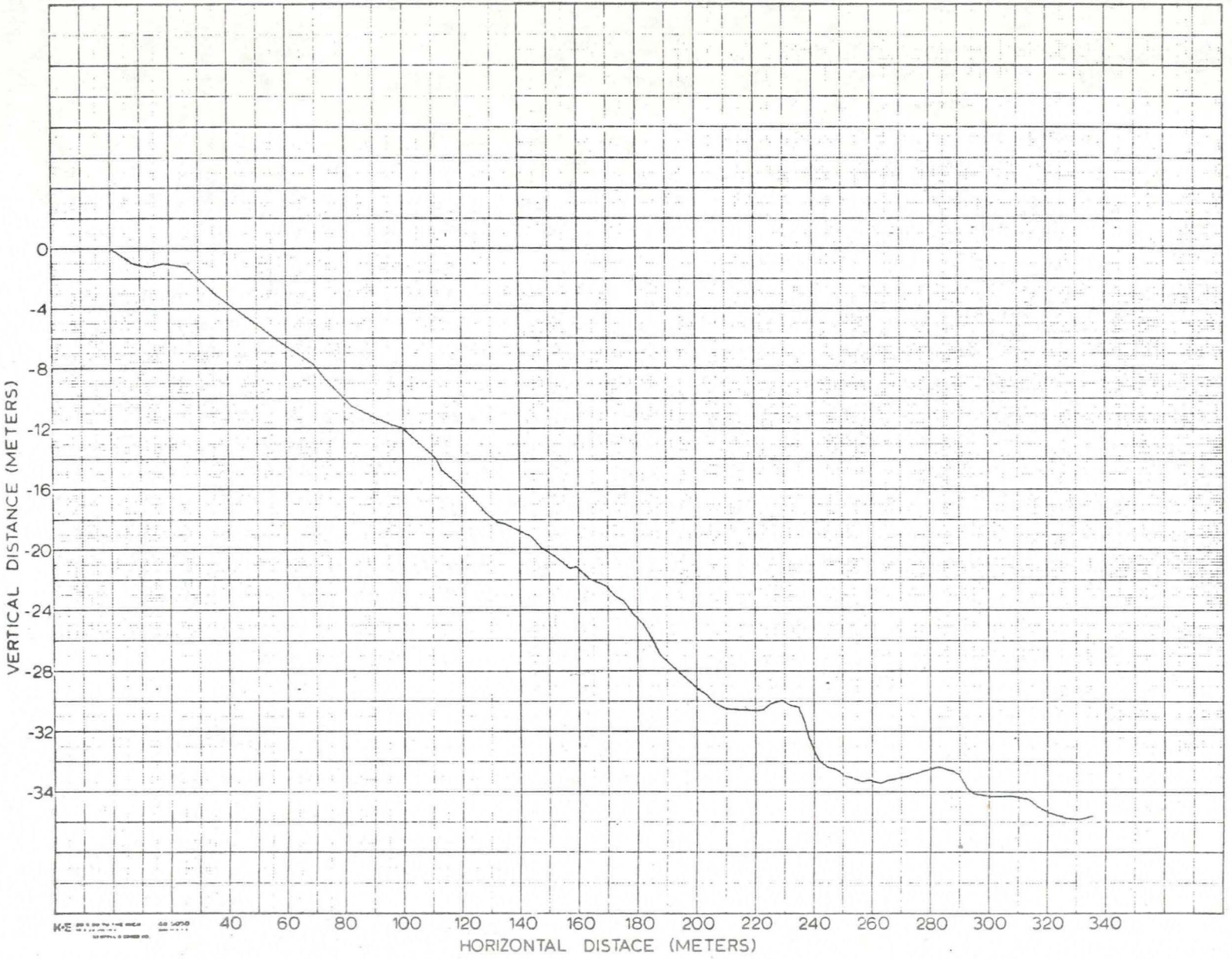

Figure 19e. Cross-sectional profile along ground surface at Slope site, Center line.

Figure 19f. Cross-sectional profile along ground surface at Slope site, North line.

were recorded over a distance of 20 m. Sequential movement upslope followed the initial measurement until the entire drift was surveyed. It became evident towards the end of the first winter season that accumulated errors in each survey made this procedure unsuitable and so it was replaced by probe measurements for the last quarter of the 1973-74 season and the entire 1974-75 winter.

Use of aluminum probes, etched at one cm intervals and coupled into three to five m lengths, allowed one person to make 350 snow depth measurements on the average day. Location stakes again controlled the profiles which were probed on an interval of three to five m. Until April when ice lense development caused extreme difficulty in reaching the ground, this technique provided excellent results.[1] During April and May, probing was still possible although the measurement interval was made 10 to 15 m where deep snow was encountered. The practical limit to the probe length was five m due to the unwieldy--and therefore time-consuming--nature of a longer probe. Snow depths greater than this forced deletion of the central portion of the main Tank Trap line for the last half of the second winter accumulation period. For interpretive purposes the snow surface was assumed to follow a straight line over the unprobed distance. Visual observations suggested this to be an appropriate assumption although a slight upward concavity may have existed.

The time interval between drift surveys varied from two to twelve days and averaged twice per week. An initial goal of the investigation was to document changes in drift surface configuration through time. Observations by other workers (e.g., R.A. Schmidt, 1974, oral comm.) suggested that during the initial phases of drift accumulation infill proceeded by addition of semi-vertical-walled wedges

---

[1] Although an absolute measure of precision does not exist since the ground surface was snow-covered, replicated probing over a small area yielded depth values within two to five cm. The total measured horizontal distance between control points was usually within .5 m of that recorded during the summery survey.

appearing similar to incipient cornices. This early phase was followed by layered infill toward the lee end of the drift. Since the model predicted a somewhat similar infill sequence, documentation of such a sequence was of particular concern. For this reason extensive drift documentation was undertaken during the first two months of the season--mid-October to mid-December--followed by a more relaxed observation schedule after the New Year. Figures 20 and 21 illustrate the infill pattern at the two largest catchments.

Meteorological Observations

Primary meteorological variables input to the drift accumulation model concern 1) definition of the wind regime evident during each blowing snow event; 2) the duration and magnitude of each event; and 3) parameters of the blowing snow itself.

Characterization of the airflow during blowing snow events could best be determined by on-site installation of wind speed and direction sensors. A 9-meter mast was erected ca. 100 m west of T-van on a local high point. A U.S. Weather Bureau standard continuous-recording F420-C three-cup anemometer and vane system (U.S. Forest Service, 1973) was erected with the sensor cups/vane located at 8.75 m height. These instruments were in continuous operation between November 2, 1973 and May 1, 1974 and October 10, 1974 and May 12, 1975. Recorders were located in a propane-heated instrument box inside T-van to minimize breaks in the data record. Additional wind speed information was obtained between mid-January and the end of March, 1975, from a second sensor positioned at .95 m height on the mast. The two speed records allowed calculation of vertical wind speed gradients. The strip chart records were transcribed to x-y coordinates by a Bendix Datagrid Digitizer and recorded on magnetic tape. Up to 5000 points were recorded per strip chart hour from which minute values were interpolated. Mean hourly wind speed values were then determined using a modified form of a computer program developed by D. Joseph of the National Center for Atmospheric Research.

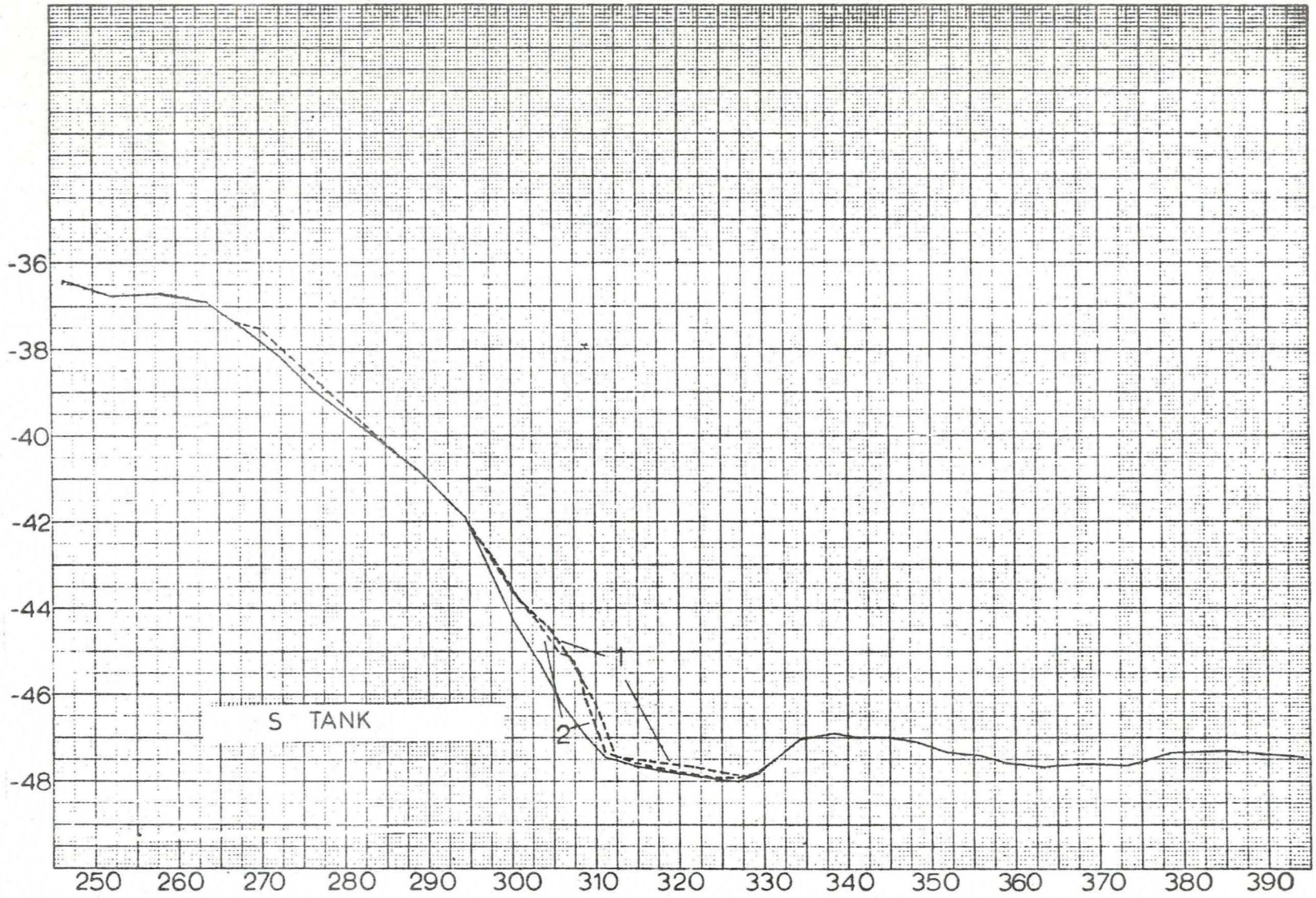

Figure 20a. Cross-sectional profiles of snowdrift accumulation at Tank Trap site, South line. Dotted line is snow surface. Vertical and horizontal scales are in meters and refer to figure 19b. 1: 10/15/74 0950 MST 2: 10/15/74 1500 MST.

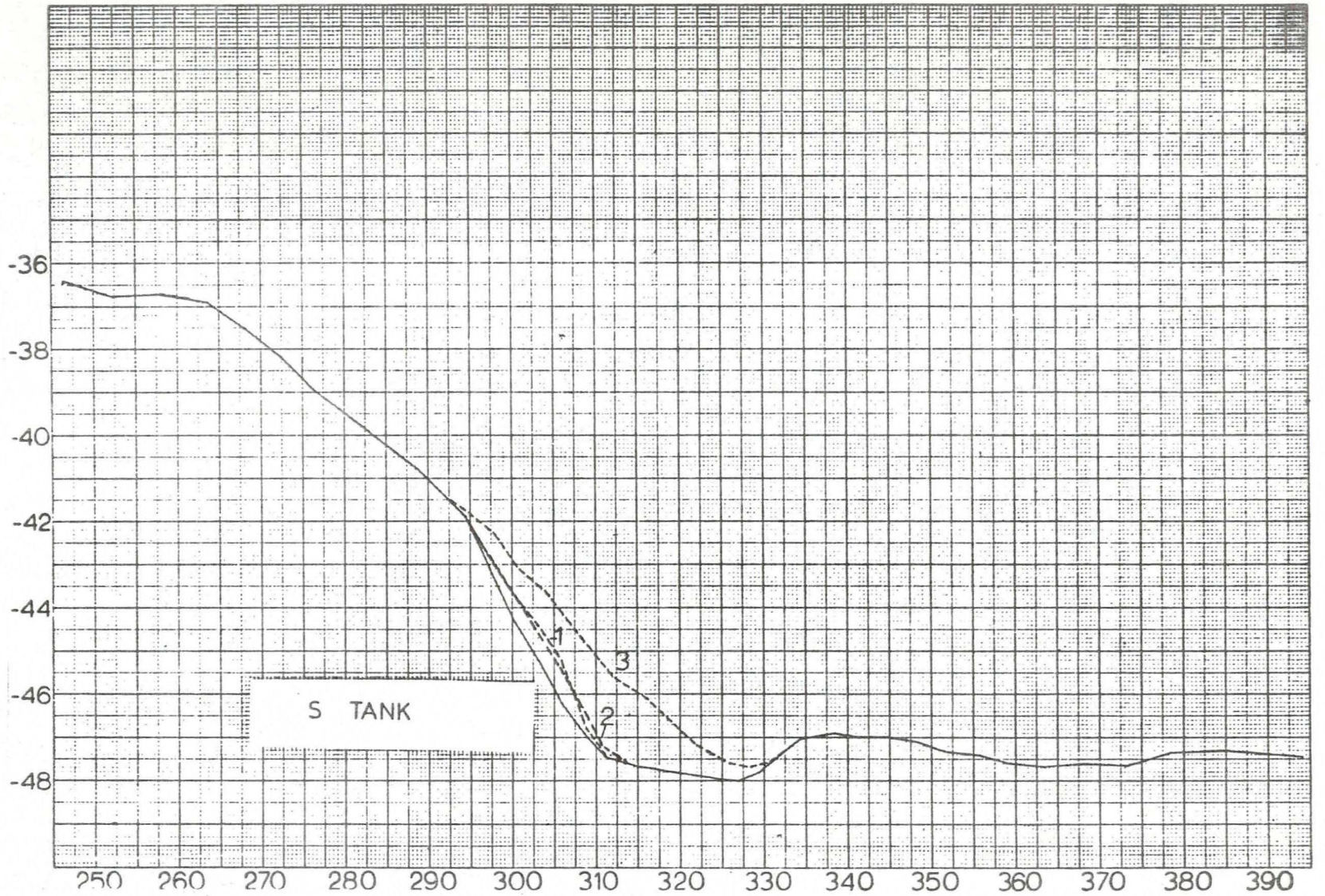

Figure 20b. Cross-sectional profiles of snowdrift accumulation at Tank Trap site, South line.
1: 10/16/74 2: 10/28/74 3: 11/1/74.

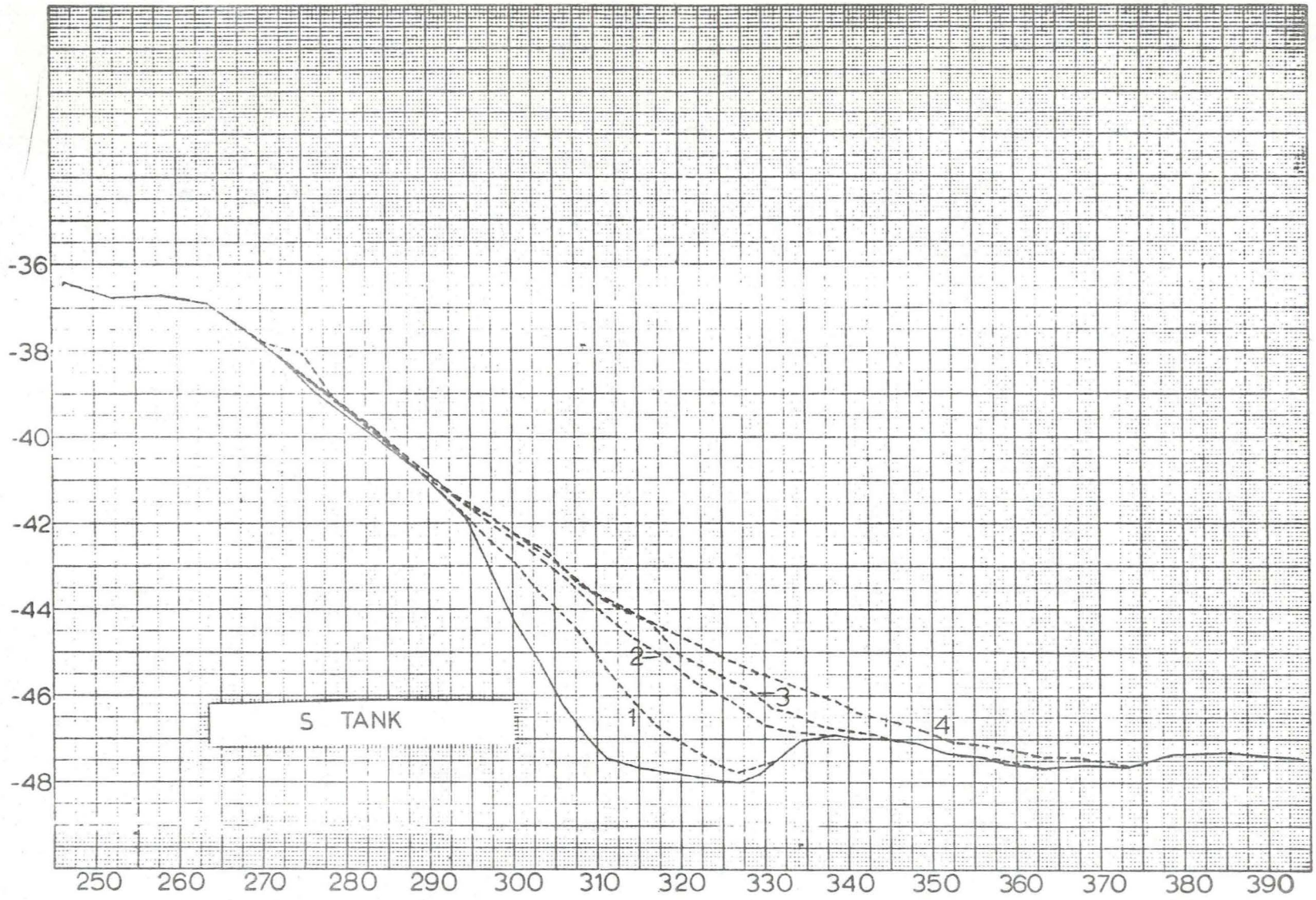

Figure 20c. Cross-sectional profiles of snowdrift accumulation at Tank Trap site, South line.
1: 11/5/74 2: 11/11/74 3: 11/13/74 4: 11/27/74.

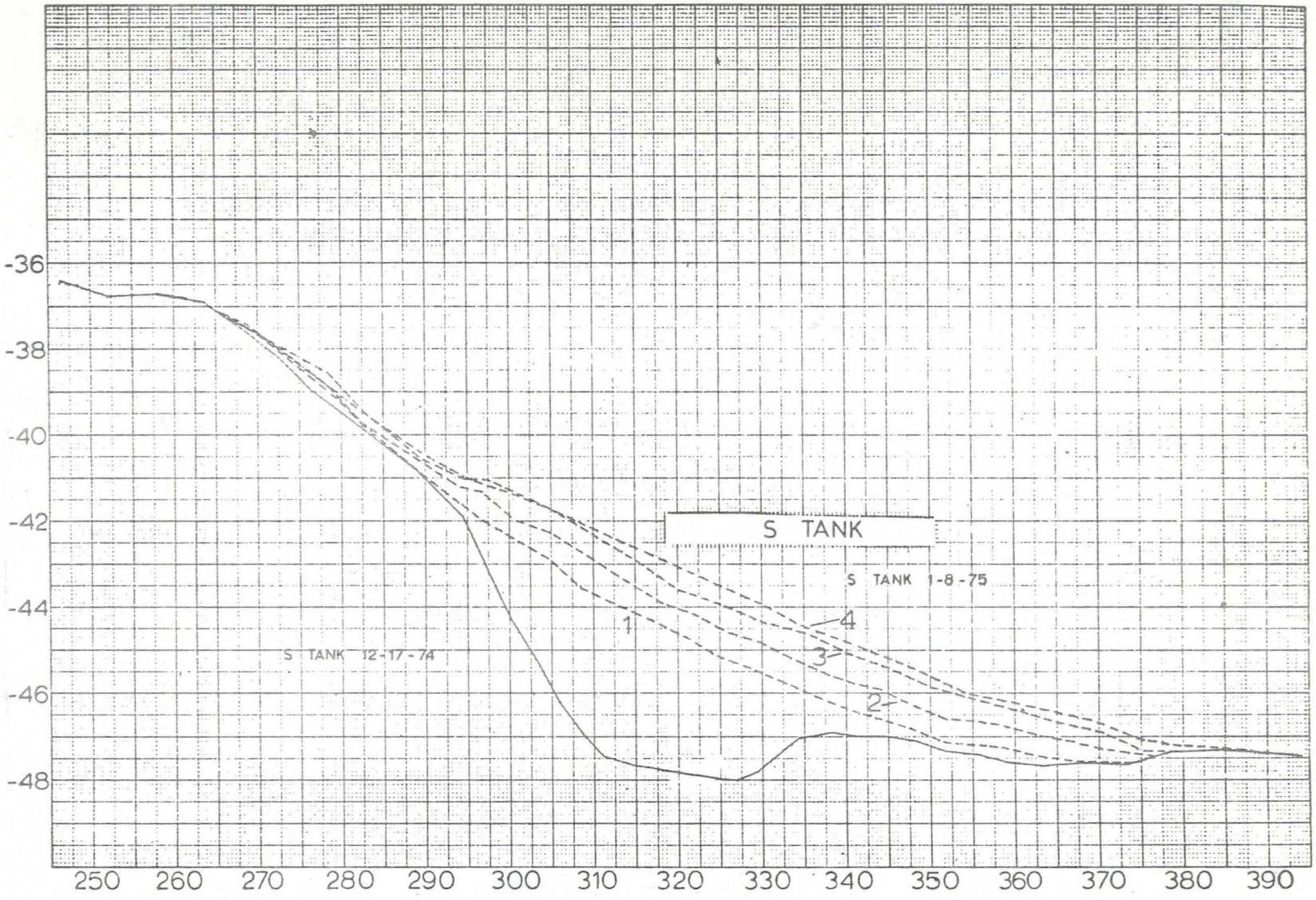

Figure 20d. Cross-sectional profiles of snowdrift accumulation at Tank Trap site, South line.
1: 12/2/74 2: 12/17/74 3: 1/2/75 4: 1/8/75.

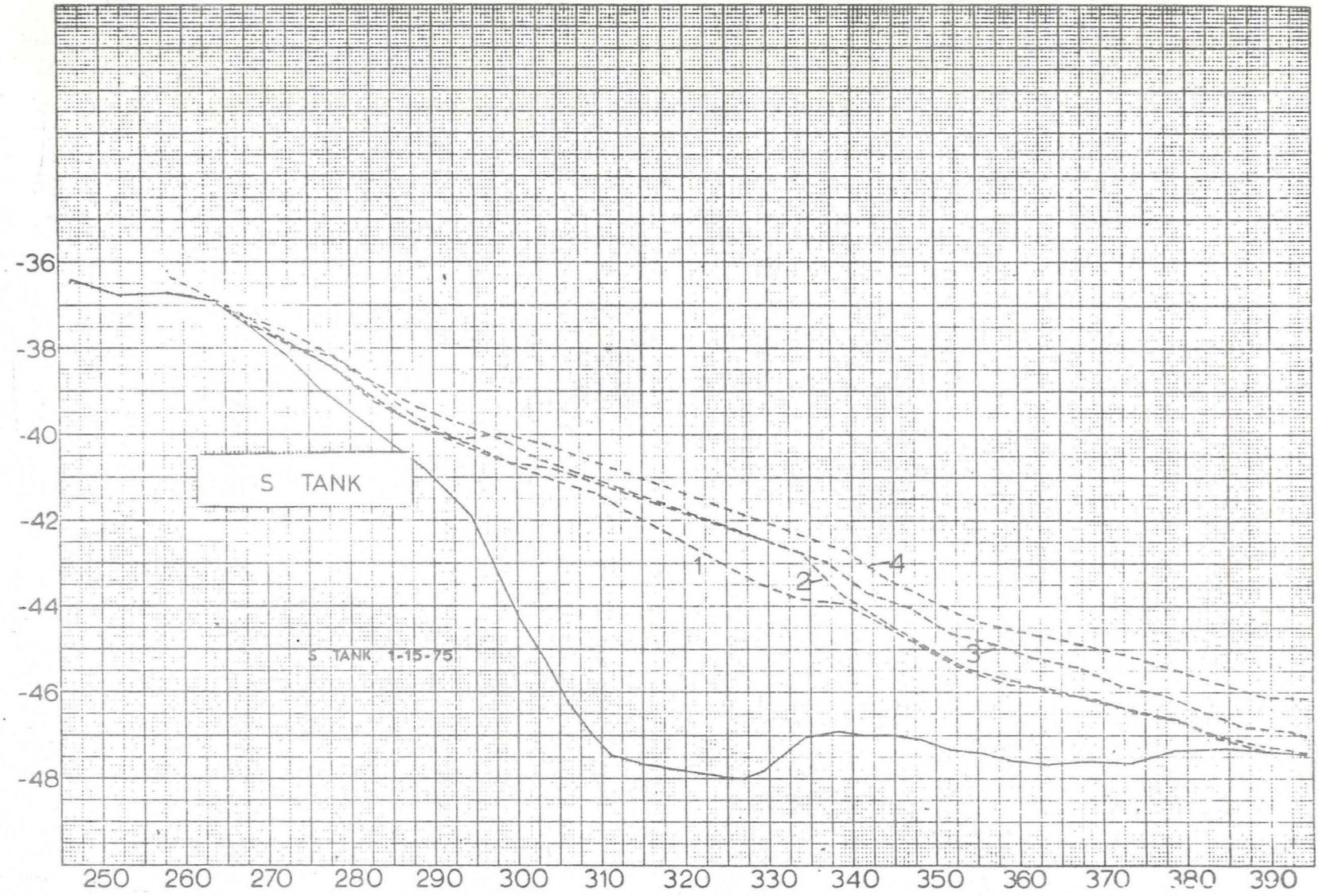

Figure 20e. Cross-sectional profiles of snowdrift accumulation at Tank Trap site, South line.
1: 1/15/75 2: 1/22/75 3: 1/30/75 4: 2/12/75.

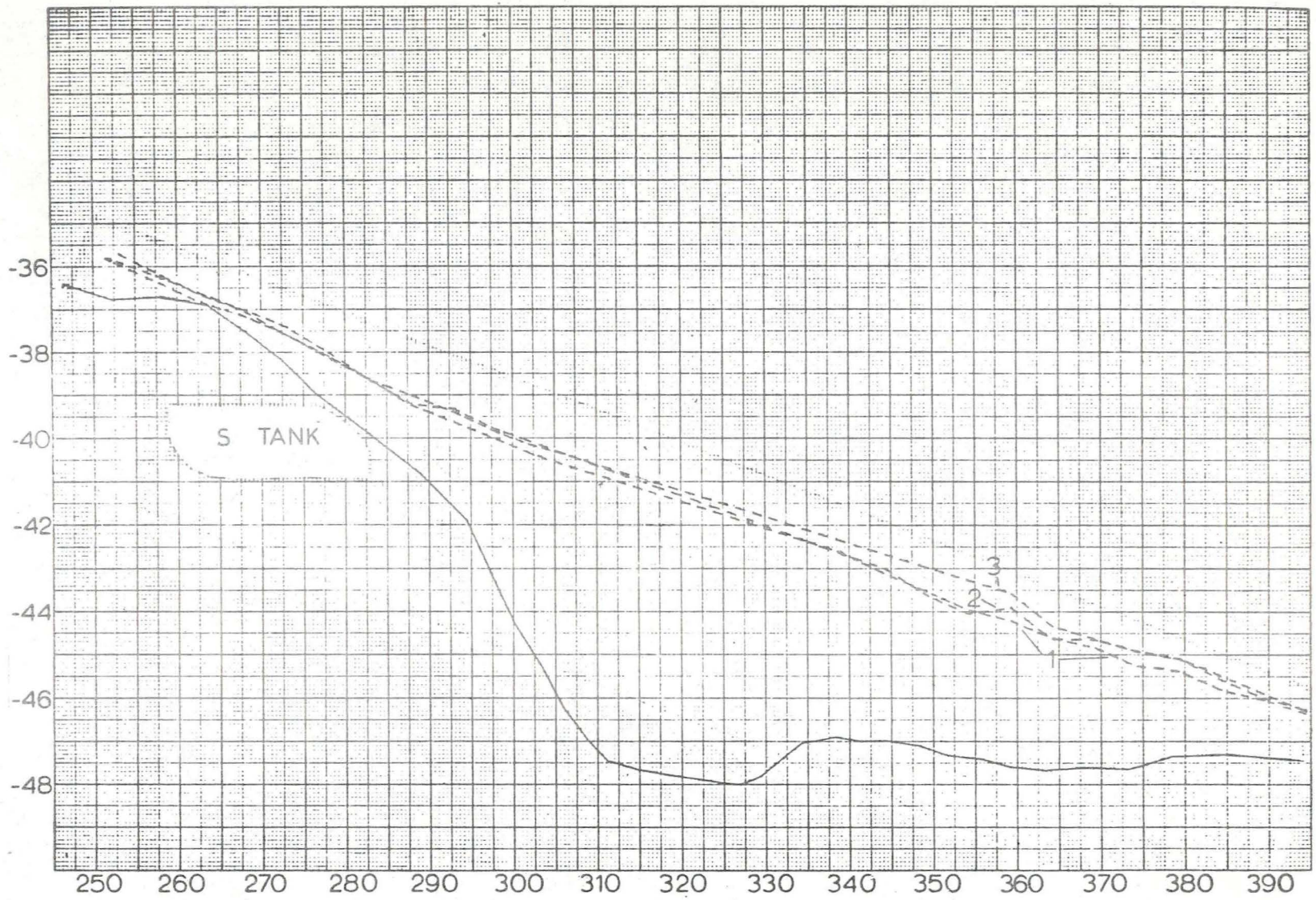

Figure 20f. Cross-sectional profiles of snowdrift accumulation at Tank Trap site, South line.
1: 2/22/75 2: 3/4/75 3: 3/14/75.

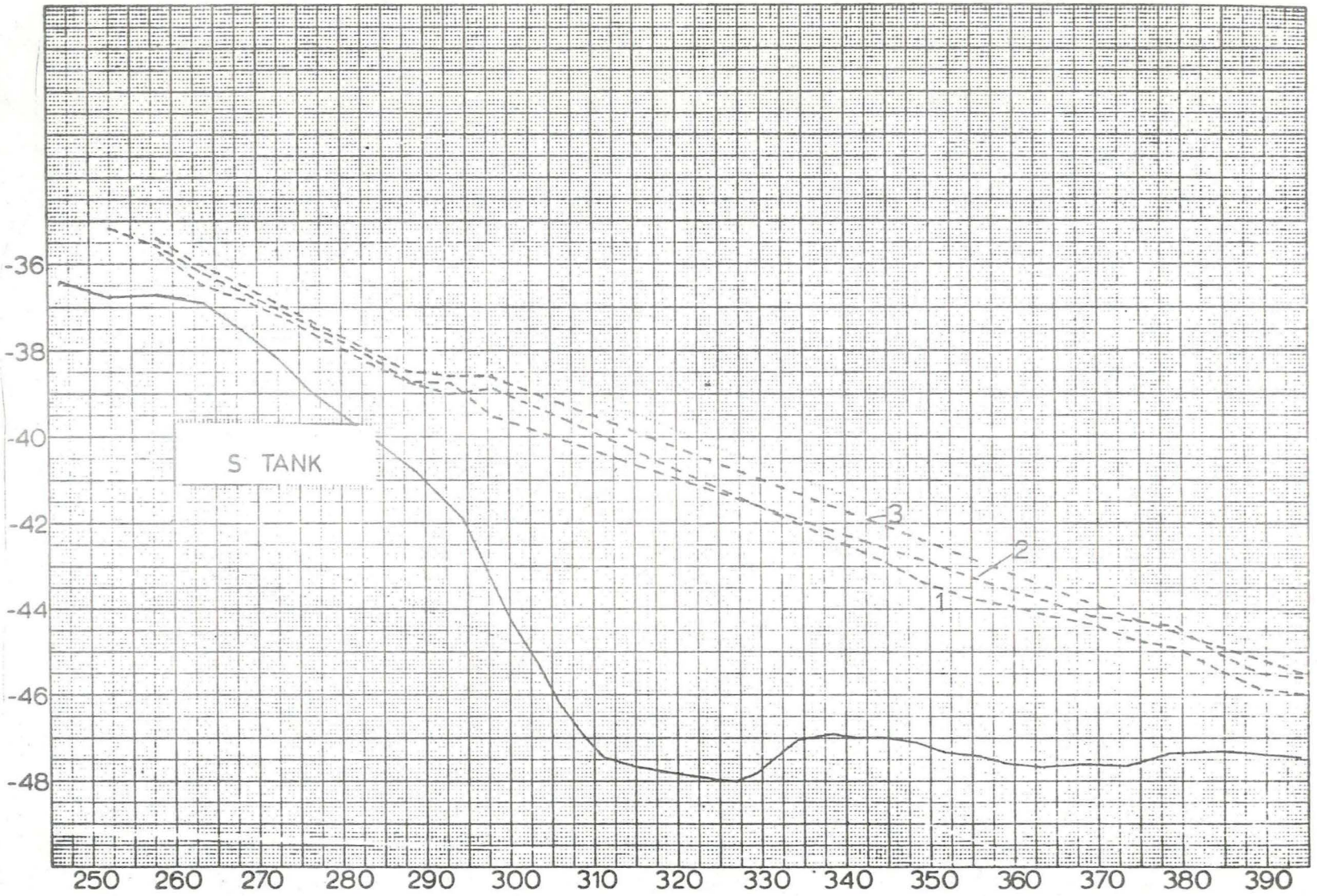

Figure 20g. Cross-sectional profiles of snowdrift accumulation at Tank Trap site, South line.
1: 3/25/75 2: 4/4/75 3: 4/22/75.

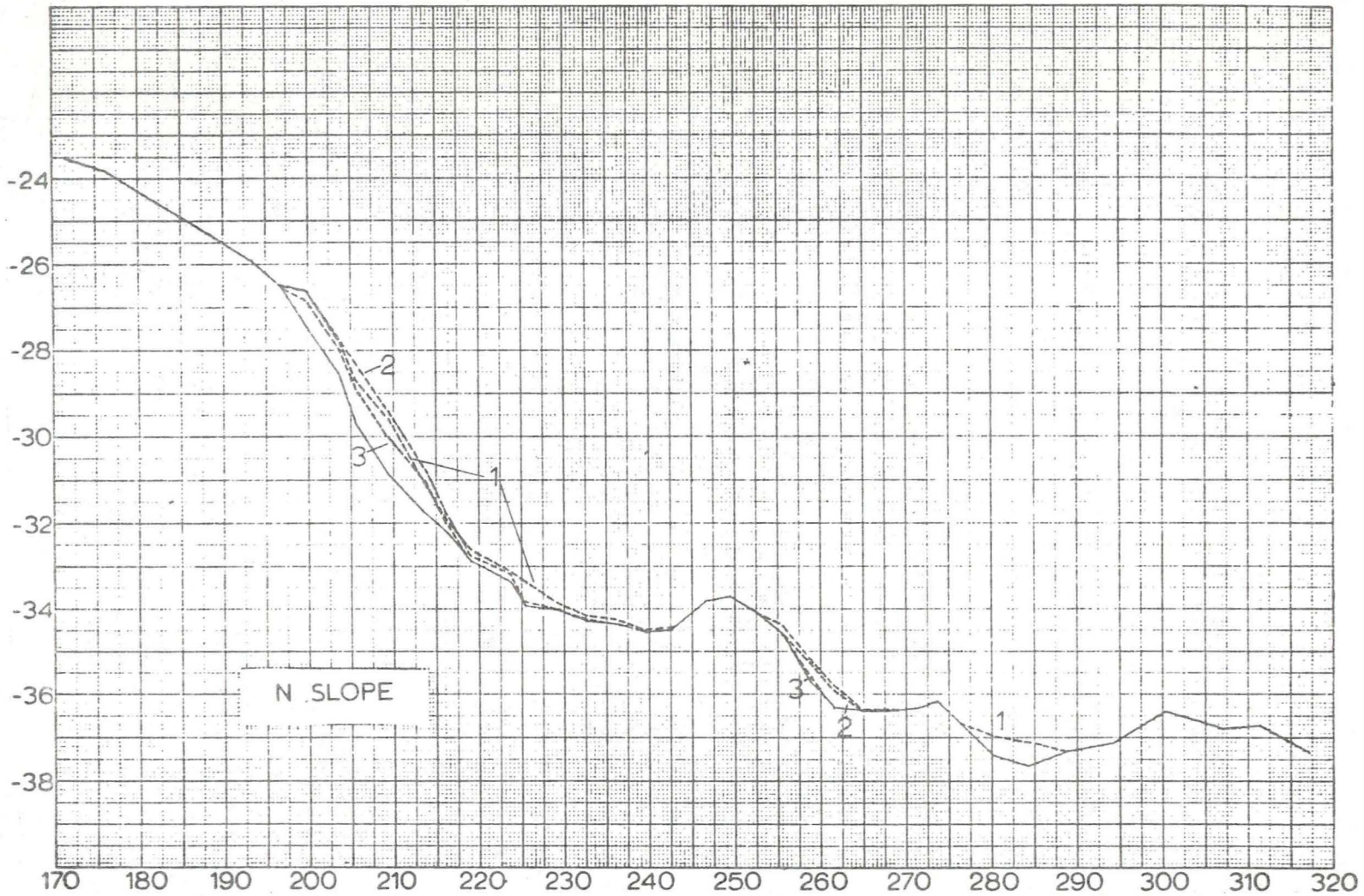

Figure 21a. Cross-sectional profiles of snowdrift accumulation at Slope site, North line. Dotted line is snow surface. Vertical and horizontal scales are in meters and refer to figure 19f. 1: 10/15/74 2: 10/16/74 3: 10/20/74.

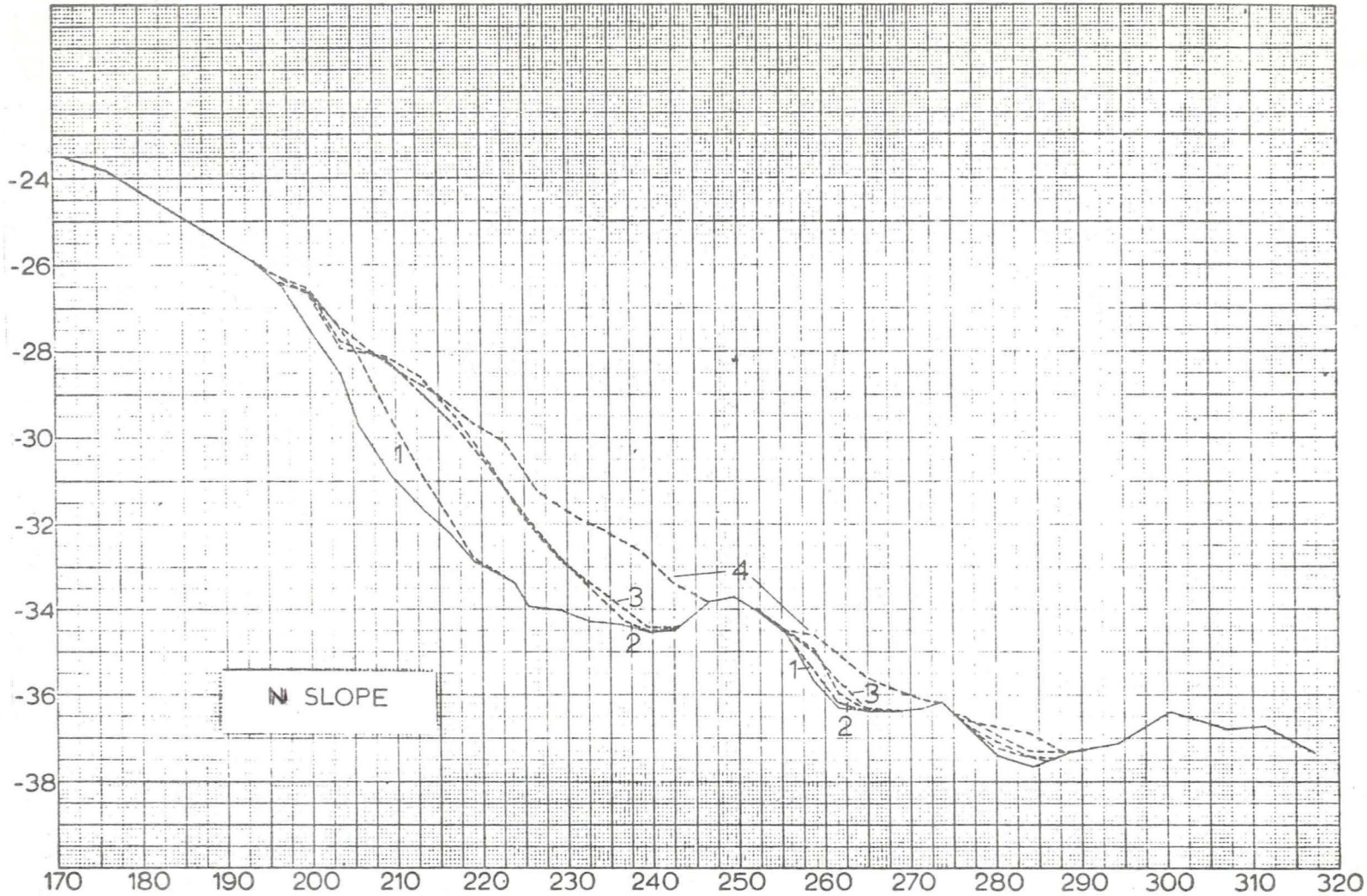

Figure 21b. Cross-sectional profiles of snowdrift accumulation at Slope site, North line.
1: 10/24/74 2: 11/1/74 3: 11/5/74 4: 11/11/74.

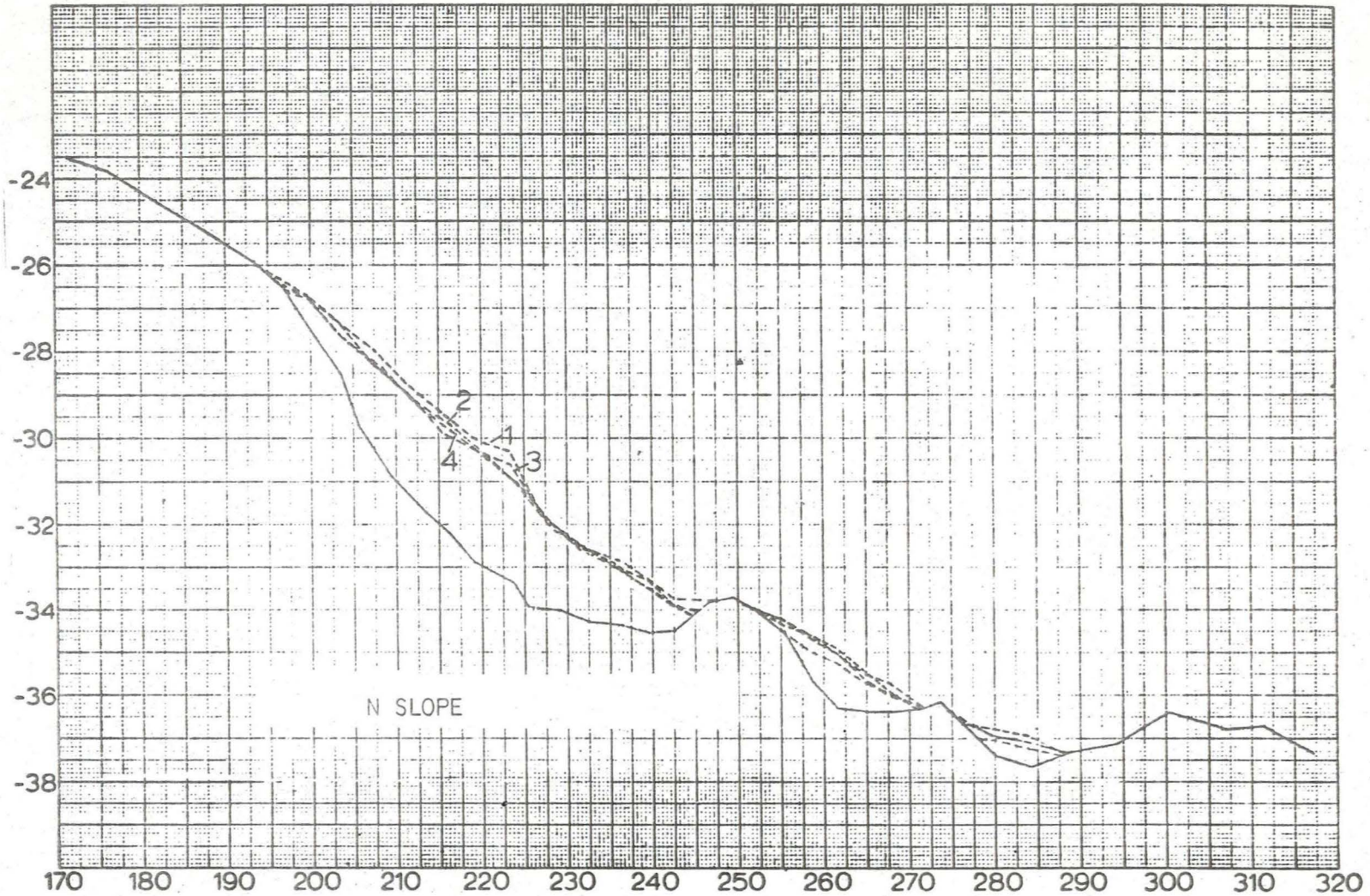

Figure 21c. Cross-sectional profiles of snowdrift accumulation at Slope site, North line.
1: 11/13/74 2: 11/27/74 3: 12/6/74 4: 12/17/74.

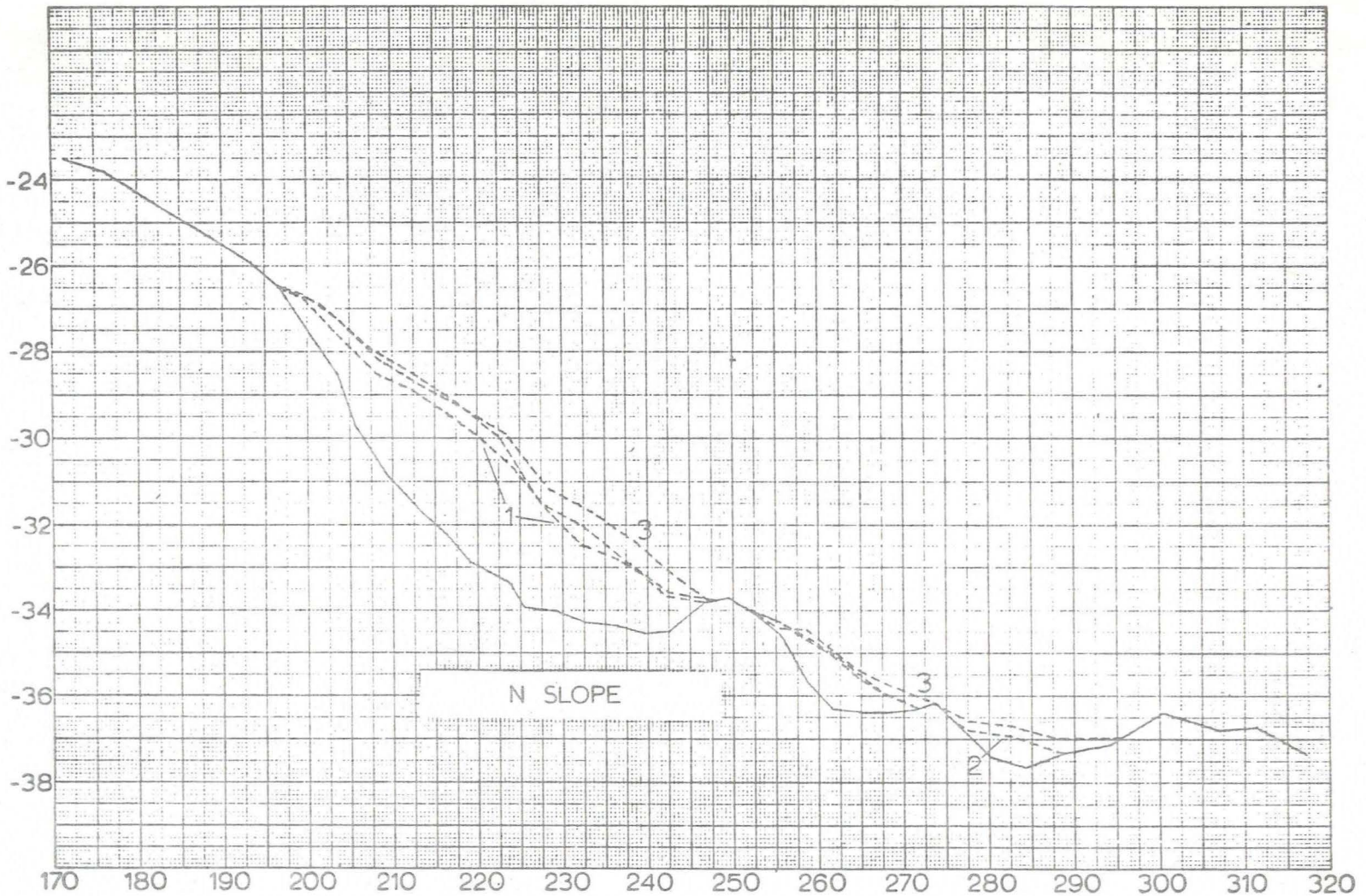

Figure 21d. Cross-sectional profiles of snowdrift accumulation at Slope site, North line.
1: 12/19/74 2: 1/2/75 3: 1/9/75.

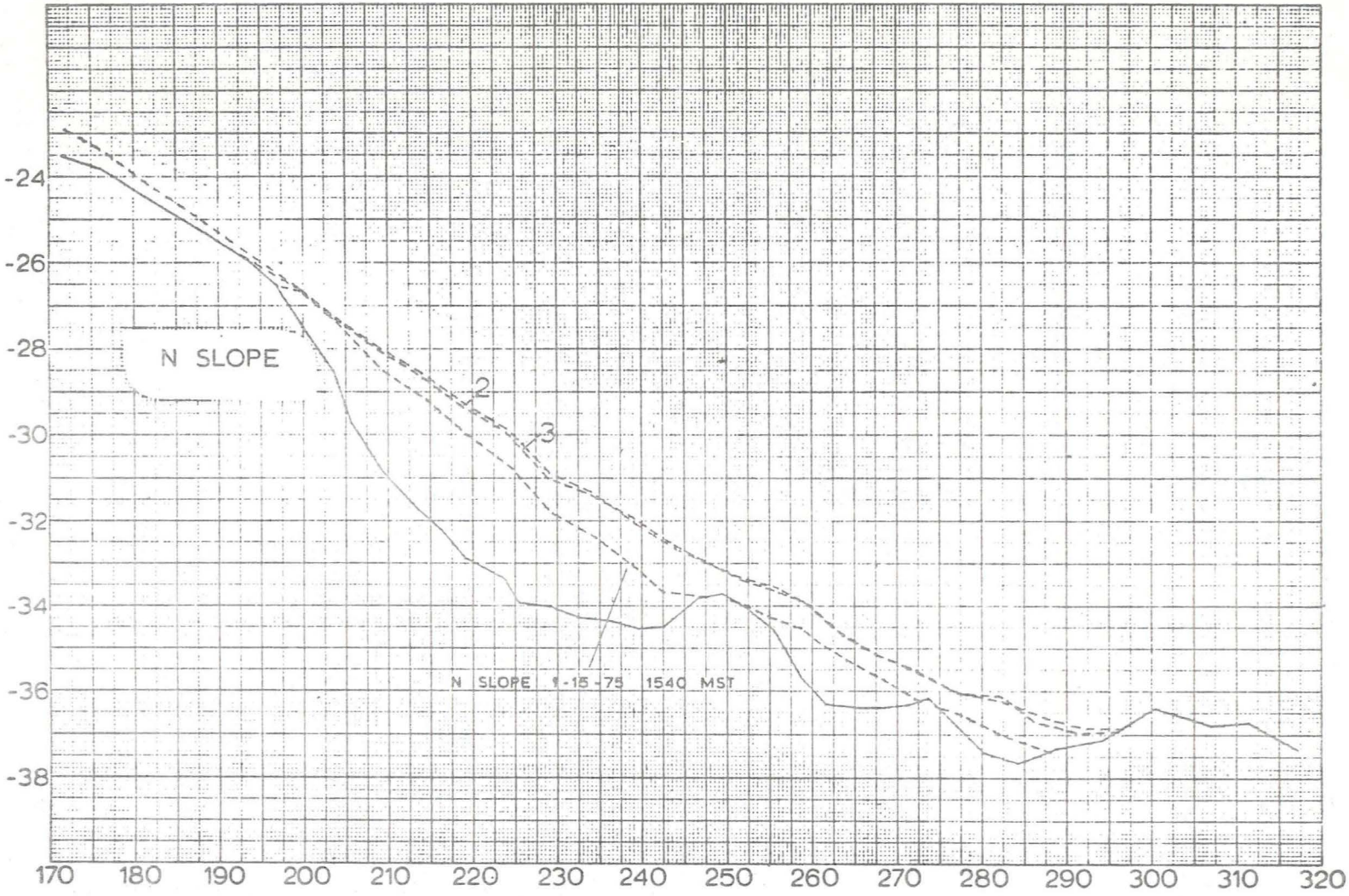

Figure 21e. Cross-sectional profiles of snowdrift accumulation at Slope site, North line.
1: 1/15/75 2: 1/28/75 3: 2/4/75.

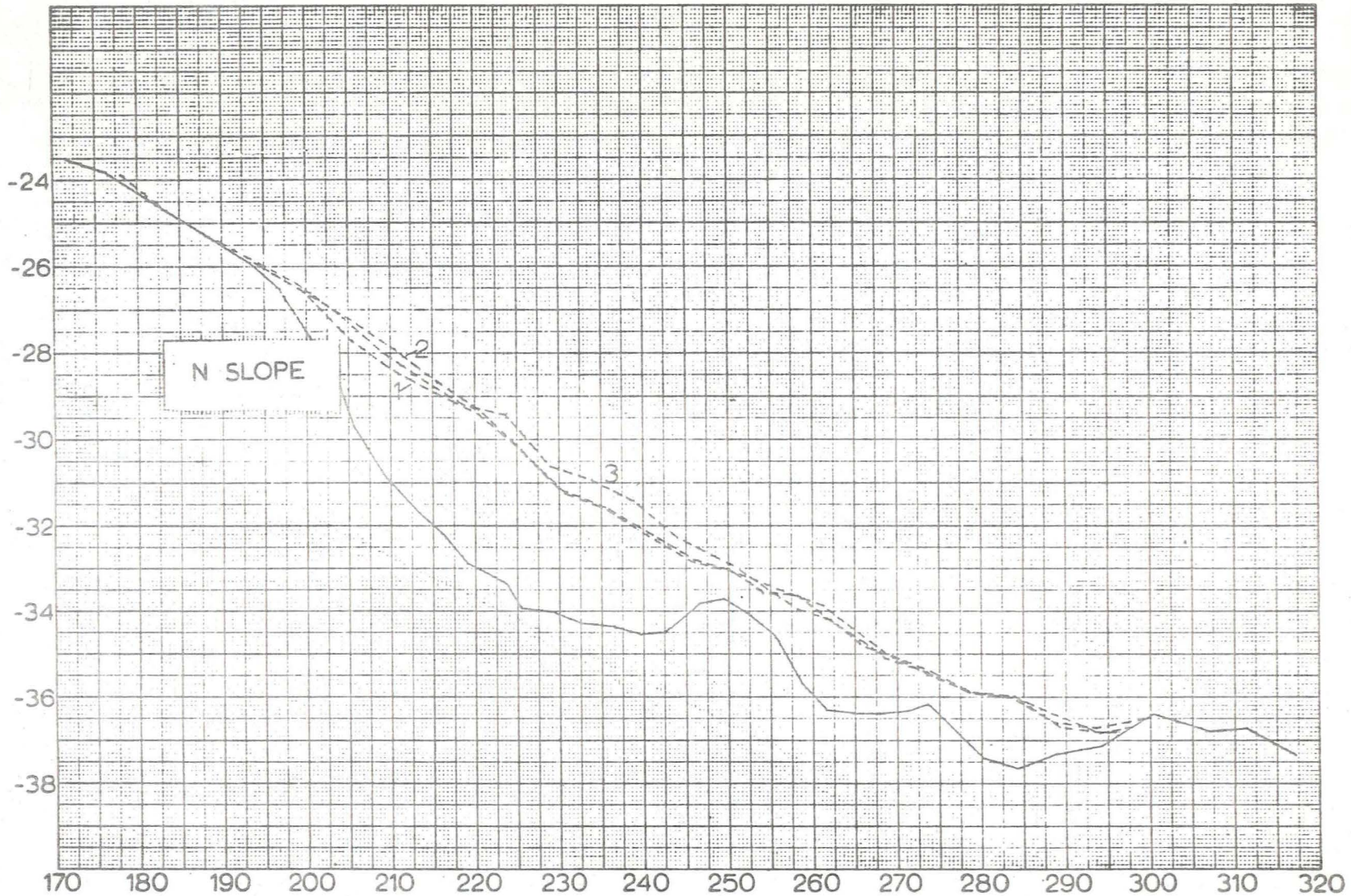

Figure 21f. Cross-sectional profiles of snowdrift accumulation at Slope site, North line.
1: 2/14/75 2: 2/22/75 3: 3/4/75.

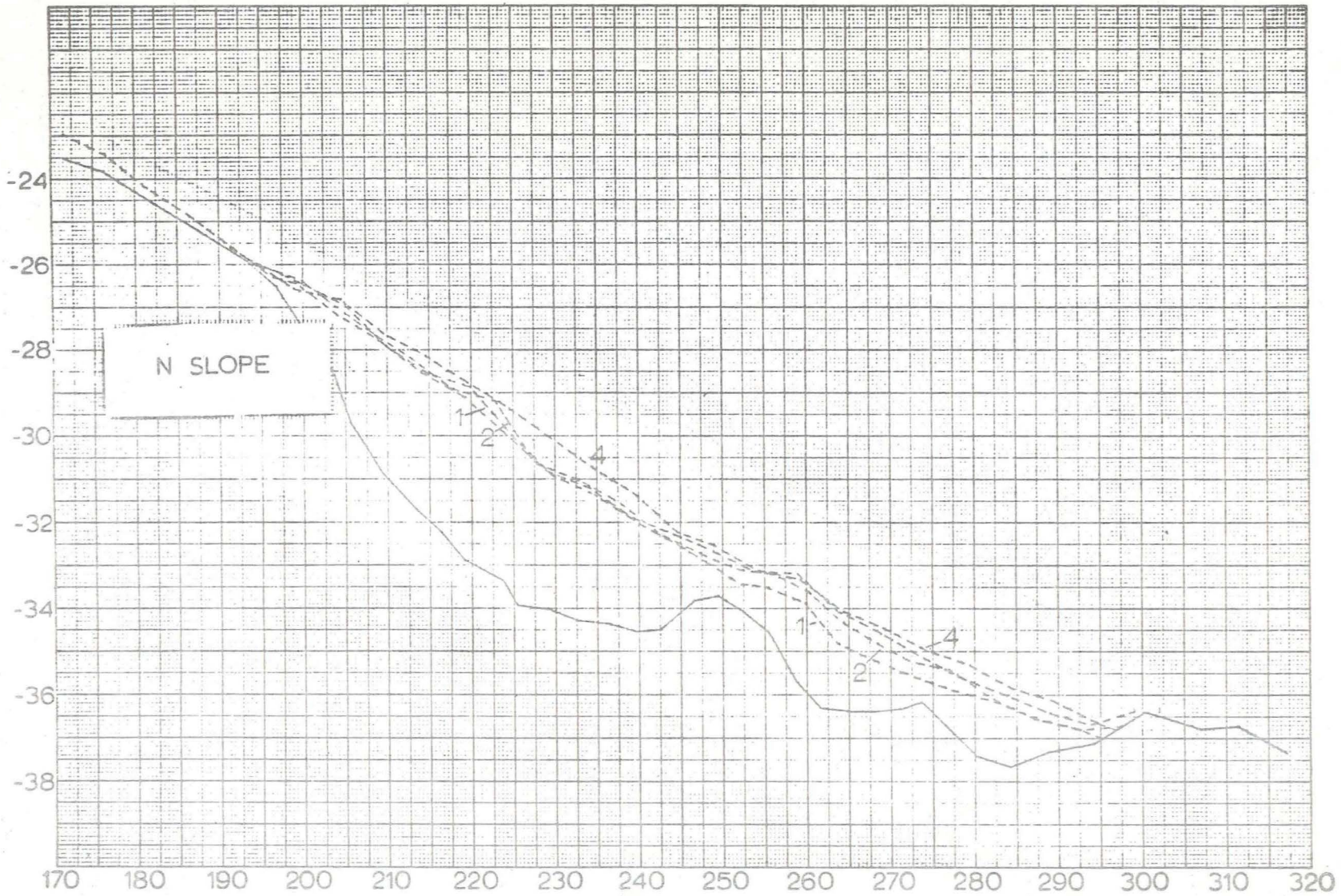

Figure 21g. Cross-sectional profiles of snowdrift accumulation at Slope site, North line.
1: 3/20/75 2: 4/3/75 3: 4/12/75 4: 4/29/75.

Blowing snow particle size and frequency were recorded by a photo-electric device developed by R.A. Schmidt (Schmidt and Sommerfeld, 1969; Schmidt, 1971). Output from this instrument is in continuous strip chart form from which the duration and relative magnitude of blowing snow events can be determined quickly without resort to automatic digitizing equipment. The "snow particle counter" was positioned at .85 m height on the mast in the anticipation that particle sizes at that height would be between .1 and .2 mm, the calibration range of the instrument. Figure 22 shows the precipitation and blowing snow frequency (0-5000 particles per second) for the 1974-1975 field season. The precipitation values are the daily weighted mean (65% to 35%) of the Niwot Ridge and Como stations. The unequal weighting derives from the consideration that the Slope and Tank Trap sites are at alpine locations and should receive precipitation more comparable to that recorded at Niwot Ridge than at Como. On figure 22 blowing snow particle frequency refers to the maximum value recorded during each event.

Figure 22. Snow precipitation and blowing snow frequency 10/11/74 to 5/11/75, Niwot Ridge, Front Range, Colorado.

Snow precipitation in cm water equivalent
Blowing snow frequency in 1000 particles per second, maximum recorded per event

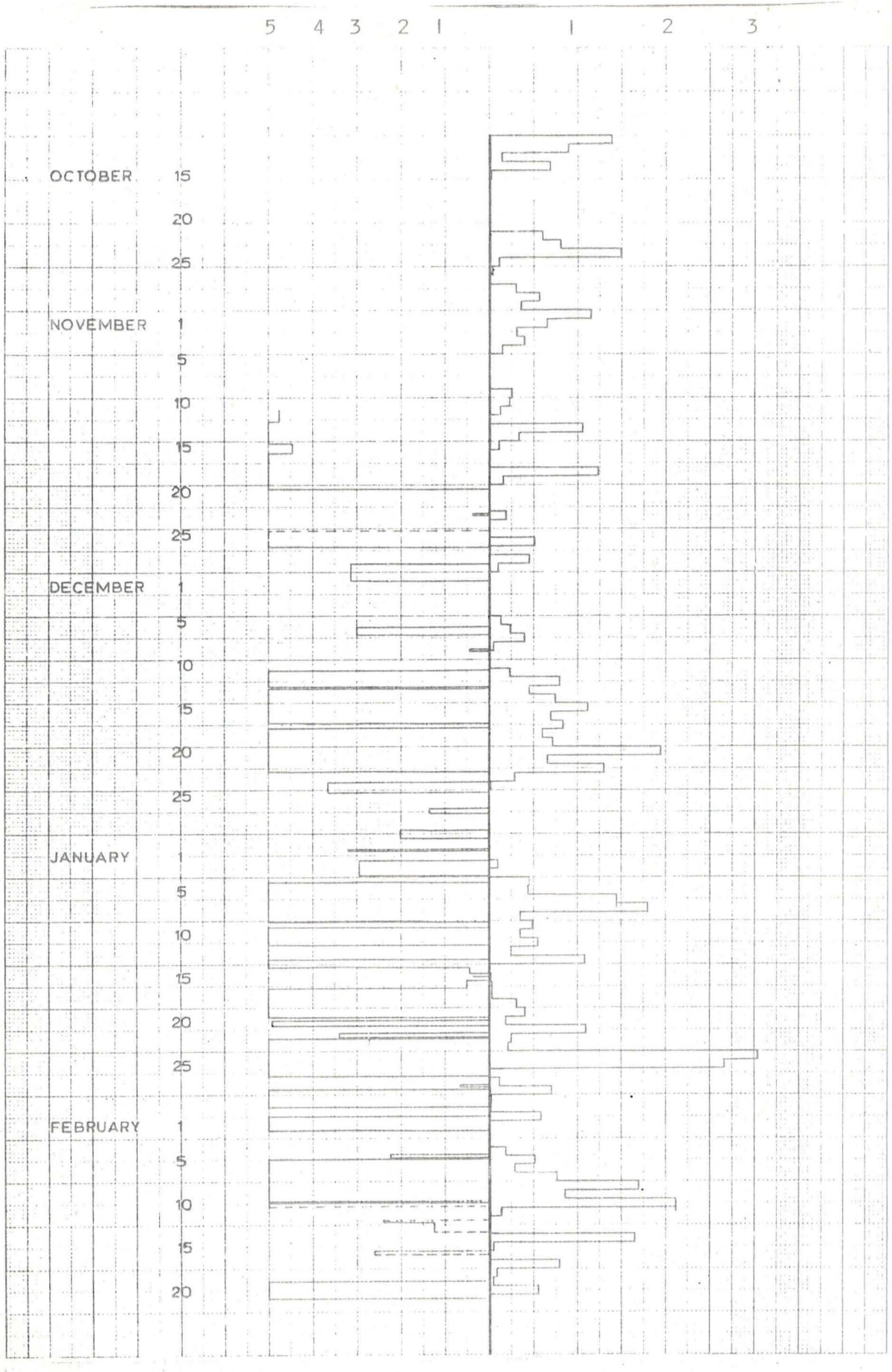
BLOWING SNOW FREQUENCY
SNOW PRECIPITATION
5 4 3 2 1
1 2 3
OCTOBER
15
20
25
NOVEMBER
1
5
10
15
20
25
DECEMBER
1
5
10
15
20
25
JANUARY
1
5
10
15
20
25
FEBRUARY
1
5
10
15
20

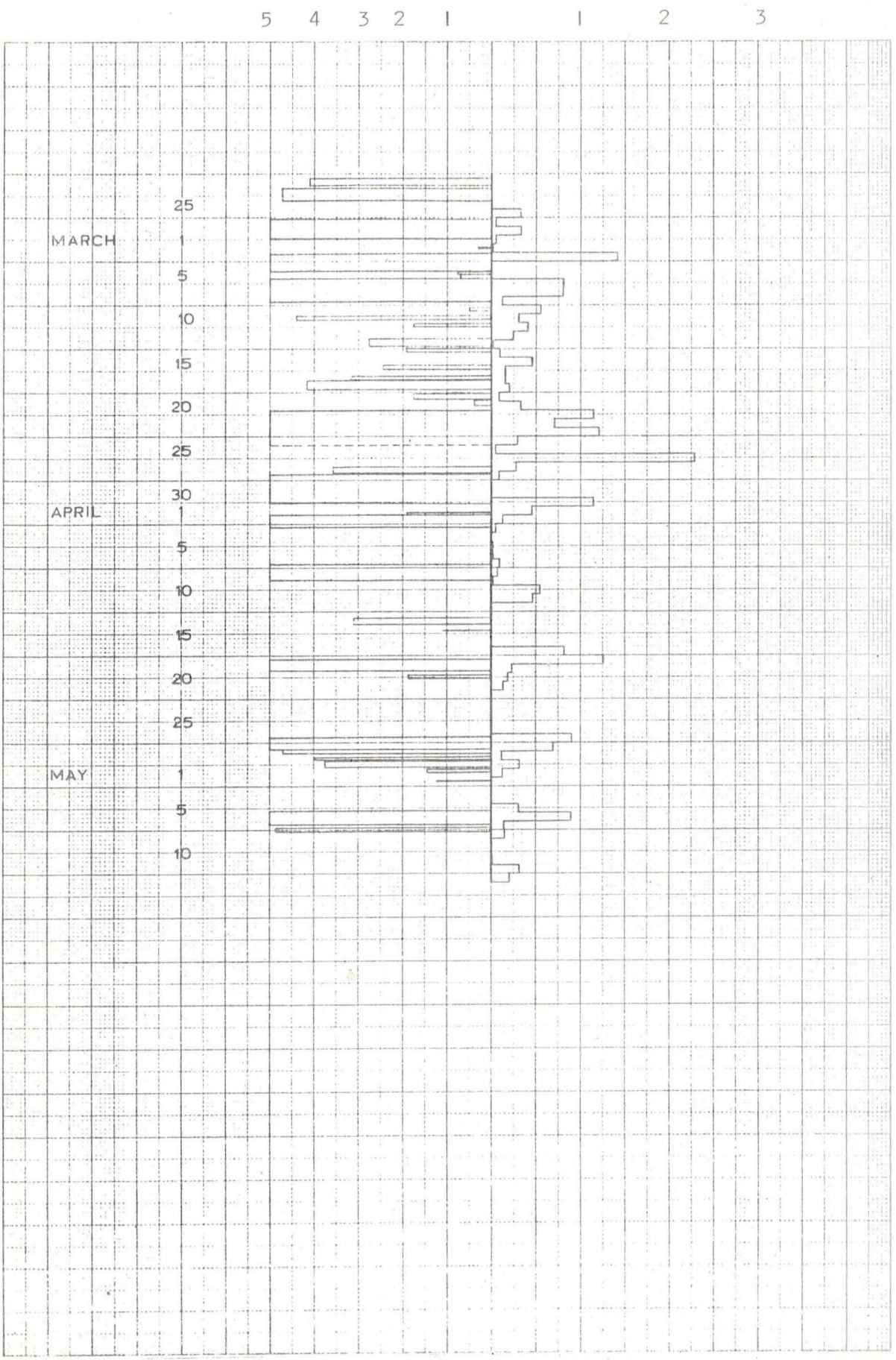
BLOWING SNOW FREQUENCY
SNOW PRECIPITATION
5 4 3 2 1
1 2 3
MARCH
APRIL
MAY
25
1
5
10
15
20
25
30
1
5
10
15
20
25
1
5
10

MODEL EVALUATION

The snowdrift accumulation model is the integration of a set of hypotheses concerning the deposition of wind-blown snow into topographic catchments. Two lines of evaluation have been applied to it. First, the response of the model to variations in selected input parameters has been estimated. Such a "sensitivity" analysis provides a means to ascertain which relationships most affect the outcome and to adjust the model accordingly. Second, the results derived from the model have been compared with compatible empirical measurements of drift accumulation from the field area. Experimentation with the model also provides a basis for suggesting improvements.

Since an original aim of the project was to consider changes in shape of the drift through the accumulation period, a visual comparison between modelled and measured cross-sectional profiles has been used. Visual comparisons of the cross-sectional profiles are also the primary method of analysis in the sensitivity experimentation.

SENSITIVITY ANALYSIS

Experimentation with the model in a sensitivity analysis allows evaluation of the contribution each input parameter makes to the outcome. Figure 23 shows a six-event series which is considered the basis for comparison. A simple three-segment slope configuration is used and the input parameters are listed in table 2. A single grain size fraction is used and the Owen procedure (equation 22) specifies the saltation layer thickness. The roughness element value, z_o, is taken equal to 0.003 m. Much lower values--between 10^{-8} and 10^{-4} m--are reported by Budd, Dingle, and Radok (1966) and Mellor (1965) for airflow over snow surfaces during blowing snow, but in alpine terrain snow seldom covers the entire surface so that z_o = 0.003 m is chosen as intermediate between 10^{-5} and LeDrew's z_o range--0.0075 to

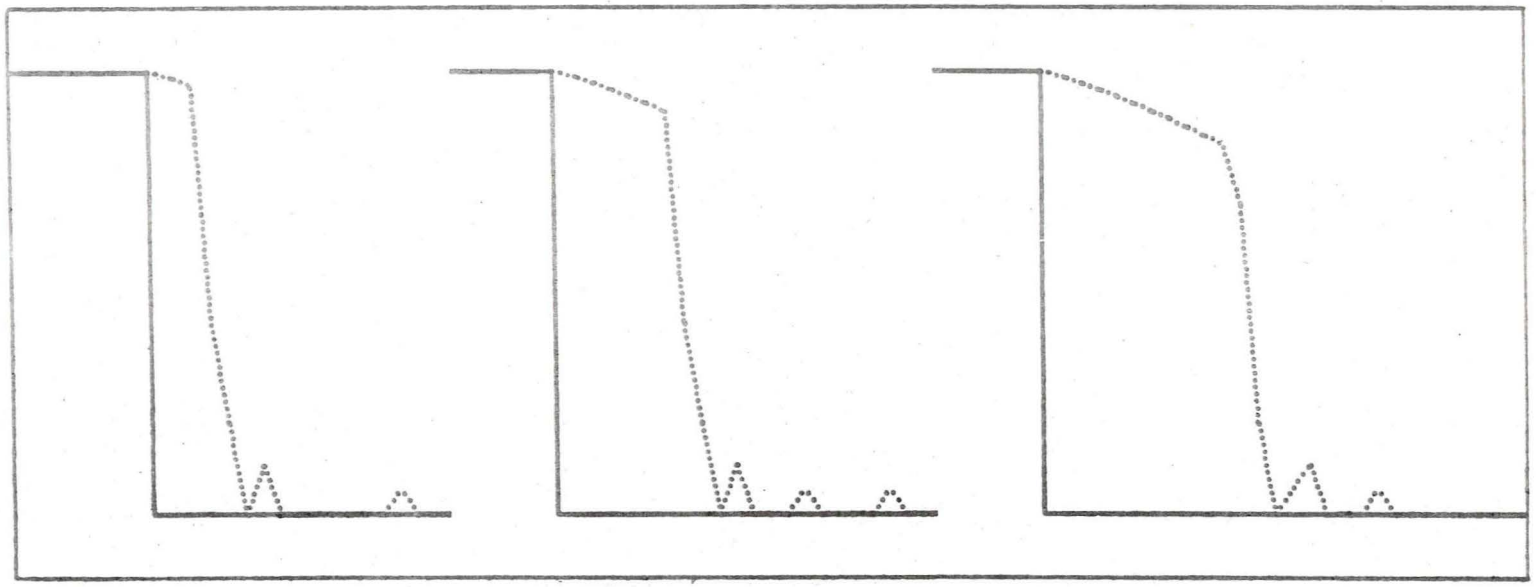

Figure 23a-c. Sensitivity analysis. Cross-sectional profile of drift infill for control case. Input parameters are listed in table 2. Three events are shown, 23a being on the far left, and each utilizes the same input values. Unless otherwise specified, all following figures also include three sequential events.

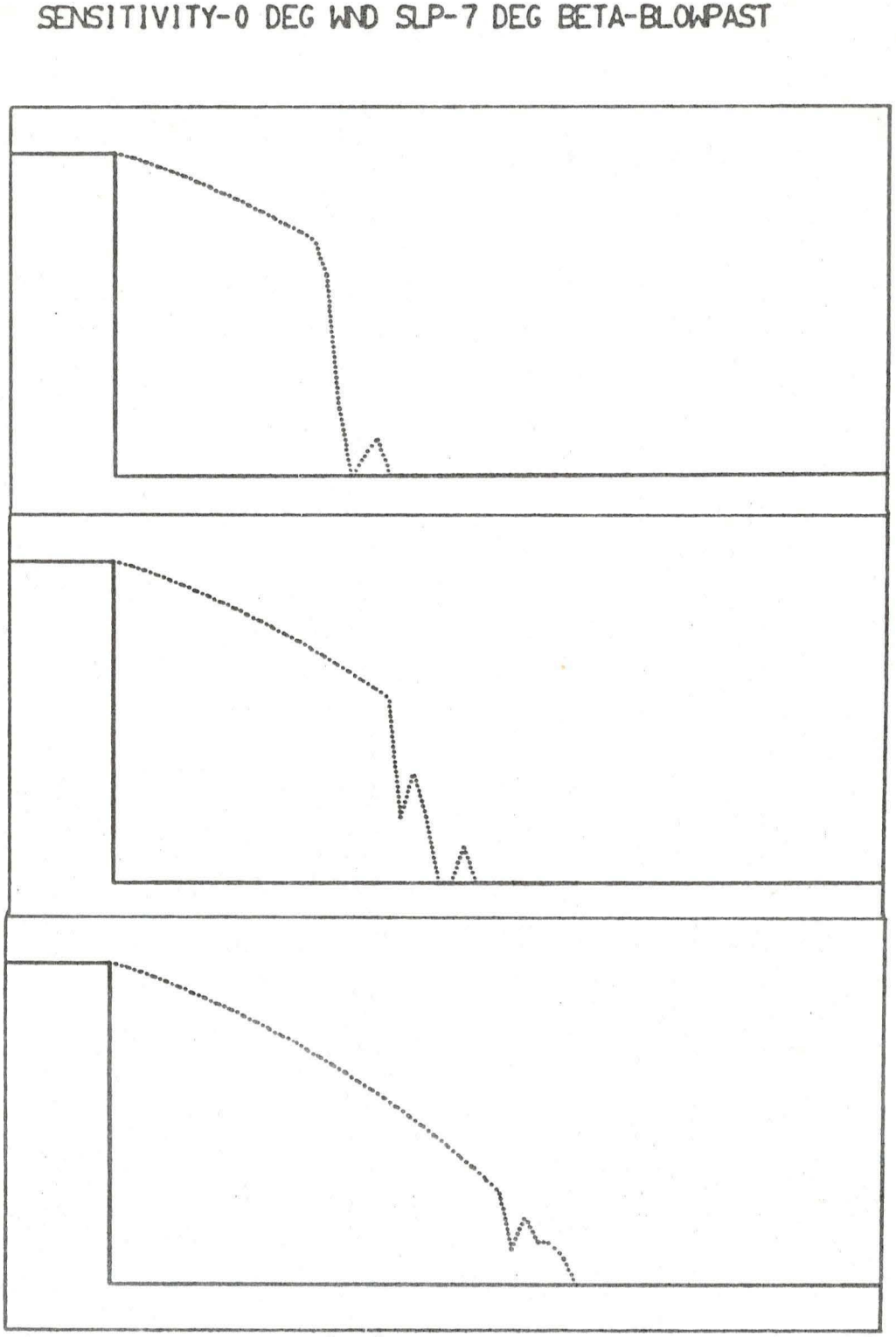

Figure 23d-f. Sensitivity analysis. Events 4, 5, and 6 for control case. Event 4, figure 23d, is on top.

Table 2. Sensitivity analysis model input parameters for control case (figure 23).

β	7^{o}
α	5^{o}
U_{t}	0.5 mps
d	15 m
k	0.4
ρ_{d}	0.4 g cm^{-3}
U_2/U_1	0.4
CREP	0.12
D	0.1 mm
ILAY	1
IANG	Subangular/subrounded
z_{o}	0.003 m
U_{max}	7 mps
q_{d}	0.15 g cm^{-1} sec^{-1}

0.01 m--measured on Niwot Ridge tundra surfaces under summer conditions (LeDrew, 1974). The mixing and eddy zone velocity distributions follow equation (6), the Naib procedure.

In the following paragraphs each parameter is classified as either a (1) snow, (2) airflow, or (3) topographic factor and is then considered individually for its influence on the model response. Figure 23 shows the basic control case which gives relatively little deposition downwind of an abrupt snow surface discontinuity, which migrates downwind with infill, and which is hereafter termed the brink of the drift. Field observations, however, show significant snow deposition leeward of the brink, hereafter termed "downwind" deposition, and a recurring concern in the model evaluation is the lack of significant downwind deposition.

Snow parameters

Grain size and angularity are clearly snow particle parameters. Also included in this section are the influence of snowdrift deposit density, saltation layer thickness, the quantity of mass transport, the creep transport coefficient, and multiple grain size fractions.

(i) Grain size, D, and angularity, IANG

In the apportionment of transport between the three transport modes q_{sus} is directly dependent upon shear velocity, U_*, and particle fall velocity, w. Snow particle diameter and angularity directly specify w. The fall velocity, in conjunction with several airflow parameters, also determines the rate of fallout from suspension and therefore deposition beyond the brink of the drift. Increased grain diameter and sphericity increase w thereby reducing both the downwind carry distance of suspended grains and the size of each suspension parcel. Figures 24 and 25 show reduction in downwind deposition when either round or large grains are used while figure 26 illustrates the increased downwind deposition which results when angular grains are specified. In these examples, grain size is more influential

SENSITIVITY-0 DEG WND SLP-7 DEG BETA-ROUND GRAINS

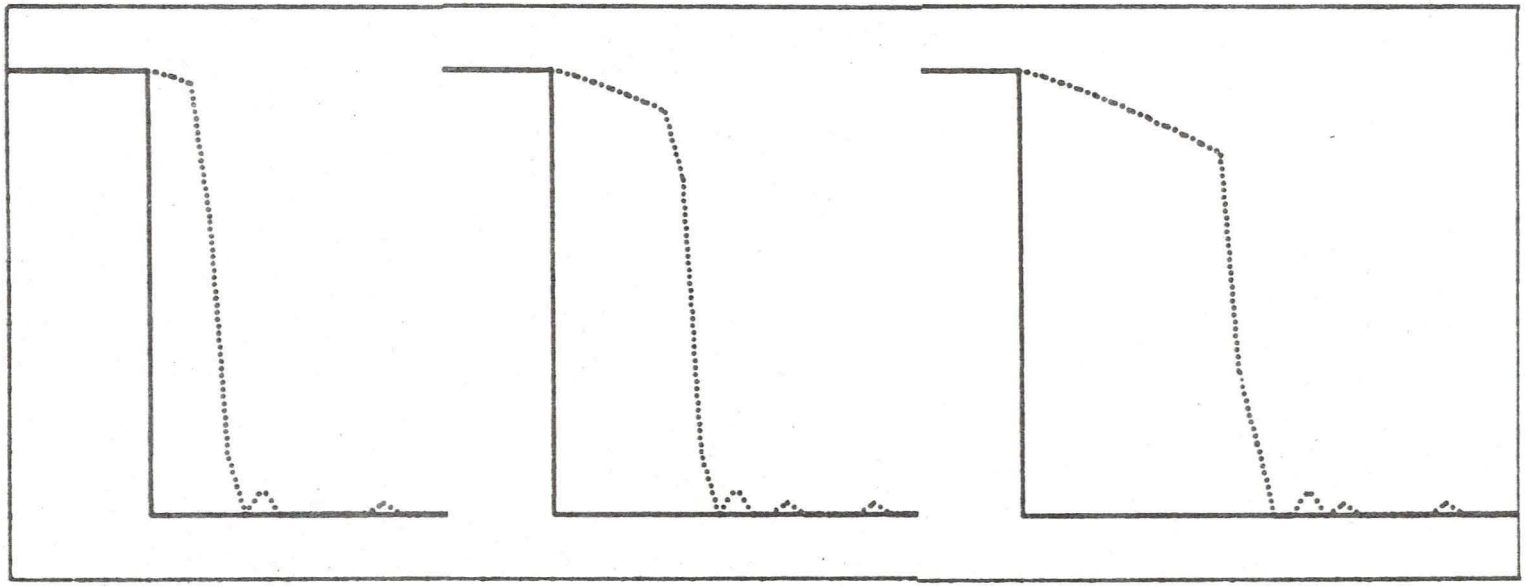

Figure 24a-c. Sensitivity analysis. All inputs are as listed in table 2 except the usage of round grains.

SENSITIVITY-0 DEG WND SLP-7 DEG BETA-.15 DIAM-UMAX=7

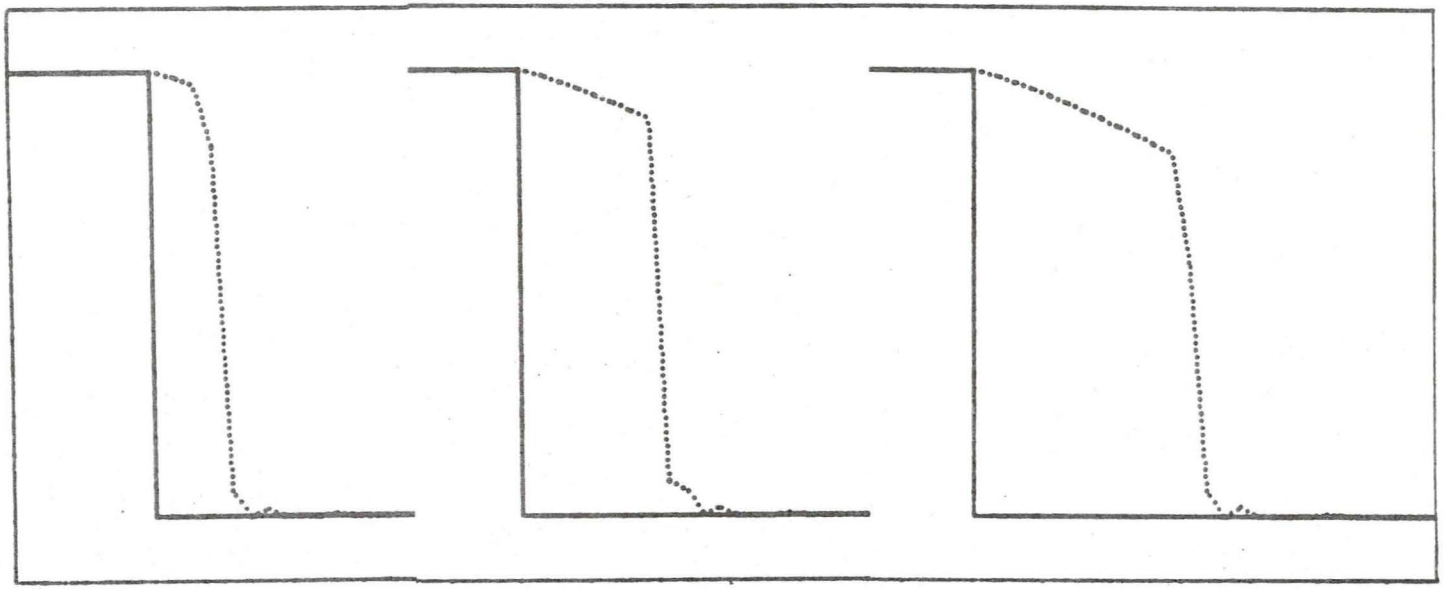

Figure 25a-c. Sensitivity analysis. All inputs are as listed in table 2 except for the usage of particles of 0.15 mm mean diameter.

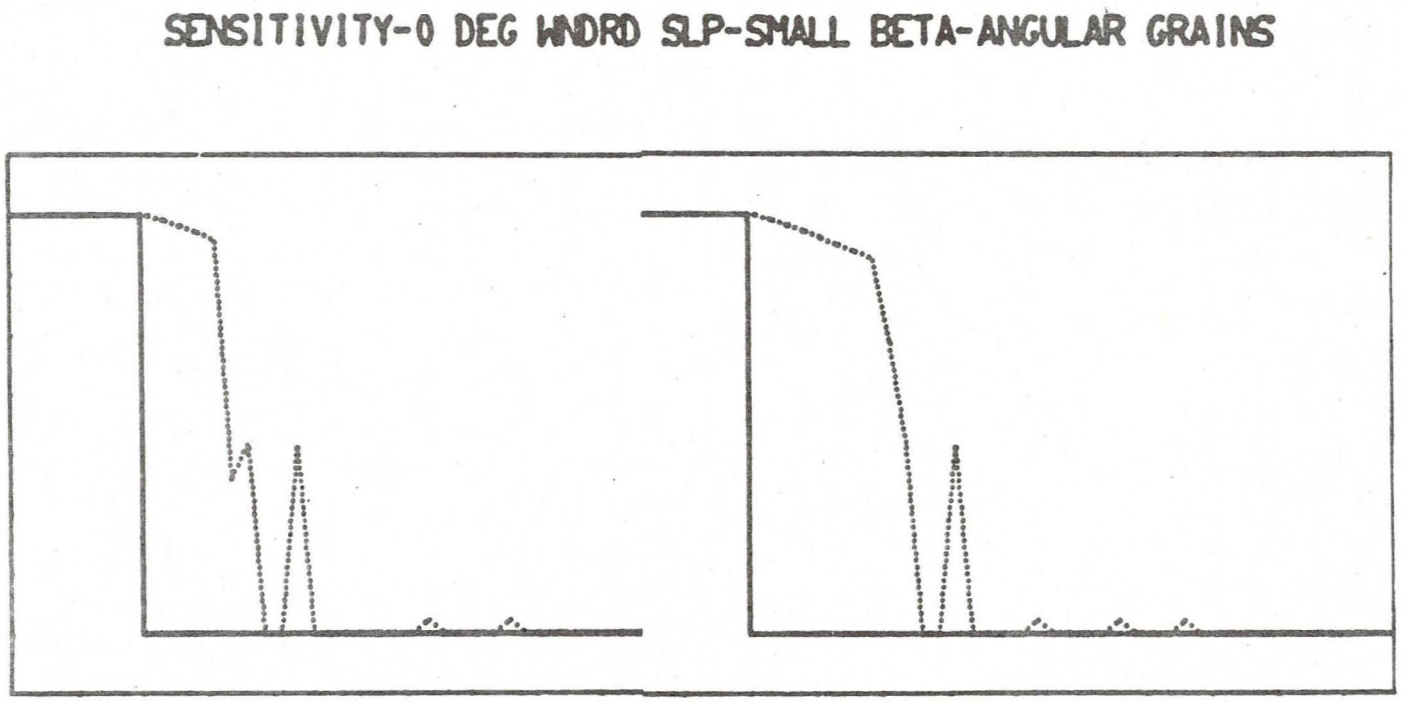

Figure 26a-b. Sensitivity analysis. All inputs are as listed in table 2 except for the usage of angular grains. Due to photographic problems the first event of the three-event sequence has not been reproduced.

than sphericity in terms of reducing downwind deposition since 1) blowpast increases from 0.1% (large grains) through 0.6% (round grains) to 2.3% (control case) and 2) the greater downwind carry distance of suspension fallout in the round grain, vs. the large diameter, case. In fact, more downwind deposition occurs in figure 24c than figure 23c since in the control case an additional snow parcel blows past by the time the third event occurs.

(ii) Snow deposit density, ρ_d

Santaford (1972) suggests that snowdrift density should range from 0.2 to 0.3 g cm^{-3} immediately after deposition. Changing ρ_d from 0.4 g cm^{-3} to 0.25 g cm^{-3} increases the cross-sectional area of each parcel so that the catchment fills more quickly (figure 27).

(iii) Saltation layer thickness, h

The Iversen saltation method (equation 23) reduces the saltation layer thickness to such an extent that it is less than z_o in all instances studied. This effectively makes saltation and creep movement indistinguishable since velocity values at heights lower than z_o equal zero.

The model allocates all saltation transport to the zone bounded on top by h, the mean value of the saltation trajectory heights. One-half of the saltation trajectories rise above h so that values of xsalt and zsalt (figure 17) should be based upon a height greater than h. This would raise the lower suspension transport levels thereby increasing the downwind carry distance of the grains in these levels. The effects of increasing h by 50% are described in a later paragraph.

(iv) The number of grain size fractions

Realistic simulation of blowing snow movement requires that the size distribution of blowing snow particles be adequately represented. In many cases, the size distribution of blowing snow has a high variance so that it would be necessary to assign varying transport quantities to different grain size fractions. In

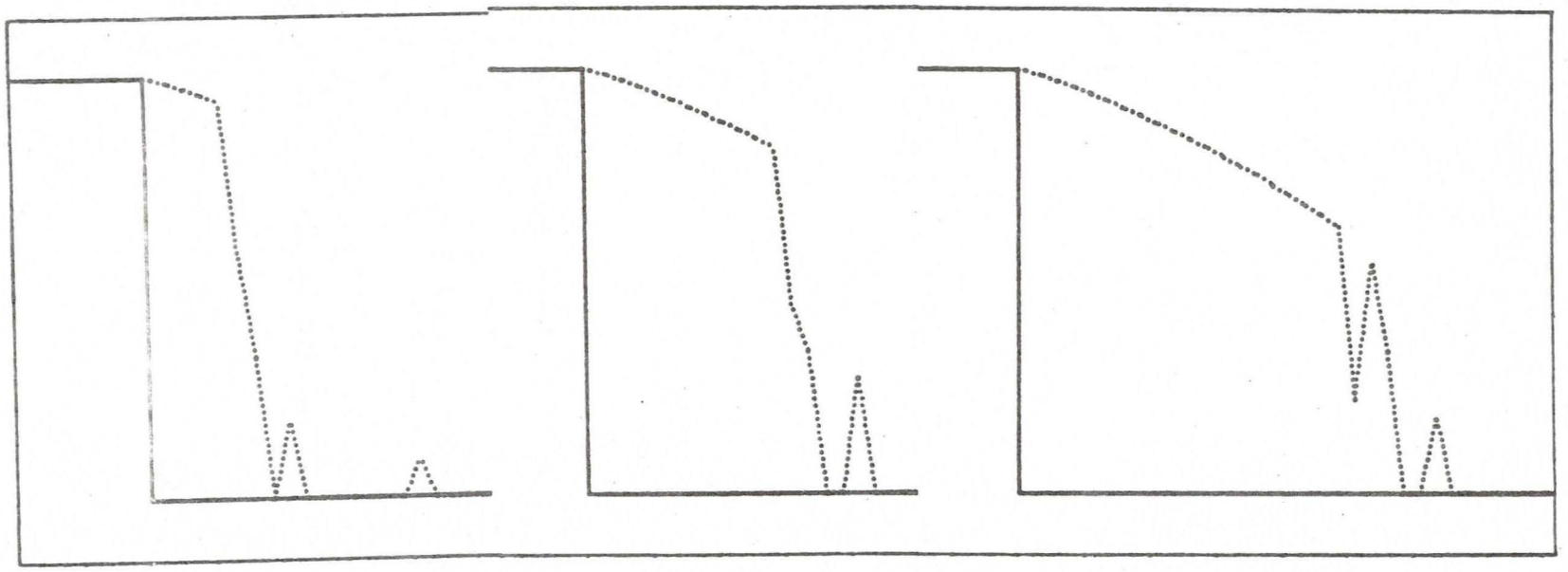

Figure 27a-c. Sensitivity analysis. All inputs are as listed in table 2 except for setting snow-drift deposit density to 0.25 g cm^{-3}.

a mixture of large and small particles the small grains should be carried further downwind and therefore increase the amount of blowpast. The use of multiple grain size fractions effectively increases the number of parcels available for movement through the system; in this way simulating the natural movement of blowing snow more realistically. In figure 28, two size fractions, 0.09 mm and 0.15 mm diameter,are used under a wind regime in which U_{max} equals 10 mps and U_2/U_1 equals 0.1. This diagram will be discussed more fully in a later section.

(v) Mass transport, q_d, and the creep transport coefficient, CREP

Neither the creep transport coefficient nor total mass transport were investigated in the current analysis. The proportion of the transport load allocated to creep transport makes no difference to the depositional pattern since in no case is saltation transport observed to reach beyond the first unfilled cell leeward of the snowdrift brink. Therefore reducing saltation by increasing the creep transport coefficient causes no changes. Since creep transport by definition has no horizontal velocity and is located at zero height, then all creep must also fall within the first unfilled cell.

Variation in the total mass transport simply alters the amount deposited but does not change the depositional pattern beyond the direct proportionality between q_d and infill rate.

Parameters specifying fluid movement can be grouped into those affecting flow through the three primary regions, 1) the undisturbed flow regime upwind of the drift catchment, 2) the mixing zone, and 3) the eddy region.

Airflow parameters--the region of undisturbed fluid flow

Use of the lagarithmic wind profile law requires information on z_o, U_{max}, and d, the boundary layer thickness. Boundary layer thickness and U_{max} are similar in that variation in either of these parameters changes wind speed at a given height. For this reason d is considered in a later section in its effect on specification of

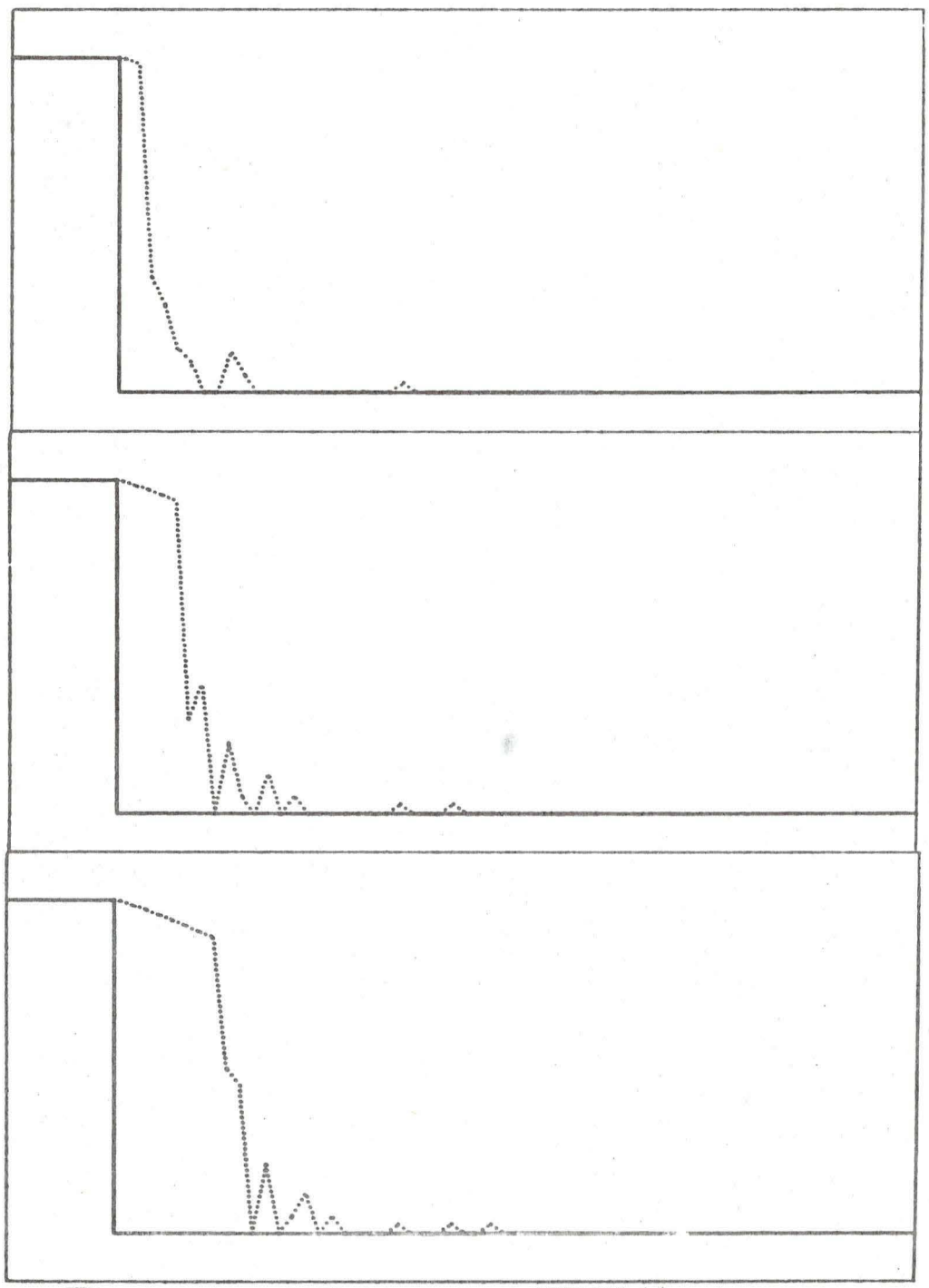

Figure 28a-c. Sensitivity analysis. All inputs are as listed in table 2 except 1) grain diameter equals 0.09 mm and 0.15 mm, 2) U_2/U_1 = 0.1, and 3) h is 50% greater than that specified by equation (22).

the lower mixing region angle β.

(i) The roughness element, z_o

The roughness element value specifies the height of zero wind speed. Reducing z_o decreases the gradient of the profile thereby decreasing U_* while increasing velocity at low levels, U_z. Frictional velocity influences q_{sus} and q_{salt} through equations (11) and (12). In figure 29 z_o is reduced from 0.003 m to 0.0005 m. Comparison with figure 23 illustrates two points. (1) Increased U_z associated with the lower z_o results in further downwind carry of the leemost suspension fallout parcel in event 1, while for following events this parcel blows past. (2) The leemost parcel is smaller in figure 29 since U_* is less than in the control case thereby reducing q_{sus} and n_z.

ii) Free stream flow velocity, U_{max}

Variation in U_{max} changes U_* and therefore transport quantities and drift densities in a manner similar to that of z_o. Increasing U_{max} 1) increases q_{sus} at the expense of q_{salt}, 2) shifts the bulk of suspension transport to higher levels, and 3) increases U_z at all levels. These factors combine to increase blowpast with increasing U_{max} since more grains are moving where higher velocities can impel the particles beyond the catchment. If the parcel crosses the separation streamline, however, it will do so further downwind from the edge of the trap and so will alight further downwind within the catchment than parcels originating from the same height but under a lower wind speed regime.

In figures 30, 31, 32, and 33, U_{max} increases through the range 7, 10, 12, and 18 mps for three blowing snow events at each velocity. In this situation, the thickness of the saltation layer is increased by 50% and U_2/U_1 equals 0.2 (rather than 0.4 as suggested by Naib) so that direct comparison with the control case (figure 23) is not possible.

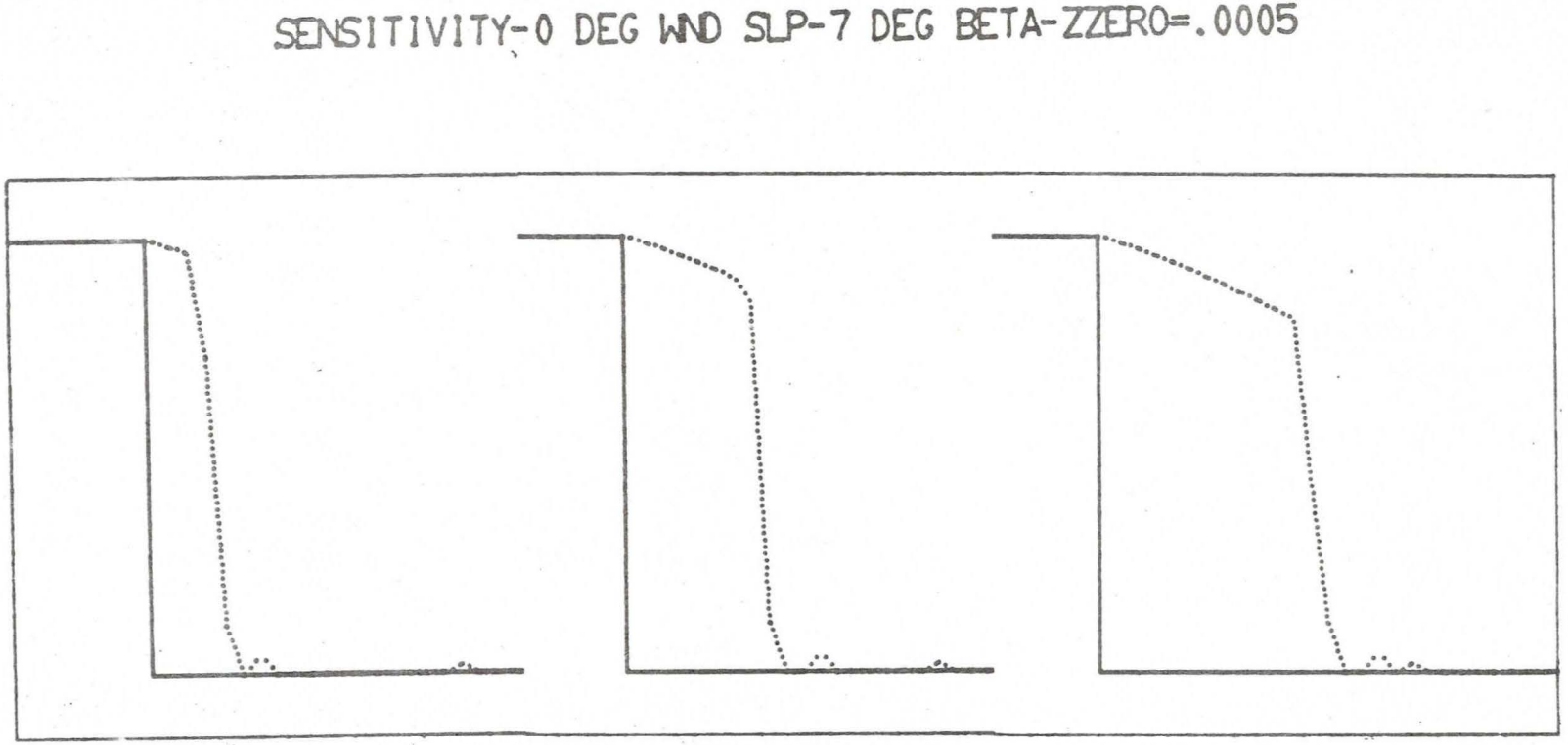

Figure 29a-c. Sensitivity analysis. All inputs are as listed in table 2 except for setting z_o equal to 0.0005 m.

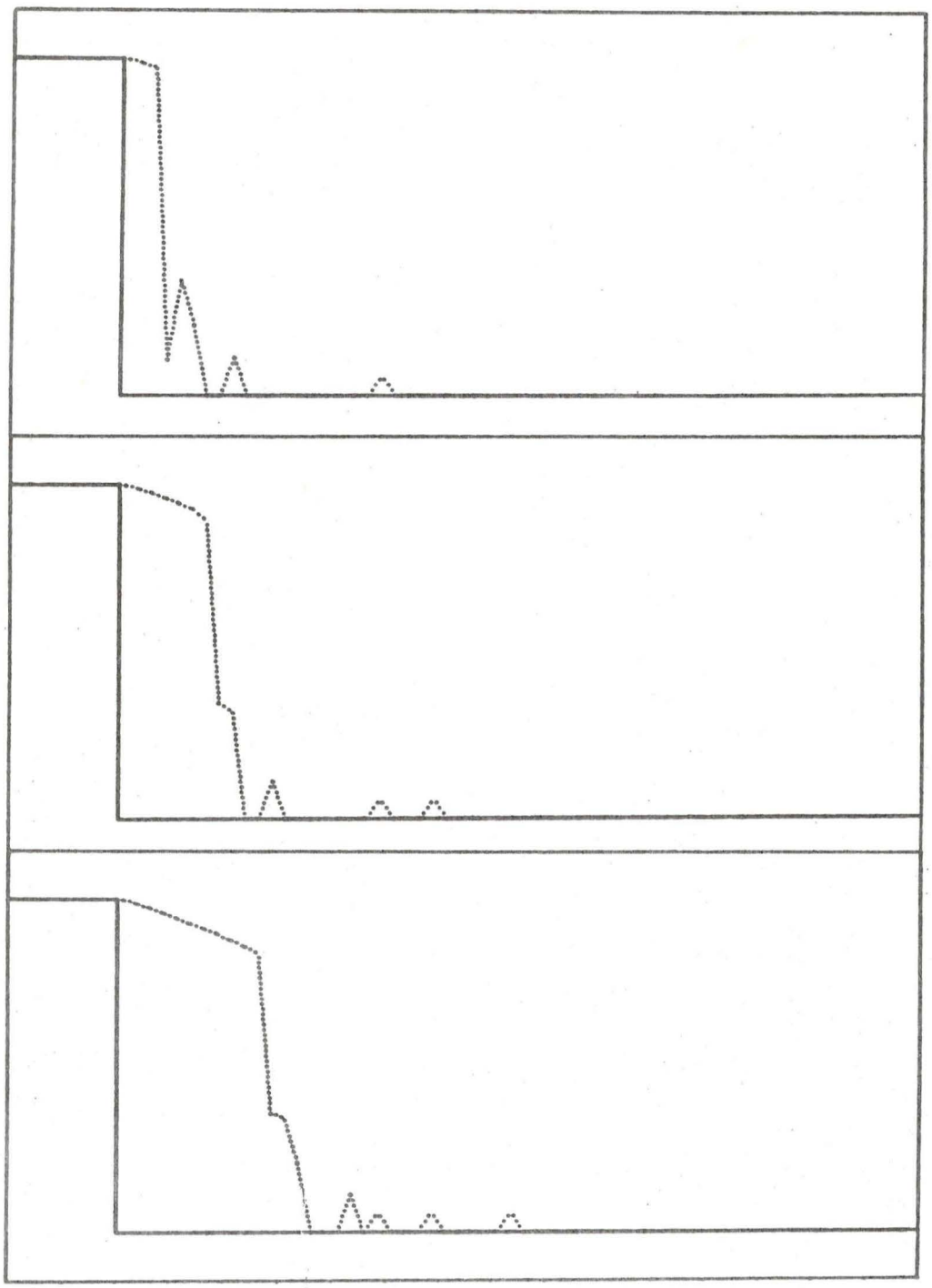

Figure 30a-c. Sensitivity analysis. All inputs are as listed in table 2 except 1) U_{max} = 7 mps, 2) h is 50% greater than that specified by equation (22), and 3) U_2/U_1 = 0.2.

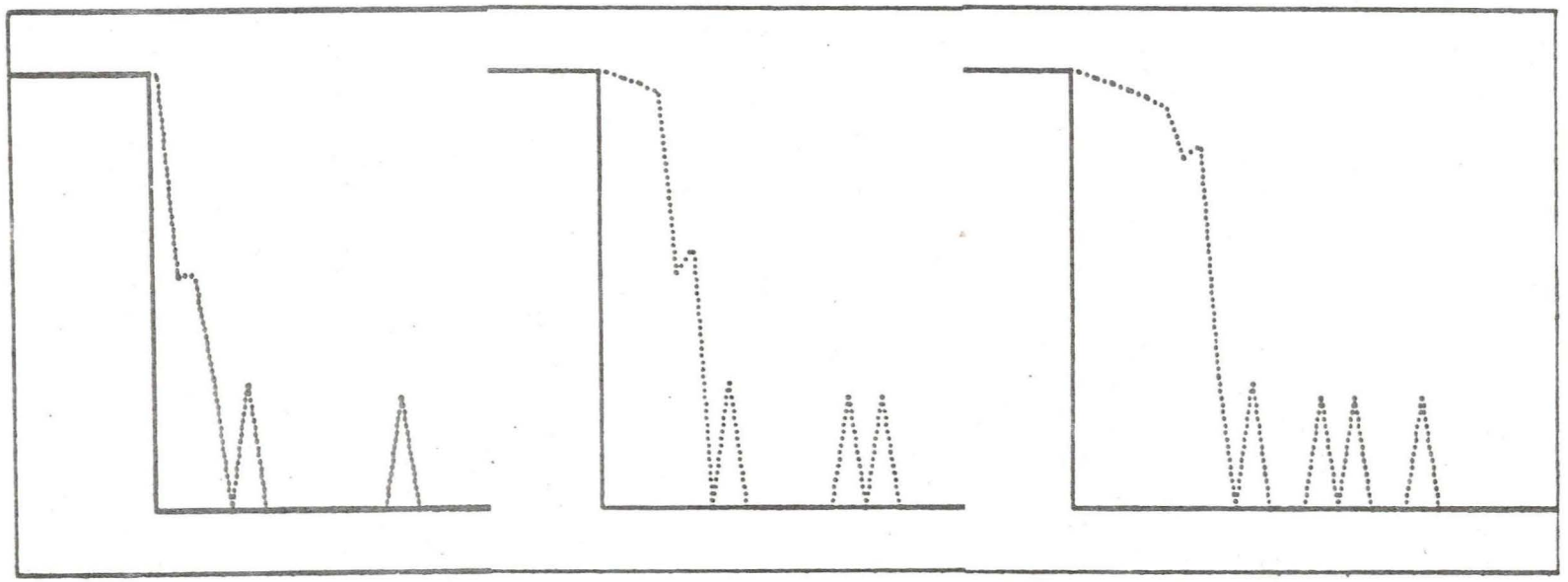

Figure 31a-c. Sensitivity analysis. All inputs are as listed in table 2 except 1) U_{max} = 10 mps, 2) h is 50% greater than that specified by equation (22), and 3) $U_2/U_1 \leq 0.2$.

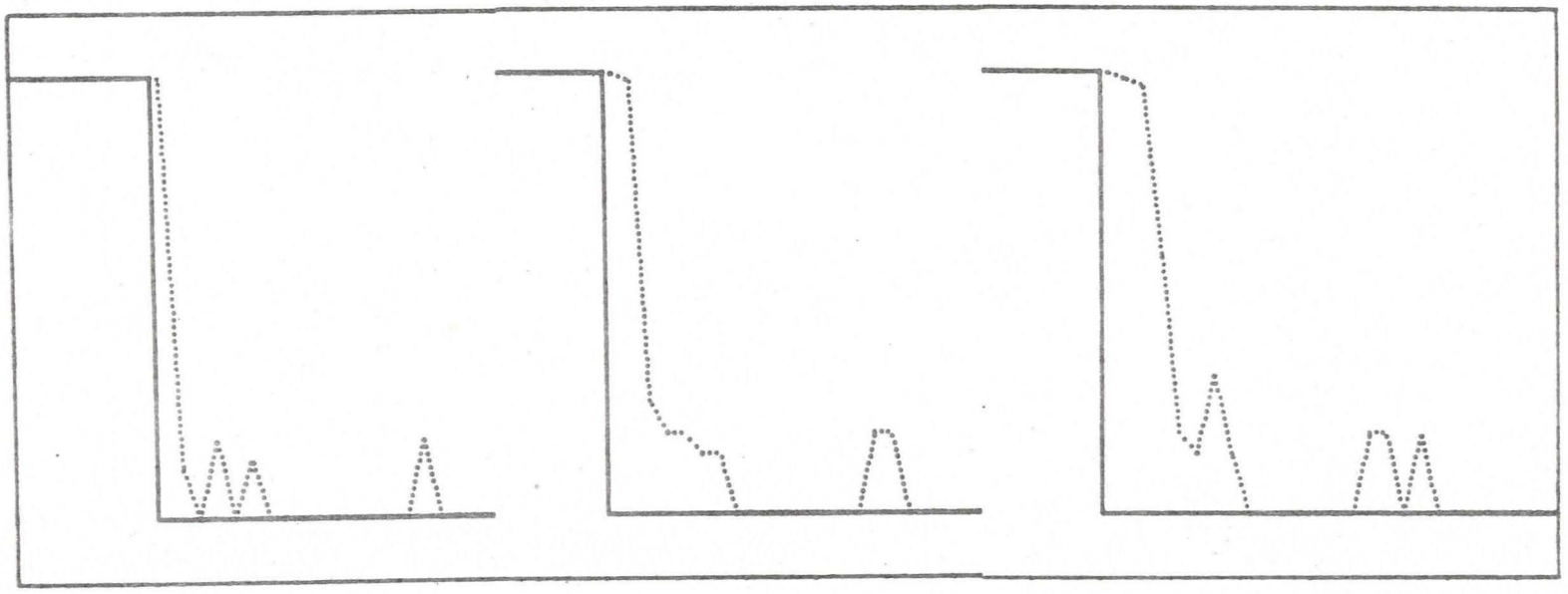

Figure 32a-c. Sensitivity analysis. All inputs are as listed in table 2 except 1) $U_{max} = 14$ mps, 2) h is 50% greater than that specified by equation (22), and 3) $U_2/U_1 \cong 0.2$.

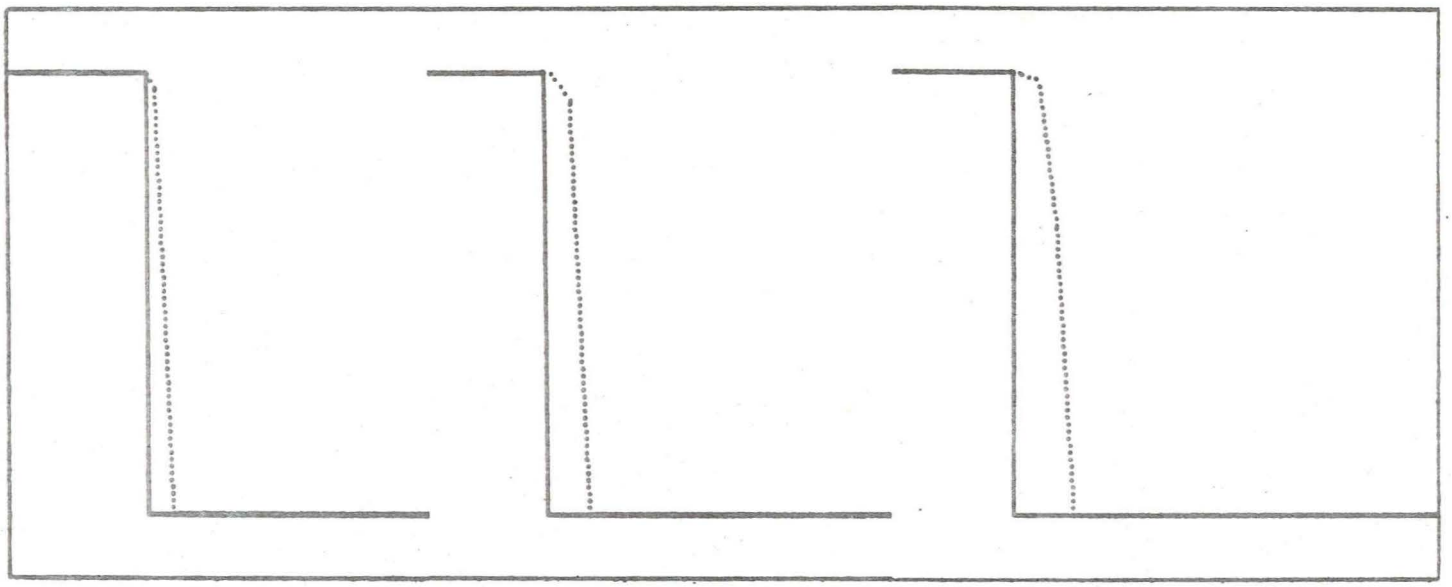

Figure 33a-c. Sensitivity analysis. All inputs are as listed in table 2 except 1) U_{max} = 18 mps, 2) h is 50% greater than that specified by equation (22), and 3) U_2/U_1 = 0.2.

As expected, blowpast increases with increasing U_{max} as shown by the reduced infill rate as U_{max} increases. For all three events where U_{max} = 7 mps, 2.3% of the total transport blows past. This snow is in the top three suspension levels (of 8 suspension layers) and includes all snow above 0.50 m height. At higher wind speeds, grains at successively lower levels blow past the trap until, in the 18 mps case, all 8 of the suspension transport levels, down to 0.07 m height and including over 77% of the total mass transport, blow past. Increasing U_{max} changes the trap configuration only slightly; it reduces the catchment length from 18.75 m (at 7 mps) to 17.75 m (at 18 mps). Thus the blowpast percentages can be compared as can the cross-sectional area occupied by snow which decreases from 19.79 square m to 4.59 square m moving from U_{max} = 7 mps to U_{max} = 18 mps.

Downwind deposition within the catchment is maximized at the lower velocities, being greatest when U_{max} = 10 mps. This results from an increase in the mass of snow moving at intermediate levels coupled with the retention of snow parcels at these levels within the catchment. Even though blowpast is 24.5% of the total mass transport and includes four levels of suspension transport (the three upper levels contain 19.1% of total transport vs. 2.3% when U_{max} = 7), particles in the lower and intermediate suspension levels, whose trajectories result in deposition within the trap and beyond the brink of the drift, account for 36% of the total transport when U_{max} = 10 mps but only 19% when U_{max} = 7 mps. The leemost deposit in figure 31a is much larger and more windward than the most downwind deposit in figure 30a since the highest suspension level contributing to the drift when U_{max} = 10 carries much more snow then the equivalent level when U_{max} = 7. Furthermore, increasing U_{max} to 10 mps forces a low level suspension layer to deposit snow downwind of the brink so that in both cases four suspension levels contribute to downwind deposition.

At higher U_{max} values saltation trajectories would be expected to thrust grains beyond the first unfilled accounting cell. In the 18 mps case this is not observed

implying that increasing h by 50% does not alter appreciably the depositional pattern of saltating grains. In the following analyses h is increased by 50%, however, to raise the level of the lower suspension transport levels.

Airflow parameters--the eddy zone

Air movement within the eddy region presupposes use of the Naib/Schlichting velocity formula (equation 6). Variables that control fluid and particle movement within this region include the location within the separation bubble at which maximum reverse flow velocity occurs and the specification of the distribution of backflow speed within the eddy zone.

(i) The location of maximum backflow

Experimentation showed no change in snow deposition pattern when the location of maximum backflow is changed from 0.80 L_b, as specified by Naib (1966), to 0.99 L_b.

(ii) Reverse flow velocity

An obvious means of increasing deposition downwind of the snowdrift brink is to decrease reverse flow velocity in the eddy zone. Input values upon which the output in figures 23 and 30 are based differ primarily in that the ratio U_2/U_1 is lower in figure 30. This change increases catchment length to 18.75 m in figure 30 and, more important, increases the downwind carry distance of suspension fallout. To test this further, a three-event run was made in which U_{max} = 10 mps, U_2/U_1 = 0.1, grain diameter = 0.07 mm and 0.15 mm, and 12 suspension layers were specified with all other parameters unchanged from the previous runs. By comparison to figure 31, figure 28 shows a longer tail of downwind deposition even though 43% of the small size fraction blows past. Two features are of interest in this regard. (1) The increased number of suspension layers coupled with the dual grain size fraction input effectively quadruples the number of parcel trajectories and as

such more realistically simulates natural movement of blowing snow. This reduces the mass apportioned to each level so that the leemost deposition is barely discernible on the figure. (2) Since the model constrains the height of the upper suspension transport layer through an input parameter and defines intermediate suspension layer heights as a power function, increasing the number of levels causes compression of the layers to the point where in this example 7 of the 12 suspension layers are below 8 cm height. Of the 12, three contribute to blowpast for the larger grain size, five cause deposition beyond the brink, and four result in deposition at the brink.

Airflow parameters--the mixing region

As will be reaffirmed in the comparison of modelled to observed drift cross-sectional profiles, the lower mixing region angle, β, and the threshold speed for particle entrainment/deposition, U_t, are important parameters since they determine the heights of the accounting cells. Thus, while most other parameters only slightly influence the shape of the trap, U_t and β profoundly alter the location of the snow surface of the potential drift and as such directly influence all depositional mechanisms.

Use of the Albertson mixing region velocity distribution also influences determination of the shape of the catchment by controlling the height at which U_t occurs. The upper mixing region angle, α, does not affect catchment shape but rather controls the point of intersection of saltation and suspension grain trajectories with the mixing region upper boundary.

(i) The upper mixing region angle, α

Variation in α affects the height at which saltating grains enter the mixing region by increasing zsalt (figure 17) as α increases. The structure of the model is such that the height of all suspension levels develop from zsalt so that it is difficult to analyze the model response to changes in α since the resulting changes

in the heights of suspension layers mask any direct effects of α by itself. However, at a given height, suspended grains enter the mixing region sooner with a higher value of α thereby allowing parcels at lower levels to enter the catchment. This is demonstrated by a comparison of cases in which $\alpha = 5^{o}$ and $\alpha = 10^{o}$ when, in the third event with $\alpha = 5^{o}$, blowpast includes an additional suspension layer which is not included when $\alpha = 10^{o}$. This data is somewhat inconclusive since 1) the difference between $\alpha = 5^{o}$ and $\alpha = 10^{o}$ is not great, 2) insufficient levels are specified to adequately isolate differences, and 3) the suspension layer heights are not directly comparable due to differences in zsalt.

(ii) Threshold speed for grain entrainment/deposition, U_{t}

With $\beta = 7^{o}$ and U_{t} increased from 0.5 mps to 2 mps (figure 34), the catchment length increases to 23.75 m, the cells are taller and the surface slope of the drift decreases. Consequently blowpast decreases, from 2.3% to 1.9%, since the leeward extent available for deposition is lengthened.

The location within the mixing region at which U_{t} occurs can have a positive value so that the surface rises with increasing distance downwind. The slight positive value for the snow surface height immediately leeward of the lip of the trap (figure 34) shows this. If U_{t} is greater than approximately 0.5 U_{max} this rising tendency is pronounced so that the potential snow surface may not intersect the ground surface downwind.

(iii) The Albertson mixing region velocity distribution

When the air speed within the mixing region is calculated to follow the normal probability distribution suggested by Albertson et al (1950) the velocity shear is great in the middle section of the mixing zone. Thus low speed flow occurs in the lower portion of this region with high speed flow in the upper portion and a steep gradient between the high and low speed regions. By comparison to the Naib velocity function for the mixing region, the Albertson method gives a lower snow

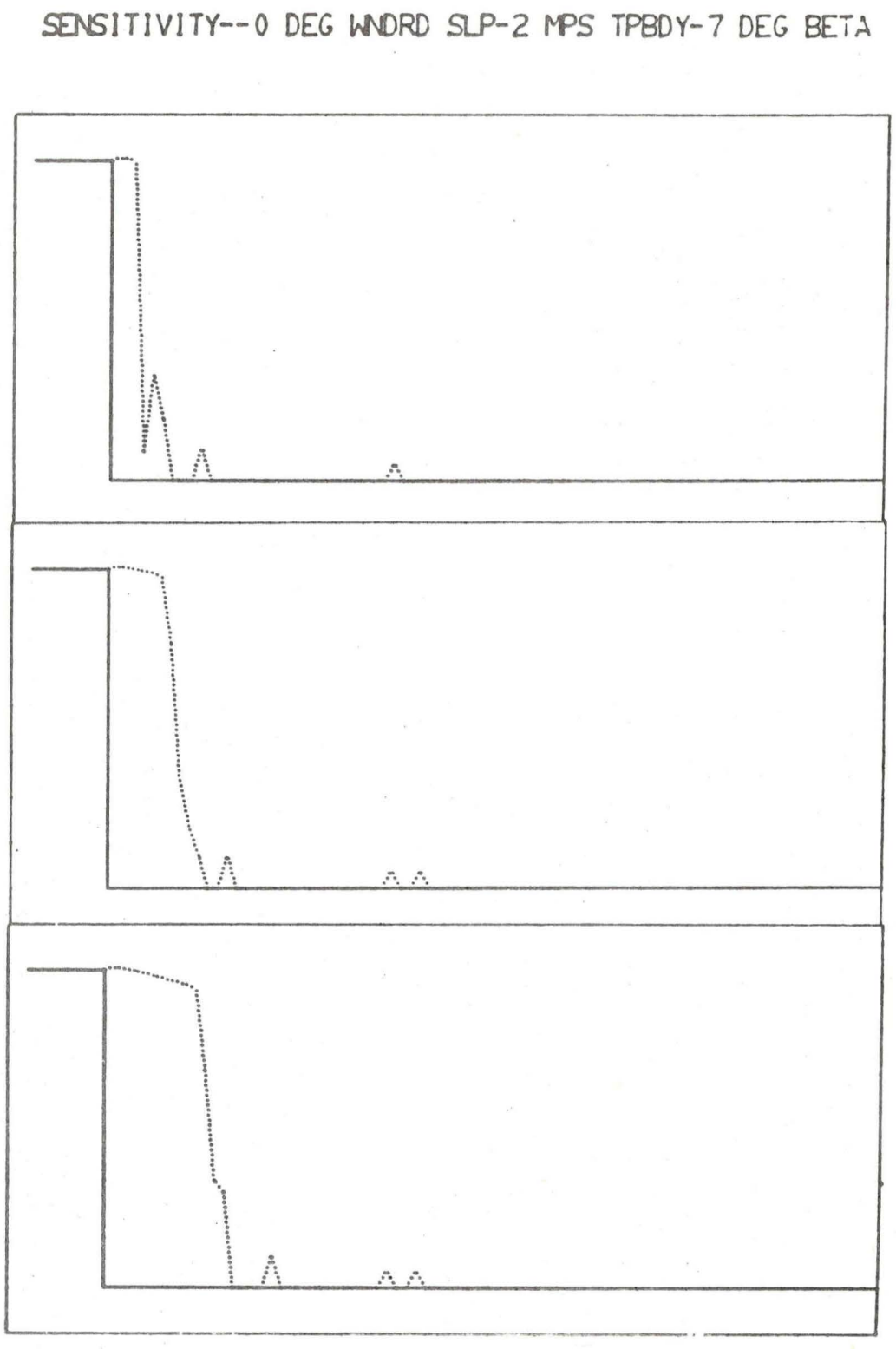

Figure 34a-c. Sensitivity analysis. All inputs are as listed in table 2 except U_t = 2 mps.

surface slope which lengthens the catchment from 18.25 to 31.75 m. This in turn decreases blowpast to 0.9% and greatly extends deposition to leeward (figure 35). In the case where $\beta = 7^{o}$ and $U_{+} = 0.5$ mps the snow surface immediately leeward of the lip of the trap rises suggesting that, as with U_{+}, the probability is high under some conditions that the drift snow surface may not intersect the ground surface to leeward.

(iv) The lower mixing region angle, β

Specification of the upper surface of the potential catchment is also highly sensitive to β. In figure 36, where $\beta = 15^{o}$, it is clear that 1) the upper surface of the drift dips more steeply than in the control case (figure 23), and 2) downwind deposition beyond the brink of the drift is negligible. The increase in β shortens the separation bubble to 11.25 m in length and, since other airflow parameters remain unchanged, blowpast increases to 15.2% of the total transport and involves 6 of the 8 suspension levels. Thus little fallout from suspension occurs downwind of the brink of the drift.

Determination of β directly by the model follows from figure 9 as $\beta = \arctan(H/L_{b})$. With all other inputs as specified in table 2, β equals 9.83^{o} (figure 37), catchment length is reduced to 14.75 m, and blowpast increases to 4.5% of total mass transport. Reduction of boundary layer thickness to 5 m lowers β to 7.31^{o} (figure 38) but also increases U_{*} by 15%. The consequent increase in blowpast to 9.2% of total transport is probably more in response to the increase in U_{*} than the reduction of β.

Before arriving at values for β and U_{+} in the comparison between observed and modelled drift cross-sectional profiles, numerous runs were made at various values of these parameters. Slight variation in U_{+} drastically shifts the leeward edge of the catchment especially when U_{max} is low. Although β is less sensitive, its value also alters the reattachment point. These results suggest that β is a function of

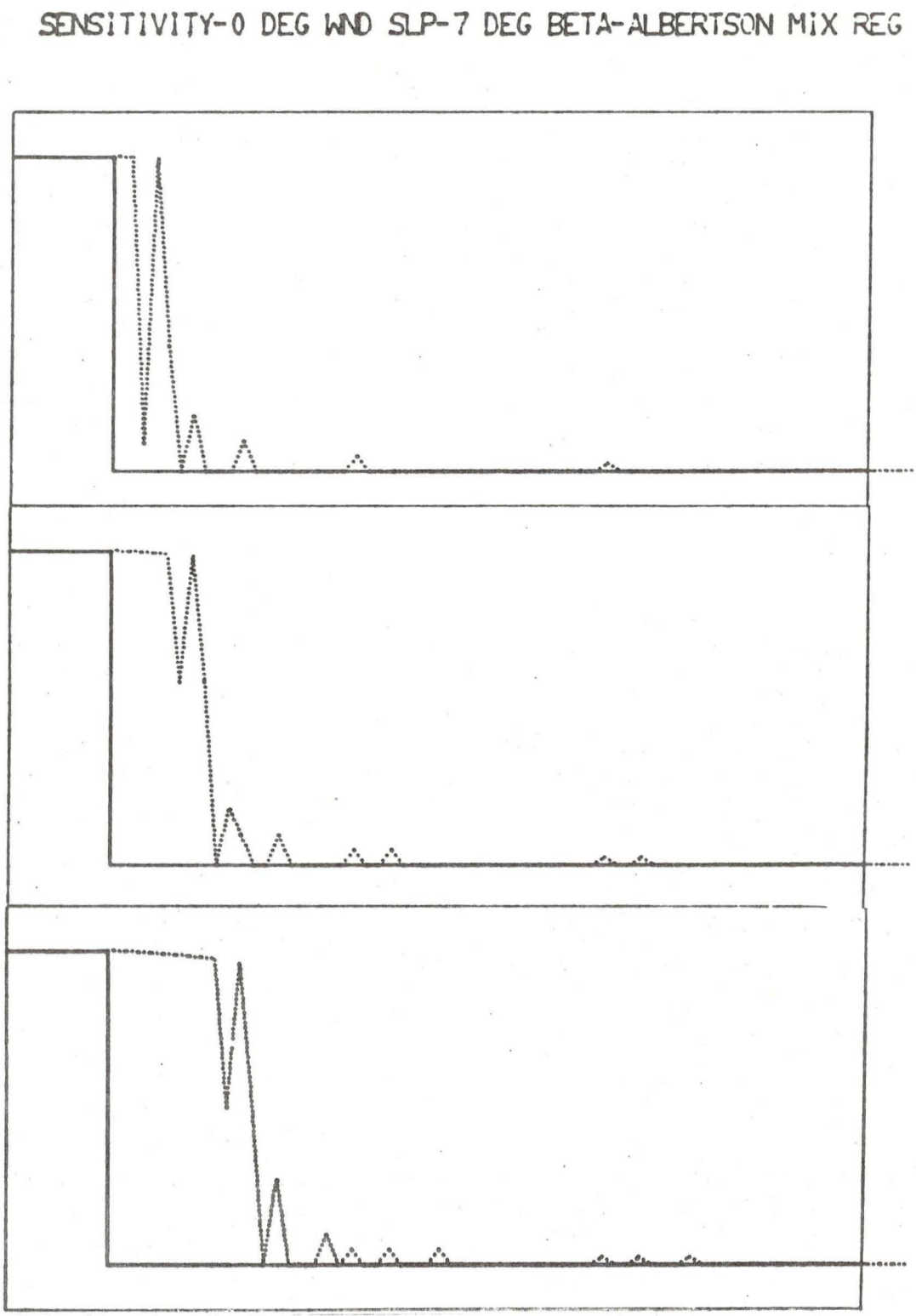

Figure 35a-c. Sensitivity analysis. All inputs are as listed in table 2 except for the usage of the Albertson et al (1950) mixing region velocity function.

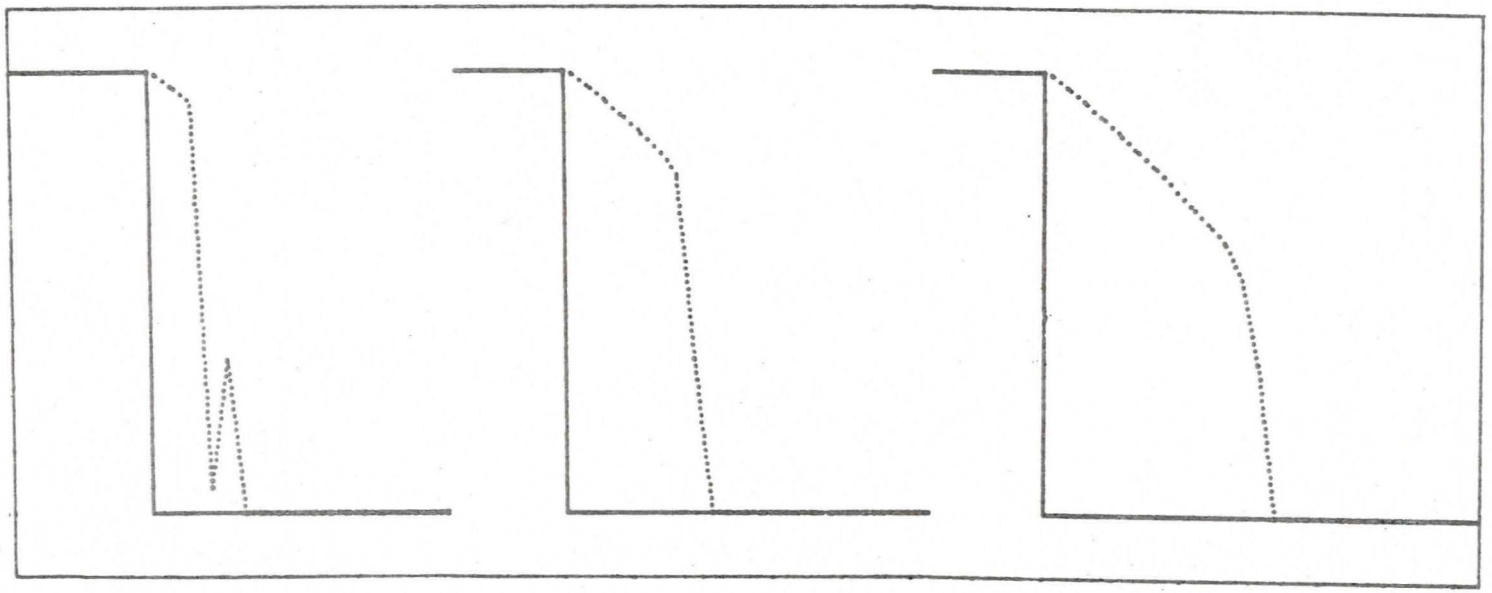

Figure 36a-c. Sensitivity analysis. All inputs are as listed in table 2 except $\beta = 15^{o}$.

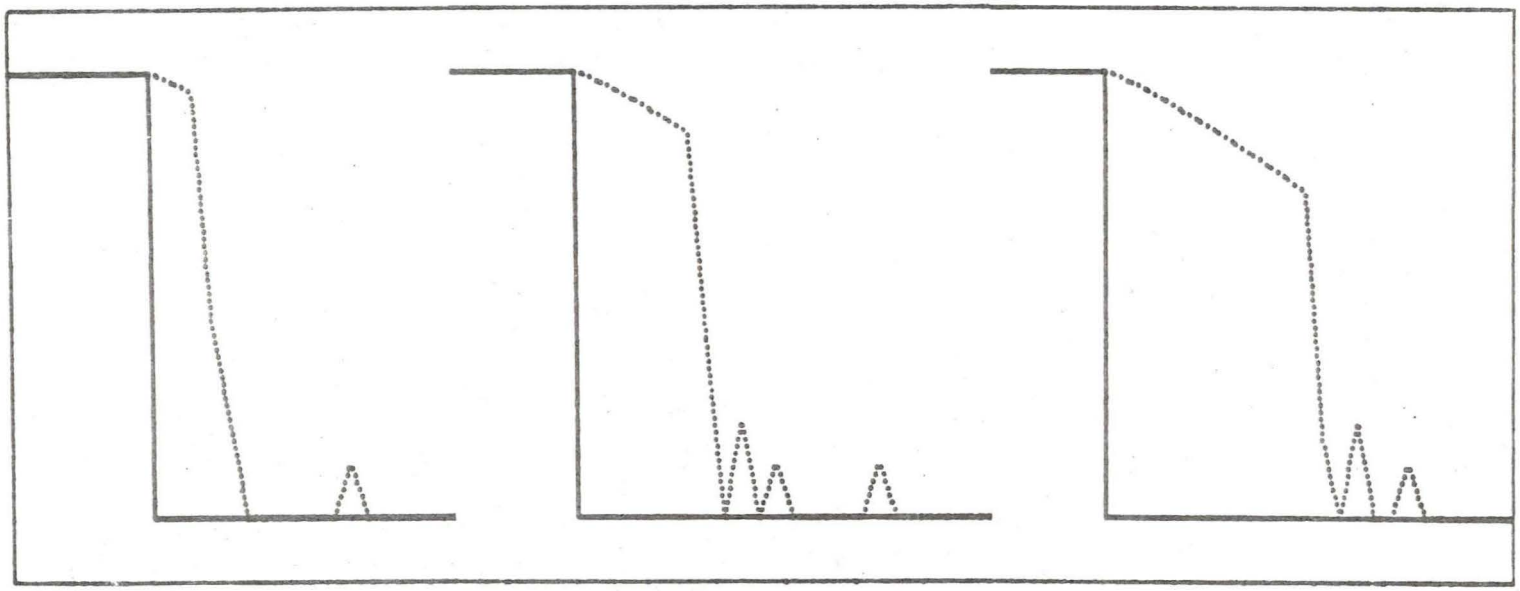

Figure 37a-c. Sensitivity analysis. All inputs are as listed in table 2 except $\beta = 9.83^{\circ}$ as determined by the model.

SENSITIVITY-0 DEG WND SLP-MODEL DEFINED BETA-BLTHK = 5

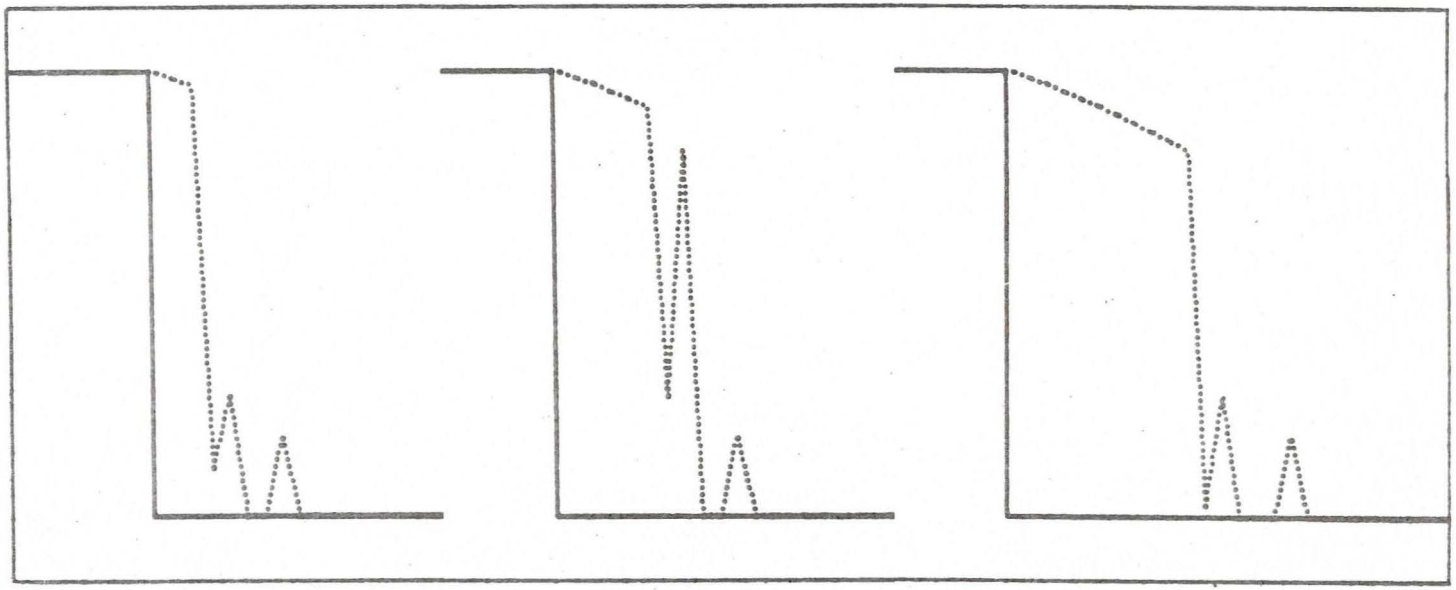

Figure 38a-c. Sensitivity analysis. All inputs are as listed in table 2 except 1) boundary layer thickness = 5 m, and 2) $\beta = 7.31^{\circ}$ as determined by the model.

windward approach slope so that the relationships shown in figure 9, based on a horizontal approach slope, may not apply when the approach angle deviates significantly from 0^{o}. This is supported intuitively by considering the extreme cases of vertical up and down flow from an orifice. There should be greater spread of the emerging flow in the "straight up" configuration wherein flow is directly against gravity than if the emerging jet faces down and the direction of flow compliments the gravitational force.

Topographic parameters

(i) Windward approach slope

The approach surface is also of interest because cornices typically develop at ridge crests where an abrupt ground slope discontinuity forces great flow expansion. It is suggested that blowpast should be great in this situation since grains have so large an upward velocity component as to be carried beyond the eddy zone. Conversely, downslope approaches should give a gradual tailing off of deposition to leeward with relatively little blowpast. The approach slope has in fact been suggested as a control for whether cornices or snowdrifts develop (Santaford, 1972). Experimentation with the model illustrates two points. (1) The area of potential drift accumulation is larger in upslope rather than downslope approach situations since flow reattachment occurs sooner when the flow is initially directed downward. (2) Such a shortening should increase blowpast but the downslope component of the initial airflow orientation tends to compensate by shortening the suspension particle trajectories. Figures 39 and 40 illustrate the two cases. In figure 39 the drift surface rises above the origin and truncates abruptly similarly to a cornice although there is some downwind deposition since the catchment extends leeward to 32.5 m. In the downslope approach case (figure 40) in which the potential trap is 10.75 m long, a tendency to taper off to leeward can be seen. Blowpast in both cases is minimal, illustrating the effects of 1) the transport of most suspended

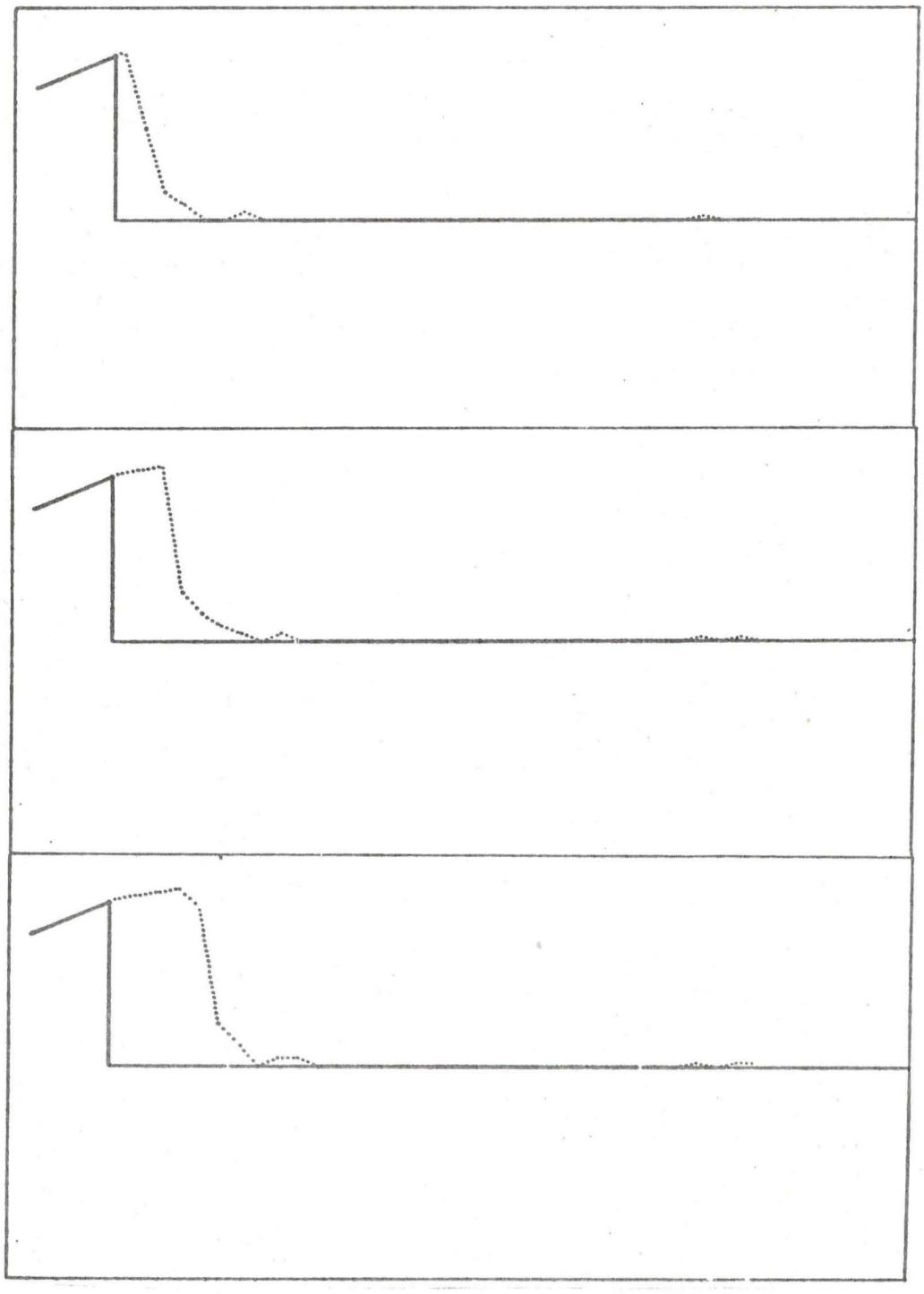

Figure 39a-c. Sensitivity analysis. All inputs are as listed in table 2 except the approach slope angle = $+10^{\circ}$.

SENSITIVITY-15 DEG DNW WND SLP-BETA=7 DEG UMAX = 7

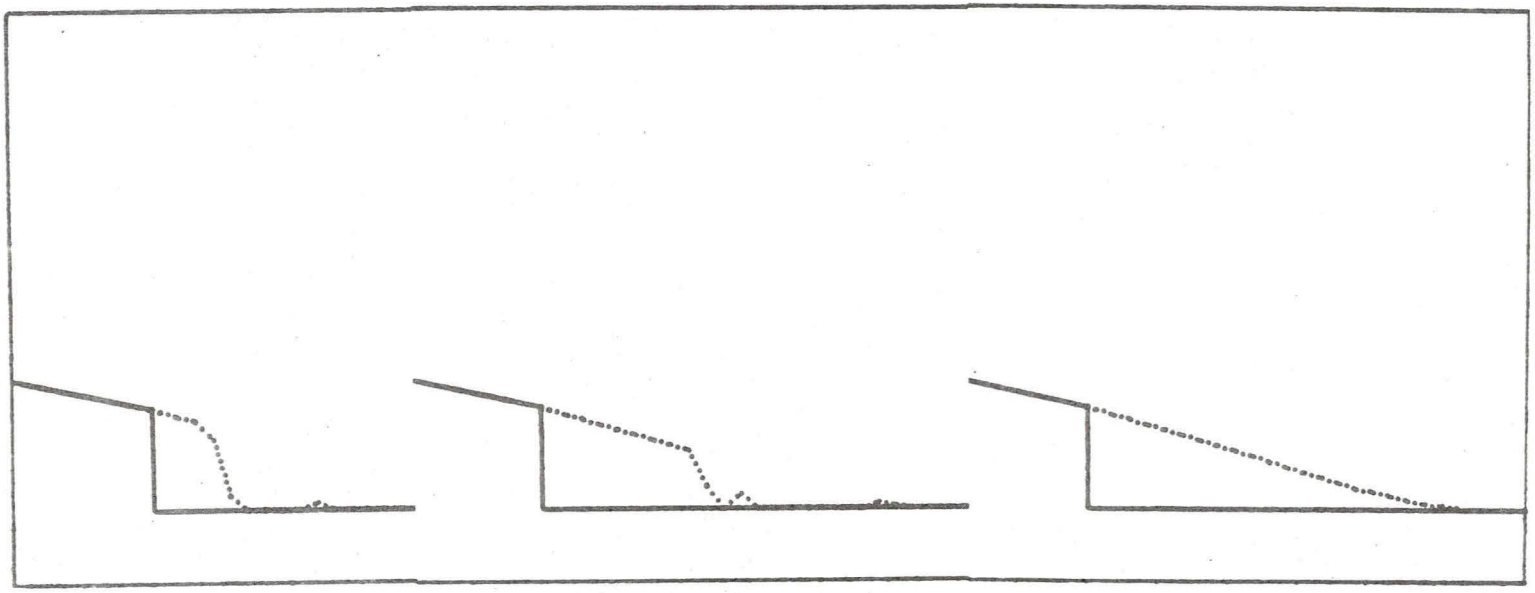

Figure 40a-c. Sensitivity analysis. All inputs are as listed in table 2 except the windward approach slope angle is 15^{o} downslope.

snow settles out beyond the cornice due to the larger catchment, and 2) the downwarping of the particle trajectories in the downslope approach situation which reduces blowpast.

Increasing U_2/U_1 to 0.7 in the upslope approach case (figure 41) better simulates natural cornice development by forcing suspension fallout back toward the brink of the drift. However, there is no reason for expecting such an increase in reversed flow velocity with increased upslope approach angle.

(ii) Exhaust slope

Exhaust slope angle influences catchment shape by altering the location of the flow reattachment point. In the upslope exhaust angle configuration the catchment is shortened to 10.75 m in length (figure 42). Catchment length increases to 19.25 m in the downslope exhaust angle situation (figure 43) even with $\beta = 10^{o}$.

Blowpast

As suggested in previous paragraphs blowpast is dependent upon several input parameters. Blowpast increases with increasing U_{max} and decreasing β and with small grain size. Since changes in U_t and the approach slope angle affect the potential drift surface configuration they, too, influence blowpast. Further, blowpast should increase with infilling, as the effective size of the trap becomes small, and this is also suggested by the model. Such a relationship between blowpast and catchment saturation has been suggested by Tabler (1972). His work shows blowpast to remain relatively constant at a low value, ca. 15%, until the catchment is ca. 80% filled. Evaluation of this relationship is difficult with the current structure of the model since judicious specification of transport quantities and/or duration of events is needed to exceed the 80% saturation level without completely filling the trap. Nevertheless the available data shows that blowpast remains constant, and usually less than 10% of the total transport, over the range up to ca. 80% saturation, and that blowpast does increase as saturation is approached--in one

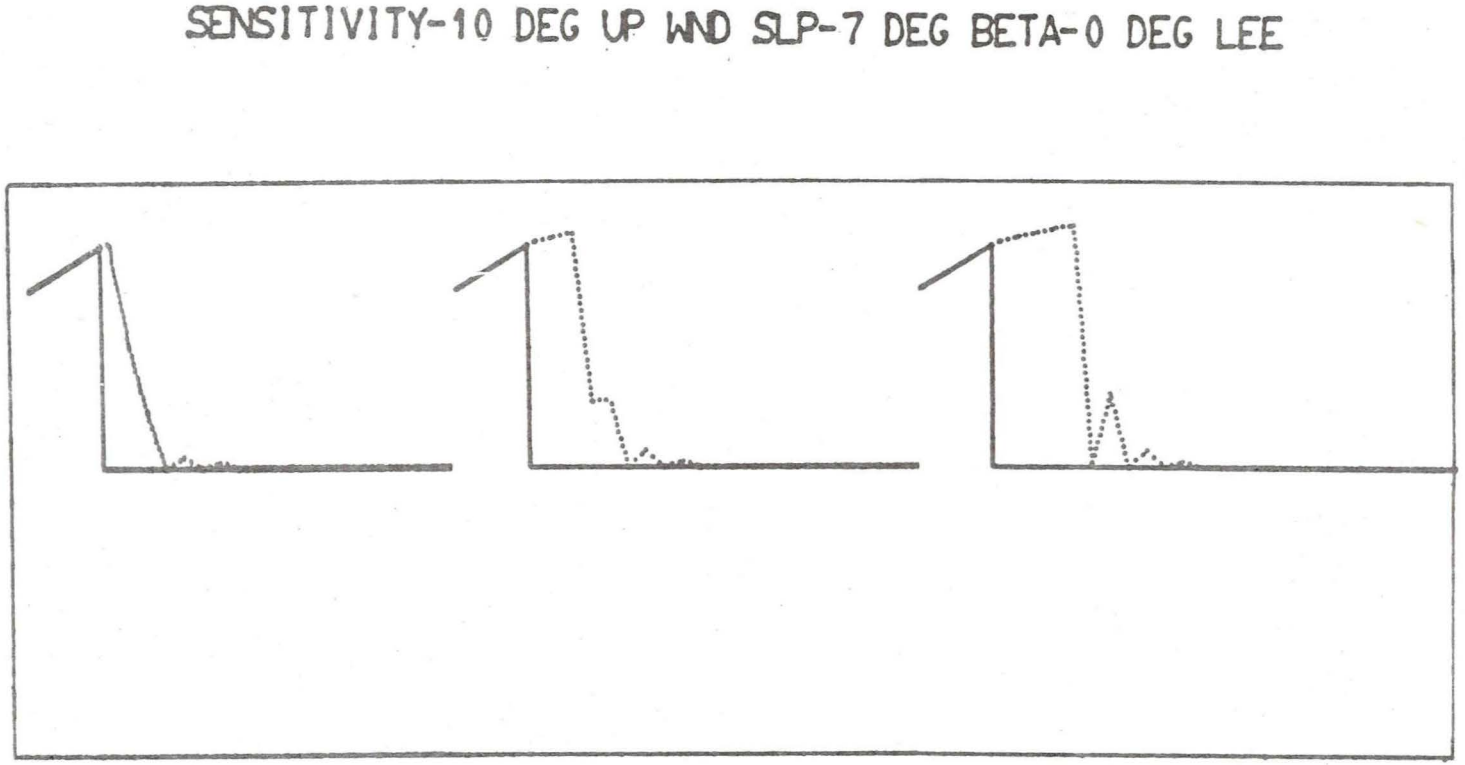

Figure 41a-c. Sensitivity analysis. All inputs are as listed in table 2 except 1) U_2/U_1 = 0.7, and 2) the windward approach slope angle is 10^{o} upslope.

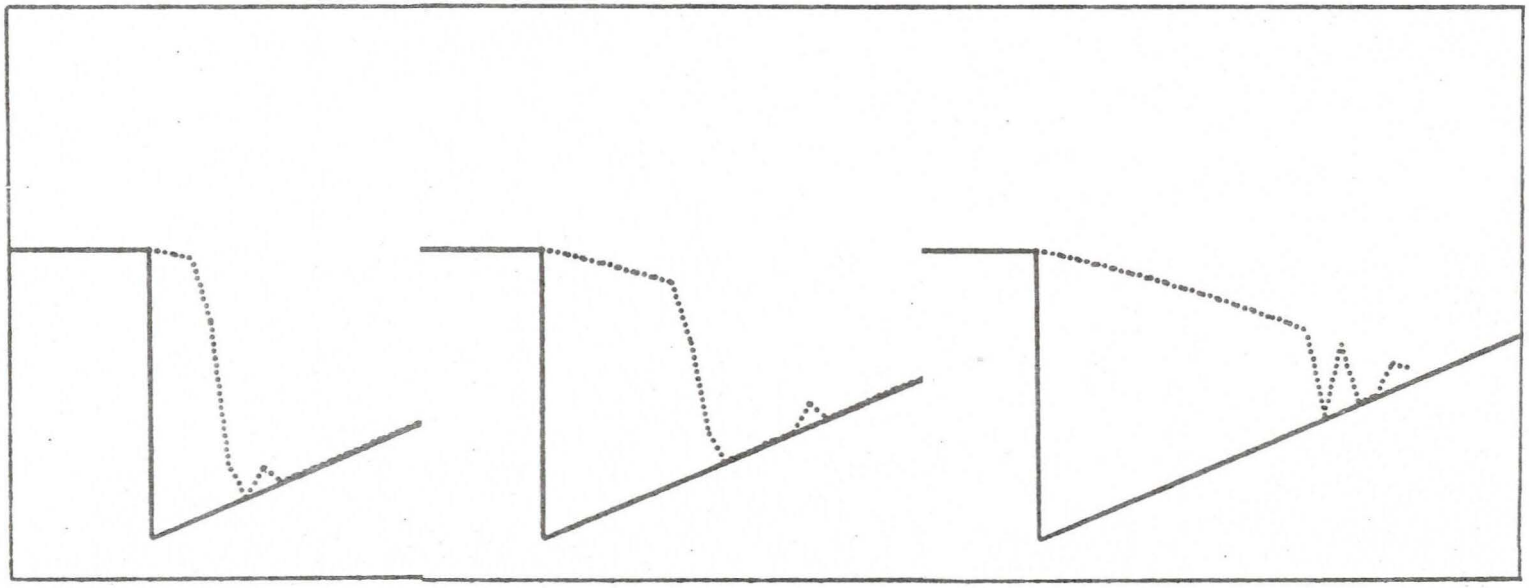

Figure 42a-c. Sensitivity analysis. All inputs are as listed in table 2 except the exhaust slope angle is 10° upslope.

SENSITIVITY-0 DEG WND SLP-5 DEG LEE DWNSLP-10 DEG BETA

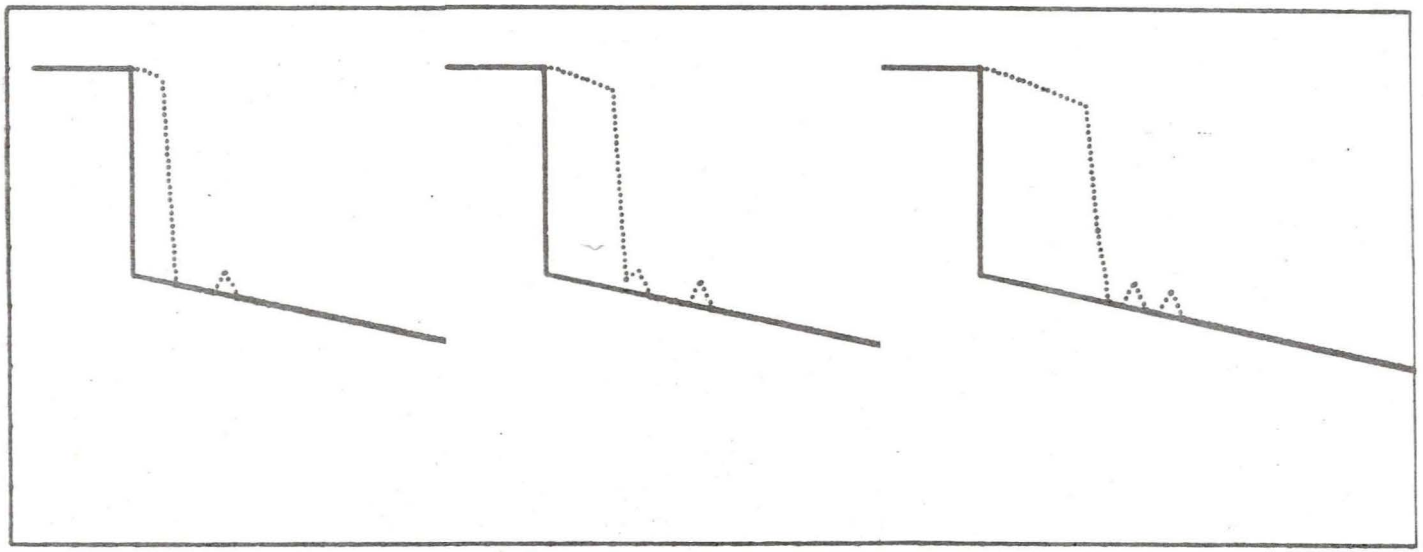

Figure 43a-c. Sensitivity analysis. All inputs are as listed in table 2 except 1) exhaust slope angle = 5^{o}, and 2) $\beta = 10^{o}$.

example at 92% saturation, blowpast was 30%. It must be stressed, however, that the main conclusion from this study with regard to blowpast is its dependence upon a multitude of parameters, particularly under conditions where the catchment is relatively empty.

Comparison with Finney's and Tabler's analyses

Recently Tabler (1975) has compared results from his regression model of snowdrift development with those from Finney's wind tunnel simulation of natural snowdrift accumulation (Finney, 1939). One result of the scale model tests was the finding that accumulation does not occur on embankments whose downslope angle is less than 17%. Experimentation with the model described here also predicts only shallow deposition on slopes approximating -17% (figure 44). On steeper embankment slopes Finney's and Tabler's results differ from those reported here in that catchment length (18.25 m for a 25% embankment, figure 45, and 18.25 m for a 20% embankment, figure 46) is shorter than that reported by other workers. However, catchment length and drift surface slope are directly dependent upon β and U_t values so that a more realistic U_t value, approximating 2 mps, would lengthen the trap.

A COMPARISON WITH FIELD OBSERVATIONS

Field observations from one of the larger catchments, North Slope site (figure 21), were chosen for comparison with the modelled output. Only the first month's accumulation during 1974 is considered since this time period is adequate for illustration of most of the comparative features. Over this period the drifts were monitored on October 15, 16, 20, 24, 28, and November 1, 5, and 11. Model input values were specified in the following manner.

Topographic data input to the model is that from the summer field surveys as shown in figure 19. The point of initial accumulation was chosen as a major break in slope (196.9 m on N. Slope).

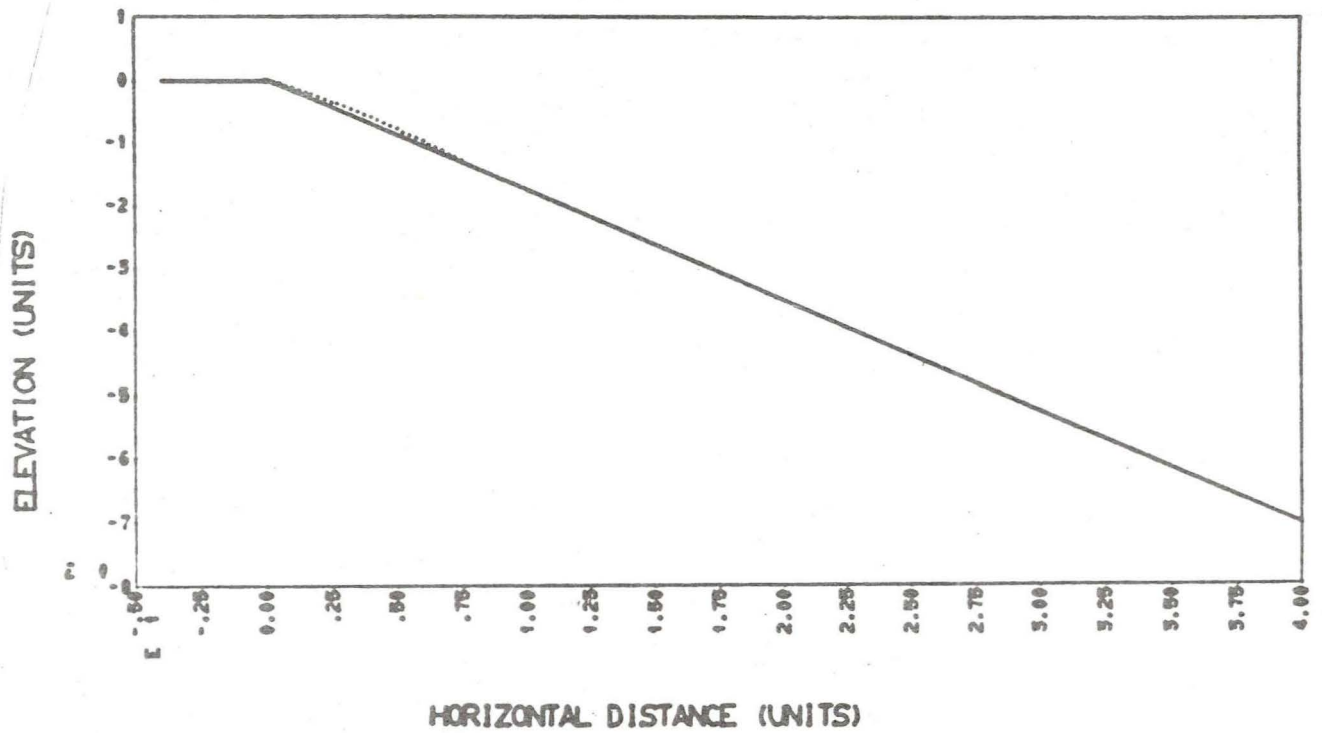

Figure 44. Comparison with Finney (1939) and Tabler (1975) analyses. Exhaust slope angle = -17%.

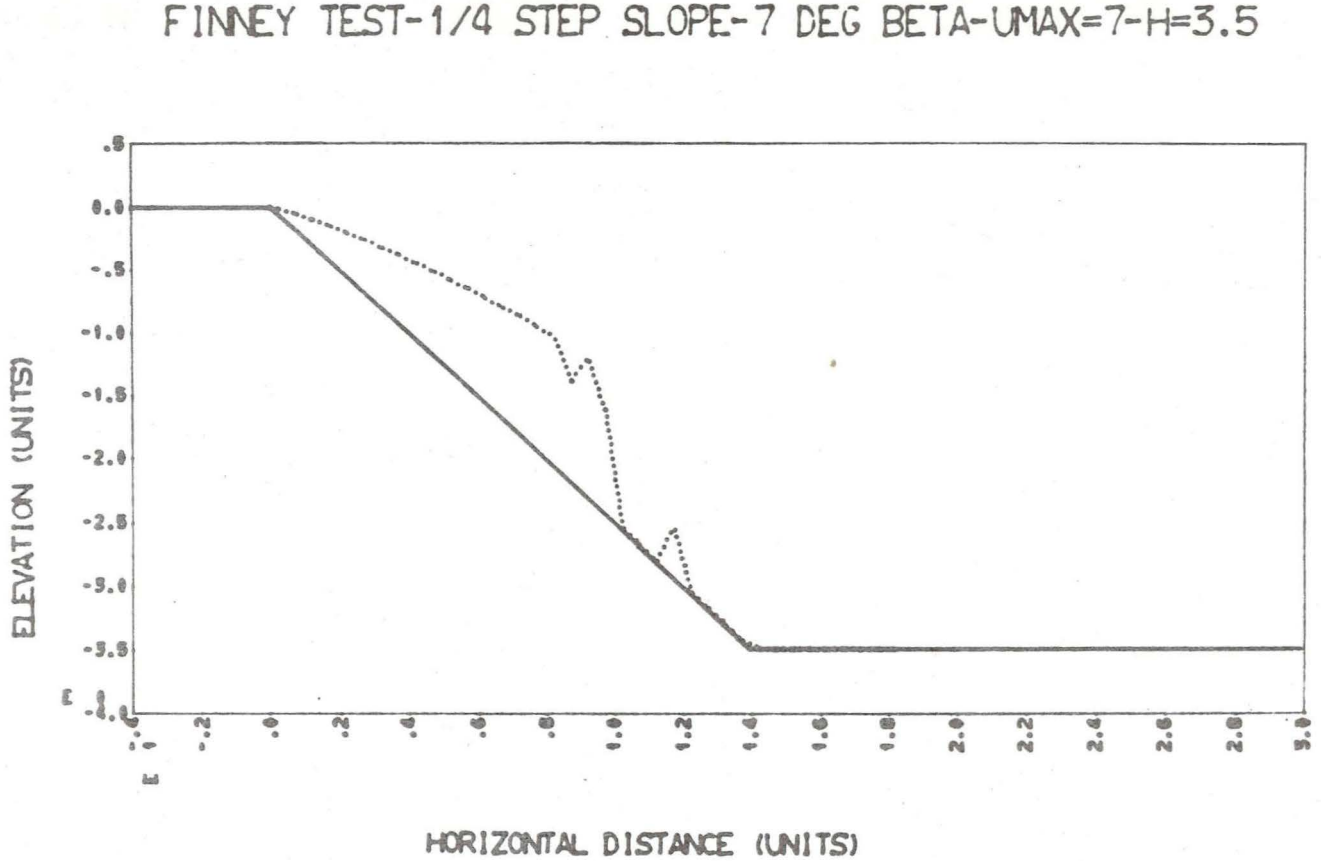

Figure 45. Comparison with Finney (1939) and Tabler (1975) analyses. Exhaust slope angle = -25%.

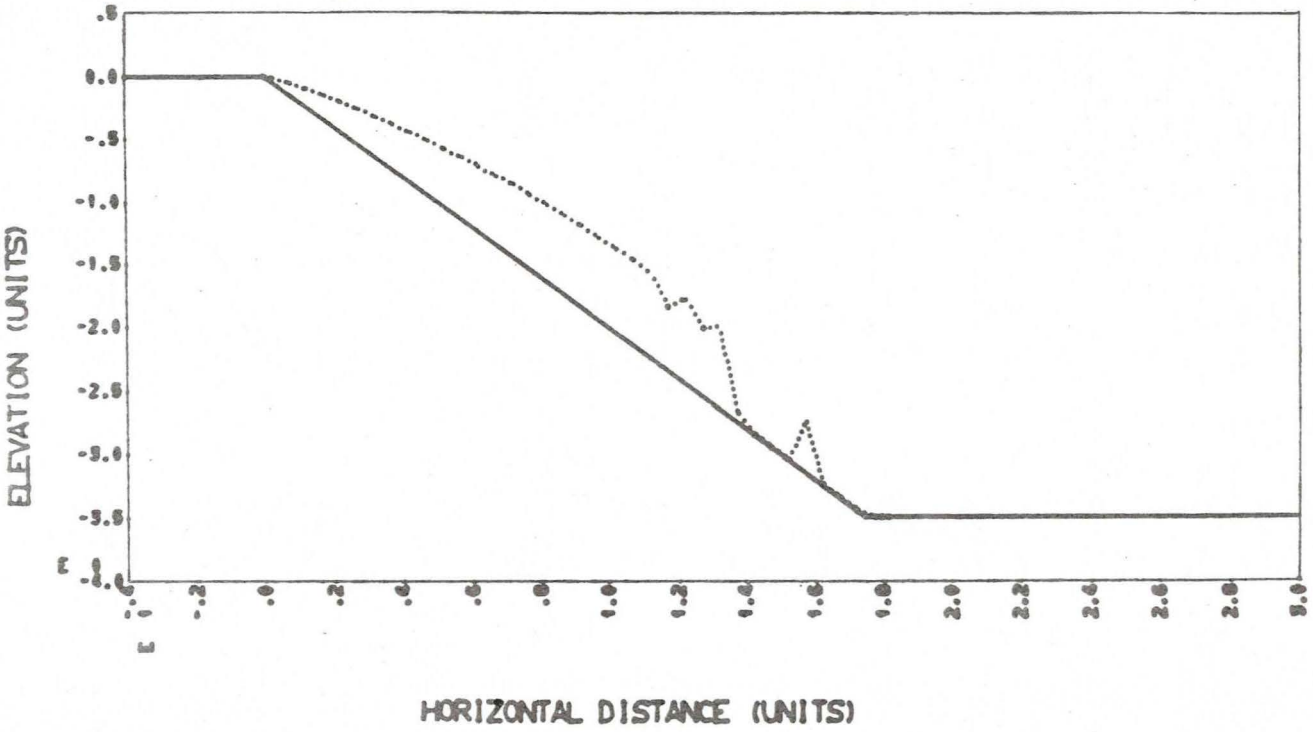

Figure 46. Comparison with Finney (1939) and Tabler (1975) analyses. Exhaust slope angle = -20%.

Several assumptions were made for the airflow data input to the model. Boundary layer thickness was assumed equal to 10 m and the wind speed at this height was calculated as a log-law extrapolation from the mast wind speed value. Twelve-hour mean values were used to economize computational cost. The roughness value was assumed equal to 0.004 m and equation (6) specified the mixing and eddy zone velocity profiles.

The best form of the model was used as determined from the sensitivity analysis. This included setting U_2/U_1 equal to 0.05, increasing saltation layer thickness by 50% over that specified by the Owen procedure (equation 22) and the use of 12 suspension levels. Values in table 3 are those for variables which remain constant through all events and table 4 shows values that vary between events. A single grain size fraction was used and α and β were defined by trial and error when it became apparent that specification of β by the model resulted in premature reattachment immediately downwind of the origin.

Since the snow particle counter was not in operation from 10/11 to 11/10, 1974, blowing snow events had to be estimated by the method described in Appendix I. Briefly, precipitation, wind speed, and temperature information was analyzed to determine time periods during which the potential for blowing snow was high. Table 4 lists the characteristics of the blowing snow events determined for the period 10/11 to 11/10, 1974.

The modelled cross-sectional profiles (figure 47) and those measured in the field (figure 21) are reasonably comparable in terms of (1) the cross-sectional area occupied by snow and (2) the general upper surface of the drift. Close inspection, however, shows discrepancies in (1) deposition beyond the brink of the snowdrift, which is often very variable in the model, showing jagged peaks of accumulation, (2) insufficient deposition at the brink and downwind of it on the modelled profile during the latter stages of the one-month period, and (3) a lack of accumulation in

Table 3. North Slope site model input parameters remaining constant through all blowing snow events.

Point (0,0)	196.9 m
β	1.96^{o}
α	5.39^{o}
U_t	2.5 mps
d	10 m
k	0.4
ρ_d	0.5 g cm^{-3}
U_2/U_1	0.05
CREP	0.1
D	0.1 mm
ILAY	2
IANG	Angular
z_o	0.004 m

Table 4. Variable input parameters for North Slope site blowing snow events between 10/11 and 11/11, 1974.

Blowing Snow Event	Date	U_{max} [1]	q_d (g cm^{-1} sec^{-1})	$U_{8.74}$	Drift Survey Date	Duration Of Event (hrs)	$m_{w(i)}$ [2]	m_T [3]
1	10/13	6.9	0.052	6.8	10/15	12	2.3×10^{3}	1.2×10^{5}
2	10/14	6.4	0.040	6.3	10/15	12	1.7×10^{3}	
3	10/14	12.1	0.275	12.0	10/15	12	1.2×10^{4}	
4	10/15	16.1	0.640	15.9	10/15	12	2.8×10^{4}	
5	10/15	14.8	0.497	14.6	10/15	12	2.2×10^{4}	
6	10/16	8.8	0.105	8.7	10/16	12	4.5×10^{3}	
7	10/30	17.5	0.820	17.3	11/1	24	7.1×10^{4}	8.3×10^{4}
8	10/31	12.2	0.280	12.1	11/1	12.5	1.2×10^{4}	
9	11/4	7.8	0.070	7.7	11/5	12	3.0×10^{3}	5.4×10^{4}
10	11/4	8.9	0.110	8.8	11/5	12	4.8×10^{3}	
11	11/6	13.1	0.340	12.9	11/11	12	1.5×10^{4}	2.4×10^{4}
12	11/7	9.4	0.130	9.3	11/11	12	5.6×10^{3}	
13	11/8	9.8	0.150	9.7	11/11	12	6.5×10^{3}	
14	11/10	11.7	0.250	11.6	11/11	12	1.1×10^{4}	
15	11/10	16.0	0.630	15.8	11/10	6	1.4×10^{4}	

[1] U_{max} refers to the mean wind speed over the duration of the specified event

[2] $m_{w(i)}$ refers to the total mass of snow transported per cm width and is calculated as the product of q_d and the duration of the event in seconds

[3] m_T refers to the total mass of transportable snow as calculated from equation (33) utilizing precipitation data from figure 22

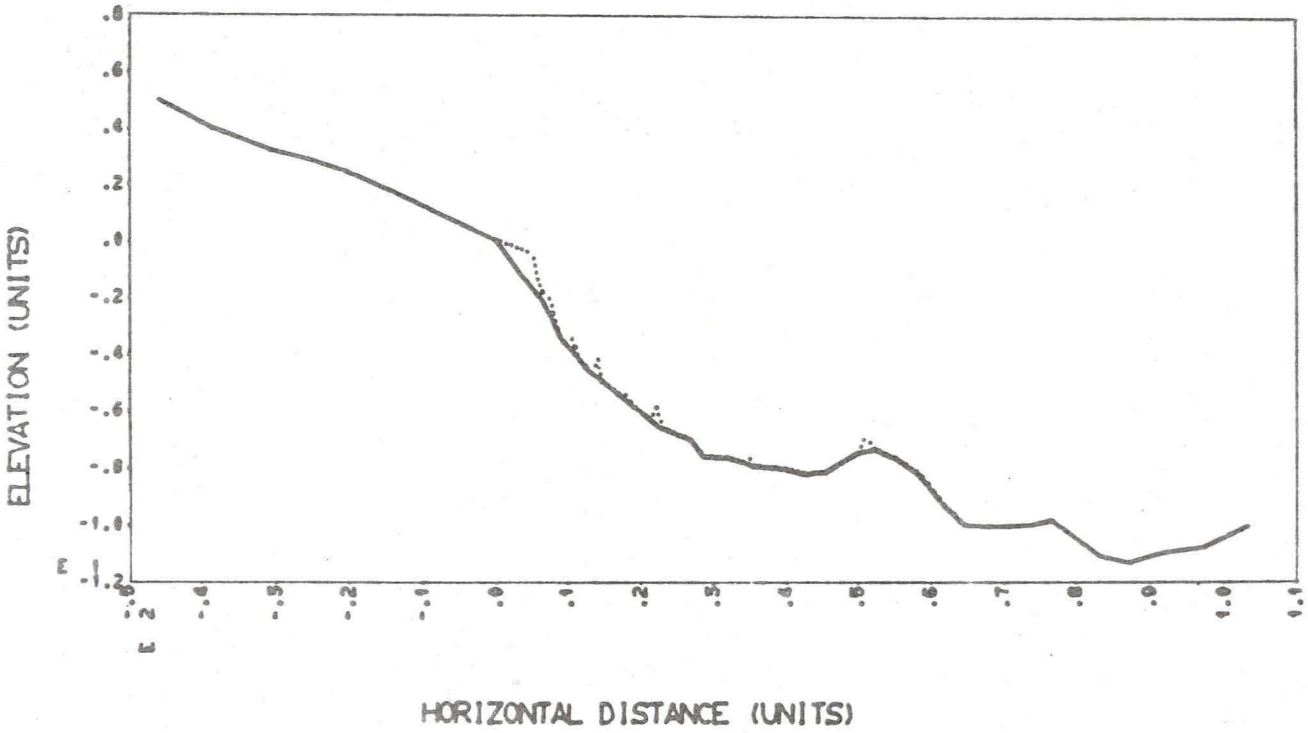

Figure 47a. Modelled snowdrift development along Slope site, North line, 10/15/74.

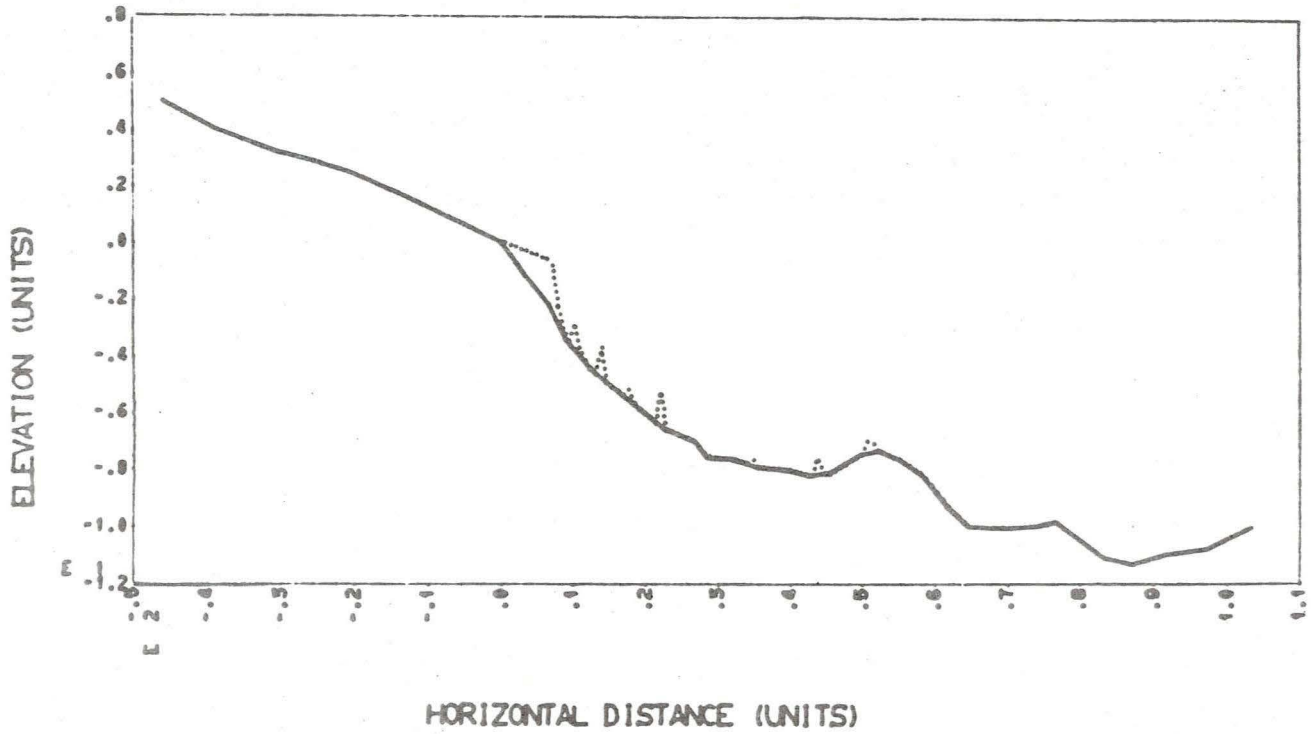

Figure 47b. Modelled snowdrift development along Slope site, North line, 10/16/74.

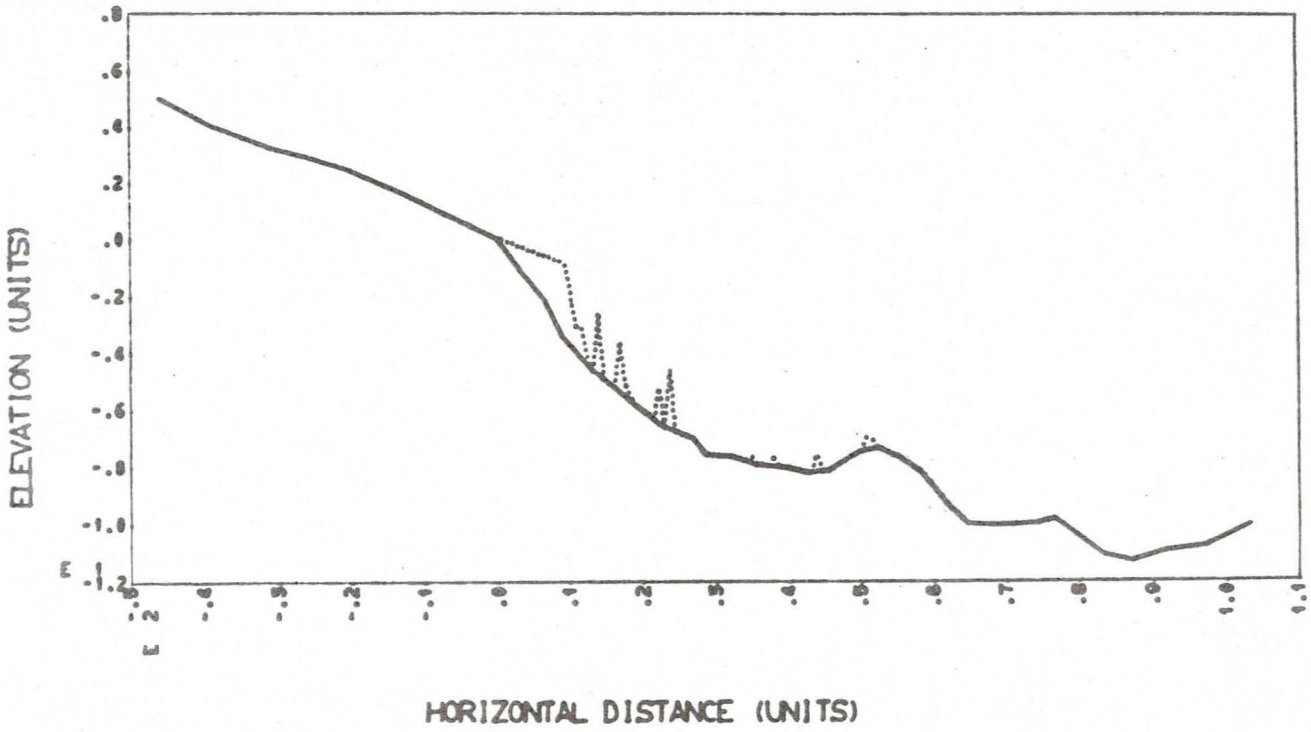

Figure 47c. Modelled snowdrift development along Slope site, North line, 10/31/74.

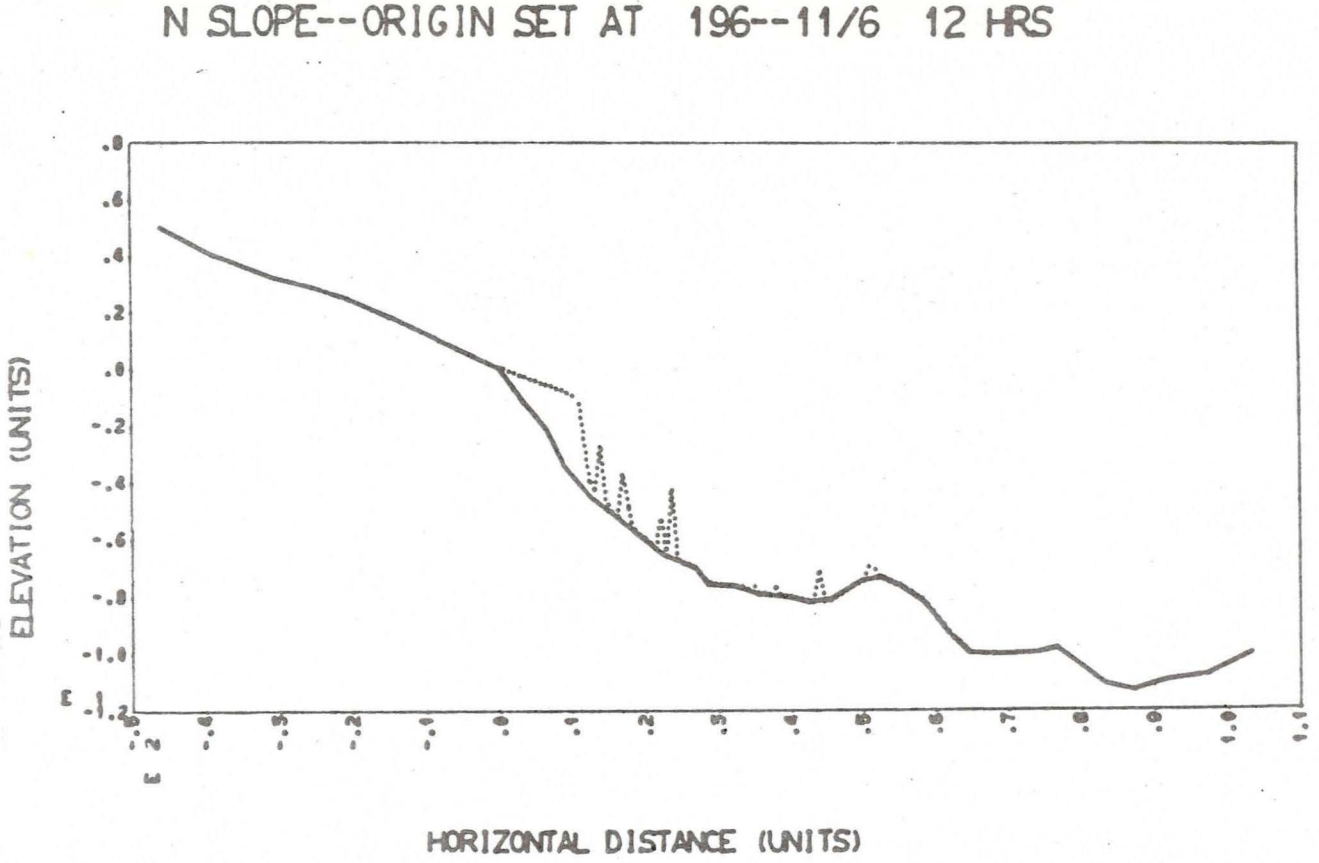

Figure 47d. Modelled snowdrift development along Slope site, North line, 11/6/74.

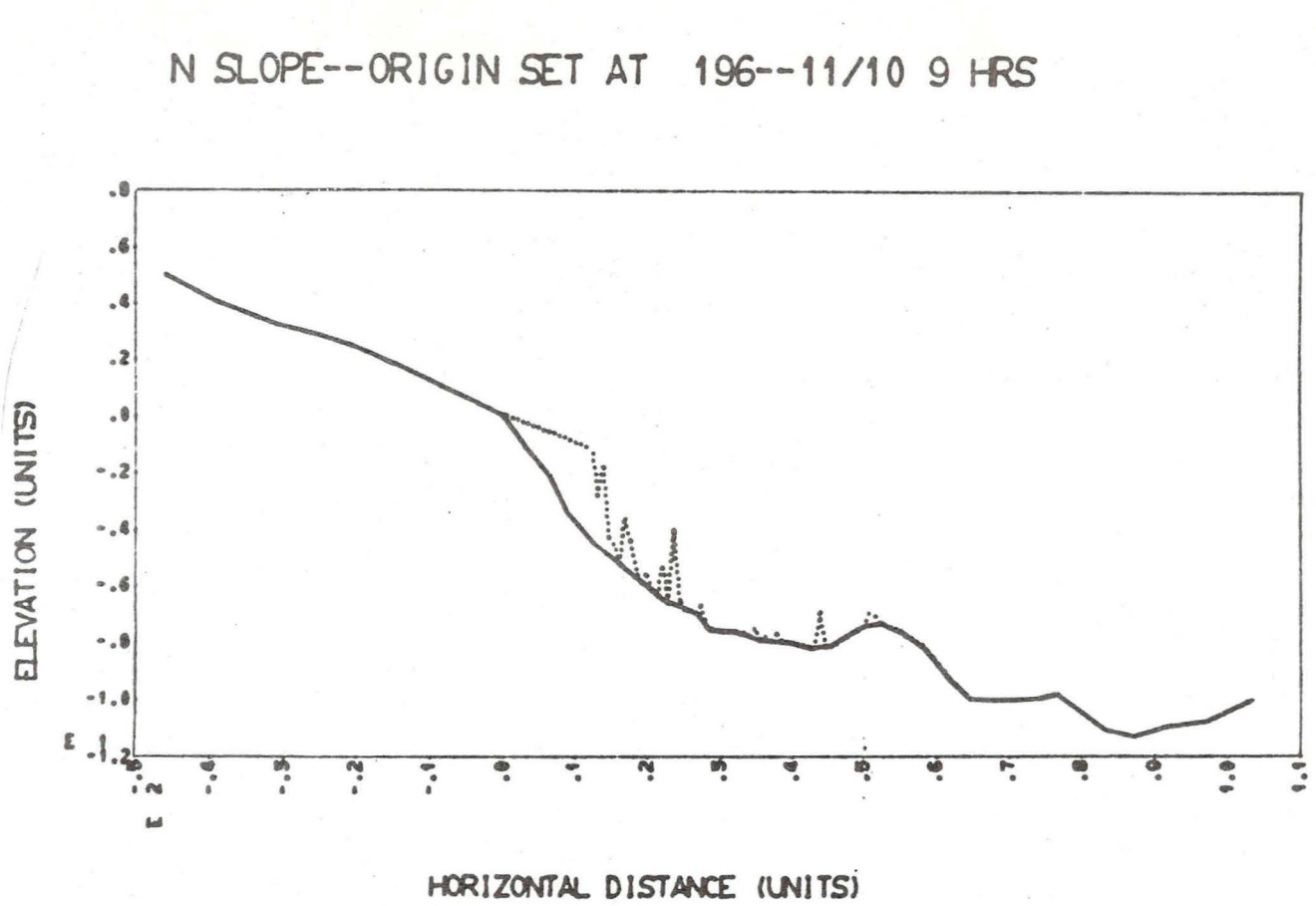

Figure 47e. Modelled snowdrift development along Slope site, North line, 11/10/74.

the second trap, at ca. 55 to 90 m (figure 47) , in the model.

The ragged profile of the depositional pattern to the lee of the brink is due partially to the fact that the model segregates the lower atmospheric layer into discrete layers rather than treating it realistically as a continuum. Thus the smooth snow accumulation surface known to exist in nature is broken into segments. Refinement of the model to estimate the snow surface by the running mean of snow depths in adjacent cells would even out the surface but cannot be justified.

Insufficient accumulation over the entire catchment may result from either 1) insufficient total mass transport, 2) excessive blowpast, or 3) low snowdrift deposit density. As explained in Appendix I the method of generating transport quantities is based upon a transport equation that produces intermediate values out of six possible formulae. It would be possible to use a different relationship so as to increase q_d although there is no clear justification for doing so. Alternatively, use of several grain size fractions with most of the transport allocated to the larger sizes should reduce blowpast and consequently increase the total cross-sectional area of snow accumulation but might also reduce deposition downwind from the brink. Perhaps the easiest modification would be to reduce ρ_d from 0.4 to 0.25, as suggested by Santaford (1972), to increase accumulation at all locations by 60%.

It is clear that the model does not adequately treat the condition in which a second catchment is located immediately downwind of an initial catchment. The ground topography between ca. 46 and 75 m (figure 47) suggests constriction of flow between 46 and 54 m, with consequent increase in fluid velocity to a value probably greater than U_t, followed by flow expansion between 54 and 75 m, over which speed decreases and snow deposition results. Thus the accumulation evident at ca. 50 to 52 m (figure 47) should be relocated to beyond the second flow separation point at ca. 56 m. This conceptual argument is supported by field observations over the

first few months of the accumulation season (figure 21) before accumulation between 28 and 53 m effectively raises the surface so that flow constriction no longer occurs between 46 and 54 m. The model treats the entire horizontal distance between 0 and ca. 70 m as one mixing/eddy zone which is improper with the topography as specified in figure 47. This problem suggests a major modification to the model and one that will be discussed in the final section of this report.

RECOMMENDATIONS AND CONCLUSIONS

A major aim of this project was the development of a semi-theoretical model of natural snowdrift accumulation. This has been achieved by specifying rules for calculating trajectories of blowing snow particles in creep, saltation and suspension transport and has been based upon the delineation of zones of reduced airflow as determined from changes in terrain slope angle.

In structure this approach is based upon sedimentological concepts developed in fluvial and eolian sand movement regimes and has potential for use in these situations. Successful verification of the model suggests that similar functional relationships exist between snow and sand movement in air.

FURTHER WORK

The computational mechanisms can be improved and expanded to more realistically simulate natural snowdrift accumulation.

The relationships specifying airflow change over varied terrain are major components in the model; several alterations can be made in this regard. (1) The location of the origin must be defined internally by the model through specification of rules by which slope angle change determines points of flow separation. (2) The lower mixing region angle must be related to approach slope angle as well as boundary layer thickness and step height. (3) Extension of the model should include the capacity for analysis of topographic conditions in which flow constriction, such as that over a forward facing step, occurs. Included would be air movement up and over an embankment or road cut; currently only movement down and across a slope discontinuity is considered. (4) Routines must be developed to adequately analyze the case where multiple drift catchments exist in immediate downwind proximity. If flow reattachment at an initial catchment has occurred then the Plate and Lin (1965) velocity distribution techniques specify airflow prior to the second catchment and

blowpast from the first trap becomes the primary mass transport input to the second drift accumulation. If, however, traps are close together, as in the N. Slope case (figure 21) complications arise. During the early part of the accumulation season the catchments respond as distinct traps. However, as infill proceeds the snow surface configuration changes so that by the later stages of accumulation infill in the first trap can drastically alter the approach slope to the second catchment or effectively bury the second trap (N. Slope accumulation between February and April, figure 21).

A final modification would incorporate the effects of the metamorphism of deposited snow. The drift deposit should settle through time so that the upper surface would lower, thereby allowing possible additional infill. A simple weighting factor defined as a function of time may be appropriate as an allowance for settlement. The cohesive properties of snow which may contribute to cornice development during intermediate stages of drift infill are only incidently accommodated in the model. It is assumed that a parcel of blowing snow impacting onto deposited snow in a specified accounting cell remains there rather than contributing to the next leeward cell. This condition implicitly assumes particle cohesion. It may, nevertheless, be useful to develop further this factor to relate to the mechanisms of cornice development.

CONCLUSIONS

If the basic functional relationships incorporated in the model are valid then experimentation with the model suggests that realistic simulation of drift accumulation is possible if

1) a relatively low reverse flow velocity within the eddy zone is specified,
2) several grain size fractions are included,
3) numerous levels of suspension transport are defined, and
4) saltation layer thickness is increased over that proposed by Owen (1964).

In its present form the model predicts the location and change of drift infill through time in cases where airflow expansion occurs in response to changes in terrain configuration. Additional work is necessary to adequately simulate conditions in which several drift accumulation traps exist in close proximity or if slope change is such that airflow constriction occurs.

REFERENCES

Abbott, D.E. and S.J. Kline, 1962, Experimental investigation of subsonic flow over single and double backward steps: Trans. ASME, Ser. D, J. Basic Eng., 84, 317-325.

Abramovich, G.K., 1963, The Theory of Turbulent Jets: MIT Press, Cambridge, Mass.

Albertson, M.L., et al, 1950, Diffusion of submerged jets: Trans. ASCE, 115, 639-659.

Allen, J.R.L., 1968, Current Ripples: North-Holland Pub. Comp., Amsterdam, 433 p.

Anderson, D.L. and C.S. Benson, 1963, Densification and diagenesis of snow: p. 391-411 in W.D. Kingery (ed.), Ice and Snow, MIT Press, Cambridge, Mass., 684 p.

Arie, M. and H. Rouse, 1956, Experiments on two-dimensional flow over a normal wall: J. Fluid Mech., 1, 129-141.

Bader, H., 1962, The physics and mechanics of snow as a material: Cold Regions Science and Eng. Mono., Pt. II, Sec. b.

Bagnold, R.A., 1936, The movement of desert sand: Proc. Roy. Soc. London, Ser. A, 157, 594-624.

_____, 1954, The Physics of Blown Sand and Desert Dunes: 2nd ed., Methuen and Comp., Ltd., London, (1941), 265 p.

Barry, R.G., 1972, Climatic environment of the east slope of the Colorado Front Range: Colorado University, Boulder, Institute of Arctic and Alpine Research, Occasional Paper 3, 206 p.

_____, 1973, A climatological transect on the east slope of the Front Range, Colorado: Arctic and Alpine Res., 5, 89-110.

Benedict, J.B., 1970, Downslope soil movement in a Colorado alpine region: rates, processes, and climatic significance: Arctic and Alpine Res., 2, 165-226.

Berg, N.H., 1975, Empirical evaluation of some eolian sand transport models: J. Sed. Petrol., (accepted for publication)

Bourque, C. and B.G. Newman, 1960, Reattachment of a two-dimensional incompressible jet to an adjacent flat plate: Aeron. Quart., 11, 201-232.

Budd, W., 1966, The drifting of non-uniform snow particles: p. 59-70 in M. Rubin (ed.), Studies in Antarctic Meteorology, Antarctic Research Series, v. 9, Amer. Geophys. Union.

_____, Dingle, R. and U. Radok, 1966, The Byrd snow drift project: outline and basic results: p. 71-134 in M. Rubin (ed.), Studies in Antarctic Meteorology, Antarctic Research Series, v. 9, Amer. Geophys. Union.

Calkins, D.J., 1975, Simulated snowdrift patterns: Cold Regions Research and Eng.Lab., Spec. Rept. 219, 15 p.

Chang, P.K., 1970, Separation of Flow: Pergamon Press, New York, N.Y., 777 p.

Chepil, W.S., 1945, Dynamics of wind erosion: II. Initiation of soil movement: Soil Sci., 60, 397-411.

_____, and R.A. Milne, 1939, Comparative study of soil drifting in the field and in a wind tunnel: Scientific Agriculture, 19,249-261.

Cooke, J.C. and G.O. Brebner, 1961, The nature of separation and its prevention by geometric design: in G.V. Lachmann (ed.), Boundary Layer and Flow Control, v. I, Pergamon Press, Oxford.

Cooke, R.U. and A. Warren, 1973, Geomorphology in Deserts: Univ. of California Press, Berkeley ard Los Angelos, 374 p.

Cooper, W.S., 1958, Coastal Sand Dunes of Oregon and Washington: Geol. Soc. Amer. Memoir 72, 169 p.

Dingle, W.R.J. and U. Radok, 1961, Antarctic snow drift and mass transport: Gen. Assem. Helsinki, Internat'l Assoc. Sci. Hydrology, Internat'l Union of Geodosy and Geophysics, pub. 55.

Diunin, A.K., 1967, Fundamentals of the mechanics of snow storms: p. 1065-1073 in H. Oura (ed.), Physics of Snow and Ice, Hokkaido University, v. I, pt. 2.

_____, and A.A. Komarov, 1954, On the construction of snow fences: Nat'l Res. Coun. Canada, Tech. Trans. 1101, 1963.

Finney, E.A., 1939, Snow drift control by highway design: Michigan Eng. Expt. Stat., Michigan State College, Bull. 75.

Horikawa, K. and H.W. Shen, 1960, Sand movement by wind: U.S. Army Coprs of Engineers, Beach Erosion Board, Tech. Memo. 119, 51 p.

Hoyt, J.H., 1966, Air and sand movements in the lee of dunes: Sedimentology, 7, 137-144.

Hsu, S.A., 1971, Wind stress criteria in eolian sand transport: J. Geophys. Res., 76, 8684-8686.

Inman, D.L., Ewing, G.C. and J.B. Corliss, 1966, Coastal sand dunes of Guero Negro, Baja, California, Mexico: Geol. Soc. Amer. Bull., 77, 787-802.

Jopling, A.V., 1960, An experimental study on the mechanics of bedding: unpub. Ph.D. dissertation, Harvard University, 358 p.

Kobayashi, D., 1972, Studies of snow transport in low-level drifting snow: Contribution 24, Ser. A, Institute of Low Temp. Sci., 58 p.

Koerner, J.M., 1969, Krumholtz influences on alpine snow accumulations: unpub. M.A. thesis, Colorado University, Boulder.

Kotlyakov, V.M., 1961, Results of study of the formation and structure of the upper layer of the ice sheet in eastern Antarctica: Gen. Assem. Helsinki, Internat'l Assoc. Sci. Hydrology, Internat'l Union of Geodesy and Geophysics, pub. 55.

Kungurtsev, A.A., 1956, The transfer and deposition of snow: Cold Regions Res. and Eng. Lab., TL 258, 27 p.

Larson, L.W., 1971, Precipitation and its measurement: a state of the art: Water Resources Res. Institute, Ser. 24, Wyoming University, Laramie.

Laursen, E.M. and A. Toch, 1959, Free-turbulence shear flow: p. 359-406 in H. Rouse (ed.), Advanced Mechanics of Fluids, John Wiley and Sons, New York.

LeDrew, E.F., 1974, Radiation and energy budget of an alpine tundra in Colorado during the growing season, 1973: unpub. M.A. thesis, Colorado University, Boulder.

Liepmann, H.W. and J. Laufer, 1947, Investigations on free turbulent mixing: Nat'l Advisory Council for Aeronautics, Tech. Note 1257.

Mellor, M., 1964, Properties of snow: Cold Regions Sci. and Eng. Mono., Pt. III, Sec. A1.

_____, 1965, Blowing snow: Cold Regions Sci. and Eng., Mono., Pt. III, Sec. A3c, 79 p.

_____, and U. Radok, 1960, Some properties of drifting snow: p. 3333-346 in Symposium on Antarctic Meteorology, Melbourne, Pergamon Press, London.

Melnik, V.M., et al, 1971, Snowfall and snow transport during snowstorms over the USSR: Nat'l Sci. Found., Washington D.C., Spec. Foreign Currency Sci. Information Program, 180 p.

Naib, S.K.A., 1966, Mixing of a subcritical stream in a rectangular channel expansion: J. Institute of Water Engrs., 20, 199-206.

Nayak, S.K., Garrison, J.A. and J.E. Cermak, 1974, Wind engineering of Johns-Manville World Headquarters: Fluid Dynamics and Diffusion Lab., Dept. of Civil Eng., Colorado State Univ., Ft. Collins, 87 p.

Odar, F., 1965, Simulation of drifting snow: Cold Regions Res. and Eng. Lab., Res. Rept. 174, 16 p.

Owen, P.R., 1964, Saltation of uniform grains in air: J. Fluid Mech., 20, 225-242.

Plate, E.J. and C.W. Lin, 1965, The velocity field downstream from a two-dimensional hill: Fluid Dynamics and Diffusion Lab., Dept. of Civil Eng., Colorado State Univ., Ft. Collins, pt. I, 43 p.

Radok, U., 1968, Deposition and erosion of snow by the wind: Cold Regions Res. and Eng. Lab., Res. Rept. 230, 23 p.

Raudkivi, A.J., 1967, Loose Boundary Hydraulics: Pergamon Press, New York, 221 p.

Rechard, P.H., 1975, Measurement of winter precipitation in windswept areas: p. 13-31 in Snow Management on the Great Plains, Research Committee Great Plains Agricultural Coun., pub. 73, Nebraska University, Lincoln, Agricultural Expt. Stat.

Rusin, N.P., 1959, Horizontal transport of snow in Antarctica: Cold Regions Res. and Eng. Lab., Trans., 1970.

Santaford, H.S., 1972, Management of windblown alpine snows: Colorado State Univ., Atmos. Sci. Paper 192, prep. for Office of Water Resources Research.

Sawyer, R.A., The flow due to a two-dimensional jet issuing parallel to a flat plate: J. Fluid Mech., 9, 543-560.

Schmidt, R.A., 1971, Processing size, frequency and speed data from snow particle counters: USDA Forest Service Res. Note RM 196, 4 p.

_____, 1972, Sublimation of wind-transported snow-a model: USDA Forest Service Res. Paper RM-90, 24 p.

_____, and R.A. Sommerfeld, 1969, A photoelectric snow particle counter: Western Snow Conf. Proc., 37, 88-91.

Schneider, T.R., 1962, Snowdrifts and winter ice on roads: Nat'l Res. Coun. Canada, Tech. Trans. 1038, by D.A. Sinclair, 200 p.

Sharp, R.P., 1964, Wind-driven sand in the Coachella Valley, California: Geol. Soc. Amer. Bull., 64, 547-560.

Shiotani, M. and H. Arai, 1952, A short note on the snow-storm: Proc., 2nd Nat'l Congress for Applied Mechanics, Sci. Coun. of Japan.

Squire, H.B., 1956, Note on the motion inside a region of recirculation (cavity flow): J. Roy. Aeron. Soc., 60, 203-205.

Svasek, J.N. and J.H.J. Terwindt, 1974, Measurements of sand transport by wind on a natural beach: Sedimentology, 21, 311-322.

Tabler, R.D., 1972, Evaluation of the first-year performance of the Interstate-80 snow fence system: USDA Forest Service, Rocky Mtn. Forest and Range Expt. Stat., Final Rept. to contract 16-247-CA, prep. for Wyoming Highway Dept. 84 p.

_____, 1975, Predicting profiles of snowdrifts in topographic catchments: paper presented at 43rd Western Snow Conference, San Diego, Calif., 18 p.

_____, 1975, Estimating the transport and evaporation of blowing snow: p. 85-104 in Snow Management on the Great Plains, Res. Committee Great Plains Agricultural Coun., pub. 73, Nebraska University, Lincoln, Agricultural Expt. Stat.

Tani, I., 1958, Experimental investigation of flow separation over a step: p. 377-386 in H. Gortler (ed.), Boundary Layer Research, Springer-Verlag, Berlin.

Theakson, F.H., 1973, Simulated snow storms-a model analysis: paper presented at the Interdisciplinary Symposium on advanced concepts and techniques in the study of snow and ice resources, Monterey, Calif., 12/73.

Tollmien, W., 1926, Calculation of turbulent expansion processes: Nat'l Advisory Coun. for Aeronautics, Tech. Memo. 1085, 1945.

United States Department of Agriculture, Forest Service, 1970, Instrumentation for snow, weather, and avalanche observations, Snow Safety Guide 2: Alta Avalanche Study Center, 80 p.

APPENDIX I. Delimitation of blowing snow events 10/11 to 11/10, 1975

Since the snow particle counter was not in operation until 11/11/74, information on the duration and magnitude of blowing snow events during this period was determined indirectly through consideration of wind speed, temperature, and precipitation data. Several criteria were stipulated in the evaluation of these parameters. It was assumed that 1) significant blowing snow will not occur when air temperature is greater than $0^{o}C$; 2) U_{t} = 4 mps at 10 m height; and 3) blowing snow will not occur more than three days after a snowfall.

Evaluation of temperature data at the alpine "Saddle" site less than one km west of T-van and at "Kiwi" station, at 3350 m elevation one km southeast of T-van, suggested little blowing snow occurrence, and in fact probable melt, between 10/16 and 10/22 and 50% probability of snow movement between 10/23 and 10/27.

Snowfall further limited potential blowing snow to periods between 10/13 and 10/17, 10/23 and 11/7, and 11/8 and 11/11. Finally, consideration of 12-hour wind speed means resulted in delimitation of the blowing snow periods listed in table 4.

Besides specification of the wind regime evident during each blowing snow event, the mass transport of wind-blown snow must be calculated. Determination of q_{d} follows a complicated procedure in which the transport capacity of the wind is compared with the amount of transportable snow upwind of the drift catchment.

From the 12-hour mean wind speed data mass transport, q_{w}, was calculated from equation (32) (Kobayashi, 1972)

$$q_{w} = 0.03\ VI^{3}/100 \qquad (32)$$

and the total mass of transported grains, $m_{w(i)}$, calculated as the product of q_{w} and the 12-hour length of the i^{th} event. Equation (32) is selected somewhat arbitrarily as yielding intermediate values when compared with five other transport formulae listed by Kobayashi (1972).

If insufficient snow is available to match $m_{w(i)}$, then the duration of the blowing snow period is shortened. Conversely, more snow may be available than is transportable by the wind in one event so that additional mass movement may occur during a following event. Specification of these relationships follows from consideration of the sublimation of wind-blown snow over the available fetch upwind of the drift catchment.

The contributing distance, R_c, over which unimpeded snow movement occurs upwind of the Slope and Tank Trap sites is approximately 500 m. Over R_c, the mass of fallen snow is assumed to be equally distributed prior to entrainment by the wind. Losses due to sublimation of wind-blown snow over R_c are calculated through equation (33) (Tabler, 1975)

$$q_T = \frac{P_r R_\mu}{2} \left(1 - (0.14)^{R_c/R_\mu}\right) \qquad (33)$$

where q_T is m^3 of water per m width perpendicular to the wind, R_μ is the distance required for evaporation of the average sized snow particle, and P_r is the relocatable snow expressed in water equivalent. Tabler (1975) gives R_μ the value 3050 m for high plains areas and P_r is assumed equal to 0.98 of the fallen precipitation in alpine tundra environments. The quantity q_T is weighted by a constant to yield the mass of water, m_T, available for transport to the drift catchment.

The upper limit for the total mass transportable during each blowing snow event is m_T so that the event ends when the sum $m_{w(i)}$ over each 12-hour period reaches m_T. Table 4 lists $m_{w(i)}$, m_T, and other characteristics of each blowing snow event

APPENDIX II. List of symbols

A_2 - coefficient

B - coefficient

c - coefficient

C - coefficient

C_2 - coefficient

C_f - wall shear stress coefficient

$C_{f(0)}$ - value of C_f upwind of separation point

CREP - creep transport coefficient

d - jet orifice width or boundary layer thickness

D - grain diameter

e - snowdrift deposit void ratio

g - acceleration of gravity

h - mean height of the saltation curtain

H - step height

IANG - snow particle angularity

ILAY - number of saltation layers

k - von Karman constant

l - vertical length used as parameter in R_s

L - mean saltation path length (Bagnold)

L_b - separation bubble length

L_s - mean saltation path length under "saturated" conditions (Kobayashi)

L_u - mean saltation path length under "unsaturated" conditions (Kobayashi)

m_T - total mass of transportable snow including sublimation losses

$m_{w(i)}$ - total mass of transported grains calculated from transport formula

n_z - drift density

P - snowdrift deposit porosity

P_r - relocated snow expressed in water equivalence

$P(W)$ - probability distribution of boundary layer atmospheric up-currents which exceed fall velocity w

q_d - mass transport of blowing snow particles (g cm^{-1} sec^{-1})

q_{sus} - transport load carried in suspension

q_{salt} - transport load carried in saltation

q_T - mass transport calculated from Tabler (1975) including effects of sublimation

q_w - mass transport calculated from transport formula

R_c - unimpeded contributing distance upwind of catchment over which snow movement occurs

R_s - step Reynolds Number

R_μ - distance required for evaporation of average sized snow grains

T - total number of suspension transport layers

U - wind speed

U_1 - maximum forward velocity at distance x/H from separation point

U_2 - maximum reverse velocity at distance x/H from separation point

U_{10} - wind speed at 10 meter height

U_f - horizontal velocity of saltating grains just prior to impact

U_h - wind speed at height h

U_{max} - velocity at upper limit of boundary layer

U_t - threshold velocity of grain entrainment

U_z - wind speed at height z

$U_{b,x}$ - maximum reverse flow speed at x within mixing region

$U_{m,x}$ - maximum forward flow speed at x within mixing region

$U_{z,x}$ - speed within mixing region at height z and distance x from separation point

v - kinematic viscosity

$V1$ - wind speed at 1 meter height (mps)

w - particle fall velocity

w_* - non-dimensional fall velocity coefficient

w' - initial vertical velocity of a saltating grain

x - horizontal distance

xsalt - horizontal distance at which saltating grains intersect upper mixing region boundary

z - height

zsalt - height of intersection of upper mixing region boundary with saltating grains

z_o - roughness element

z_{int} - median height of a specified creep, saltation, or suspension layer

$z_{tot(i)}$ - width of i^{th} layer within mixing zone used for calculation of grain movement within mixing zone

$z_{b,x}$ - height at which $U_{b,x}$ occurs

$z_{m,x}$ - height at which $U_{m,x}$ occurs

α (A) - upper mixing region angle (also noted as angle A)

β (B) - lower mixing region angle (also noted as angle B)

ϕ - angle of saltation grain impact

ρ_d - snowdrift deposit density

ρ_f - fluid density

ρ_i - ice density

ρ_s - particle density